LA-UR-12-24019

Approved for public release; distribution is unlimited.

Title: Proton Radiography: Its uses and Resolution Scaling

Author(s): Mariam, Fesseha G.

Intended for: SPIE, 2012-08-12/2012-08-16 (San Diego, California, United States)

Disclaimer:
Los Alamos National Laboratory, an affirmative action/equal opportunity employer,is operated by the Los Alamos National Security, LLC for the National NuclearSecurity Administration of the U.S. Department of Energy under contract DE-AC52-06NA25396. By approving this article, the publisher recognizes that the U.S. Government retains nonexclusive, royalty-free license to publish or reproduce the published form of this contribution, or to allow others to do so, for U.S. Government purposes. Los Alamos National Laboratory requests that the publisher identify this article as work performed under the auspices of the U.S. Departmentof Energy. Los Alamos National Laboratory strongly supports academic freedom and a researcher's right to publish; as an institution, however, the Laboratory does not endorse the viewpoint of a publication or guarantee its technical correctness.

Proton Radiography: Its Uses and Resolution Scaling

Fesseha G. Mariam

For the LANL Proton Radiography Team

Aug. 15, 2012

SPIE, San Diego

Abstract

Charged Particle Radiography

Los Alamos National Laboratory has used high energy protons as a probe in flash radiography for over a decade. In this time the proton radiography project has used 800 MeV protons, provided by the LANSCE accelerator facility at LANL, to diagnose over five-hundred dynamic experiments in support of stockpile stewardship programs as well as basic materials science. Through this effort significant experience has been gained in using charged particles as direct radiographic probes to diagnose transient systems. The results of this experience will be discussed through the presentation of data from experiments recently performed at the LANL pRad.

Outline:

• proton interactions
•history of proton radiography
•How modern proton radiography works
•The prad facility at the Los Alamos Neutron Science Center (LANCE)
•Some results: experiments on energetics, tomography, miscellaneous uses of prad
•Way forward: Resolution improvements
•Conclusion

Proton Interactions

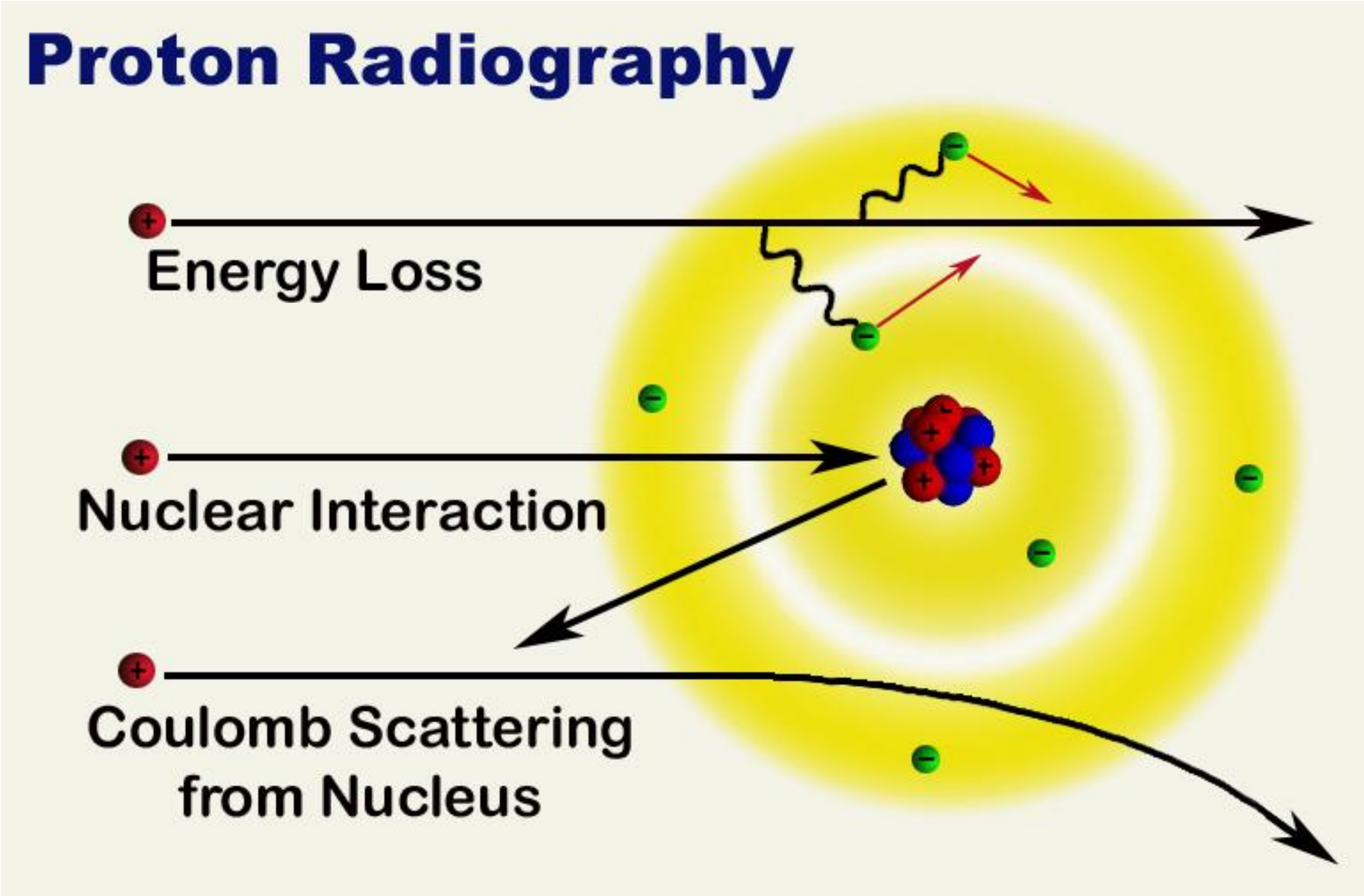

Early Proton Radiography

A. M. Koehler, *et al.* *Science* **160**, 303 (1968).

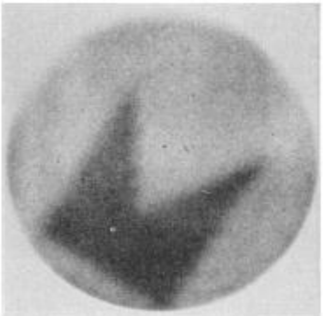

Fig. 1. Proton radiograph of aluminum absorber 7 cm in diameter and 18 g/cm² thick, with an additional thickness of 0.035-g/cm² aluminum foil, cut in the shape of a pennant, inserted at a depth of 9 g/cm². The addition of 0.2 percent to the total thickness produces a substantially darker area on the film.

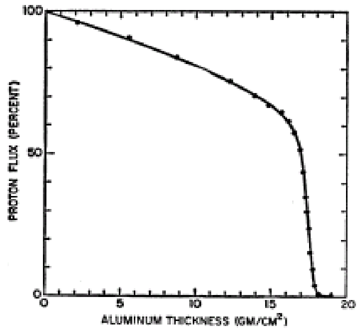

Fig. 2. Proton flux as a function of depth in aluminum. The steeply falling portion of the curve near 18 g/cm² is used to obtain the high contrast of Fig. 1.

J. A. Cookson Naturwissenschaften 61, 184—191 (1974)

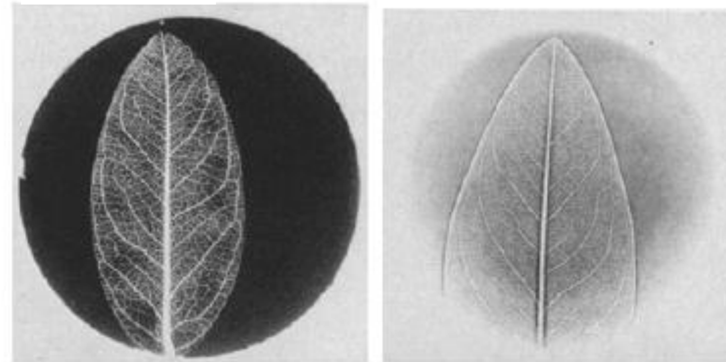

Fig. 6a and b. Radiographs of leaves by a) marginal range radiography with 196 mg/cm² of extra Al absorber, and b) scattering radiography with leaf sandwiched between two 6.9 mg/cm² Al layers and 14 mm from the film

<u>Marginal Range Radiography</u>

- Reduce proton beam energy to near end of range.
- Use steep portion of transmission curve to enhance sensitivity to areal density variations.
- Coulomb scattering at low energy results in poor resolution >1.5 mm.
- Contrast generated through proton absorption.

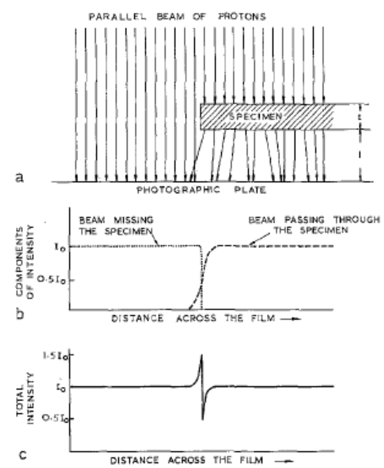

Fig. 7. Illustration of how multiple scattering produces its characteristic edge pattern

<u>Scattering Radiography</u>

- Edge detection only
- Limited to thin objects
- Contrast generated through position dependent scattering

LANL Transmission Radiography (1995)

[Morris et al.]

188 MeV secondary proton beamline at LANSCE

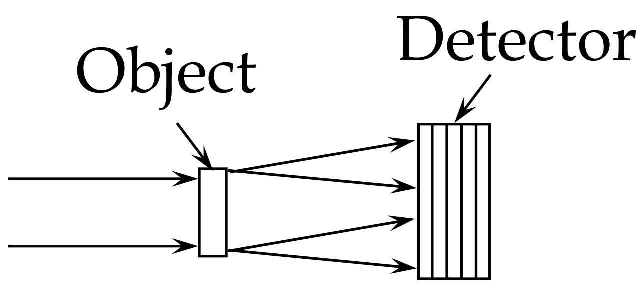

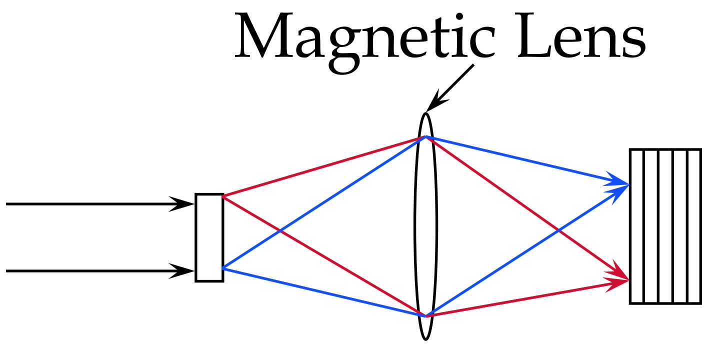

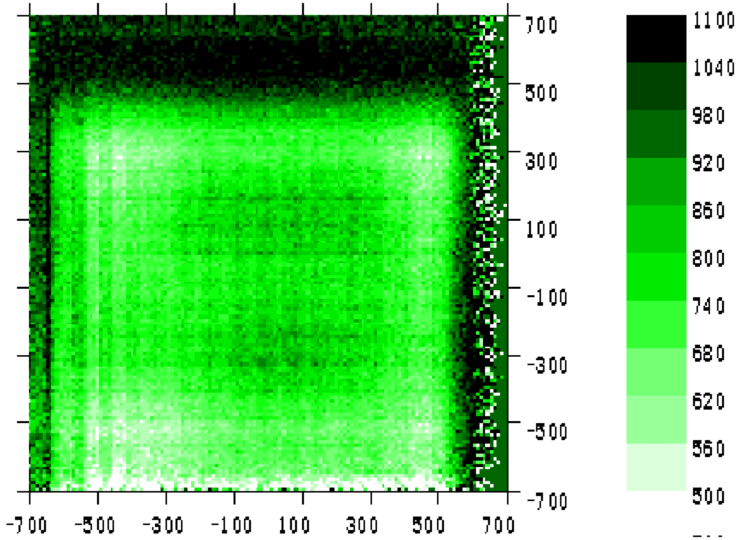

Image at the detector is substantially blurred.

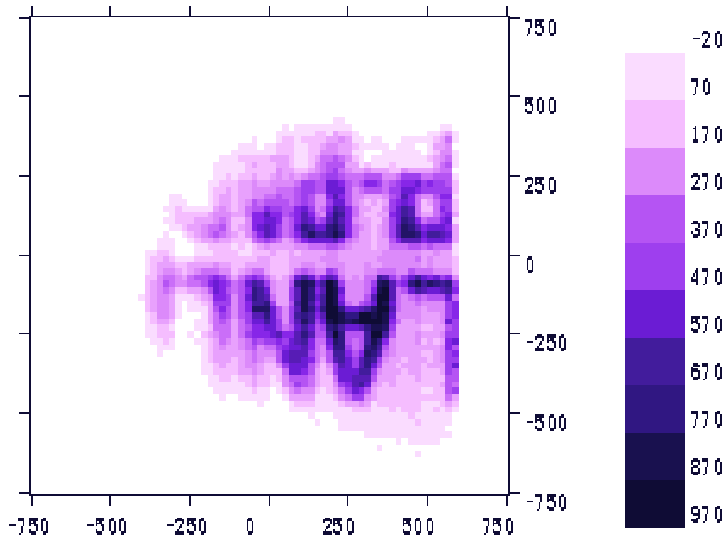

Magnetic imaging lens preserves image with high resolution.

Significant blur Correction (Matching)

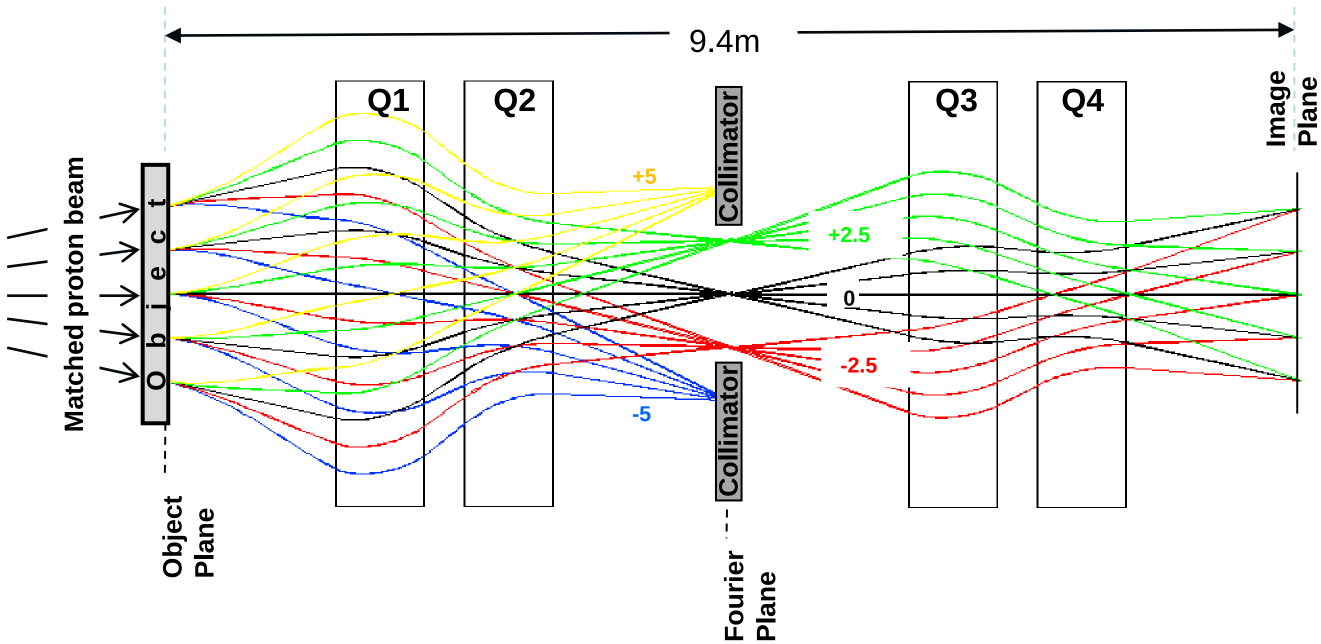

$$x_I = M_{11}x_o + \Delta x$$

$$y_I = M_{33}y_o + \Delta y$$

$$\Delta x = (T_{116}x + T_{126}\delta\theta)\frac{\delta p}{p}$$

$$\Delta y = (T_{336}y_o + T_{346}\delta\theta)\frac{\delta p}{p}$$

Δx, Δy are chromatic blur terms

MATCHING

Inject beam with position-angle correlation is such a way that the T_{116} and T_{336} (position dependent) terms are eliminated

We are then left with the blur terms:

$$\Delta x = T_{126}\delta\theta\frac{\delta p}{p} \quad \Delta y = T_{346}\delta\theta\frac{\delta p}{p}$$

Controlled by size of collimator

Also: Matching ➔results in the sorting of protons at the Fourier plane by their angle of scattering regardless of the position at the object location suggesting that the remaining chromatic blur can further be reduced by using a collimator at the Fourier plane

* C.T. Mottershead and J. D. Zumbro, “Magnetic Optics for Proton Radiography”, Proceedings of the 1997 Particle Accelerator Conference

800 MeV x3 Magnifying Imaging Lens

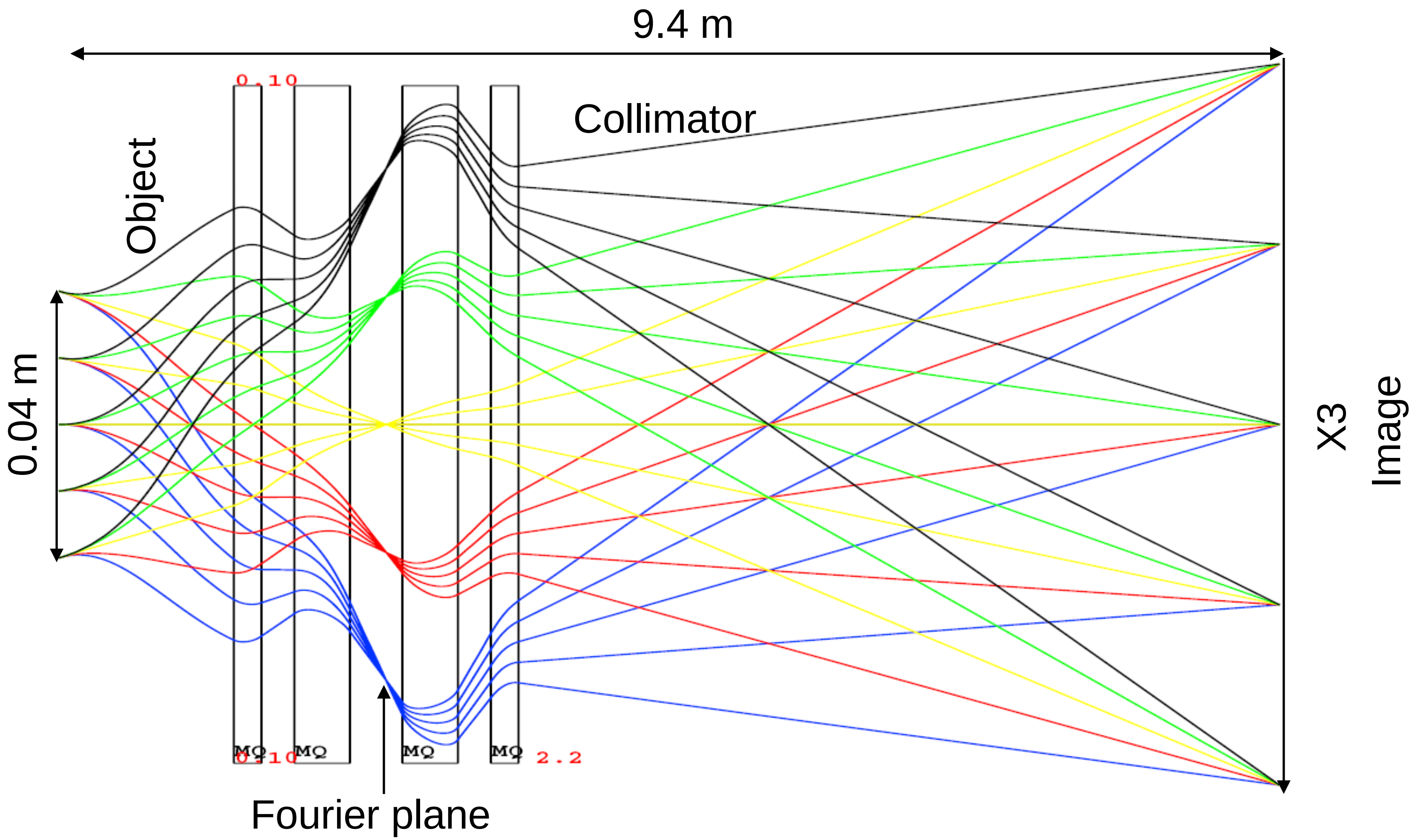

Transmission Calculation

$$T_{nuclear} = e^{-x/\lambda_c}$$

Nuclear removal processes:

λ_c - nuclear attenuation length (g/cm^2)

x - areal density

$$T_{MCS} = 1 - e^{-\theta_c^2 / 2\theta_o^2}$$

$$\theta_o = \frac{14.1MeV}{p\beta}\sqrt{\frac{x}{x_o}}$$

Multiple Coulomb Scattering with collimation:

θ_o - scattering angle (radians)

θ_c - collimator size (radians)

x - areal density

x_o - radiation length (g/cm^2)

p - momentum (MeV)

β - relativistic velocity

$$T = e^{-x/\lambda_c}\left(1 - e^{-\left(\frac{\theta_c p\beta}{14.1MeV}\right)^2 \frac{x_o}{2x}}\right)$$

Total EstimatedTransmission:

Good to 5-10%

LANSCE Experimental Areas

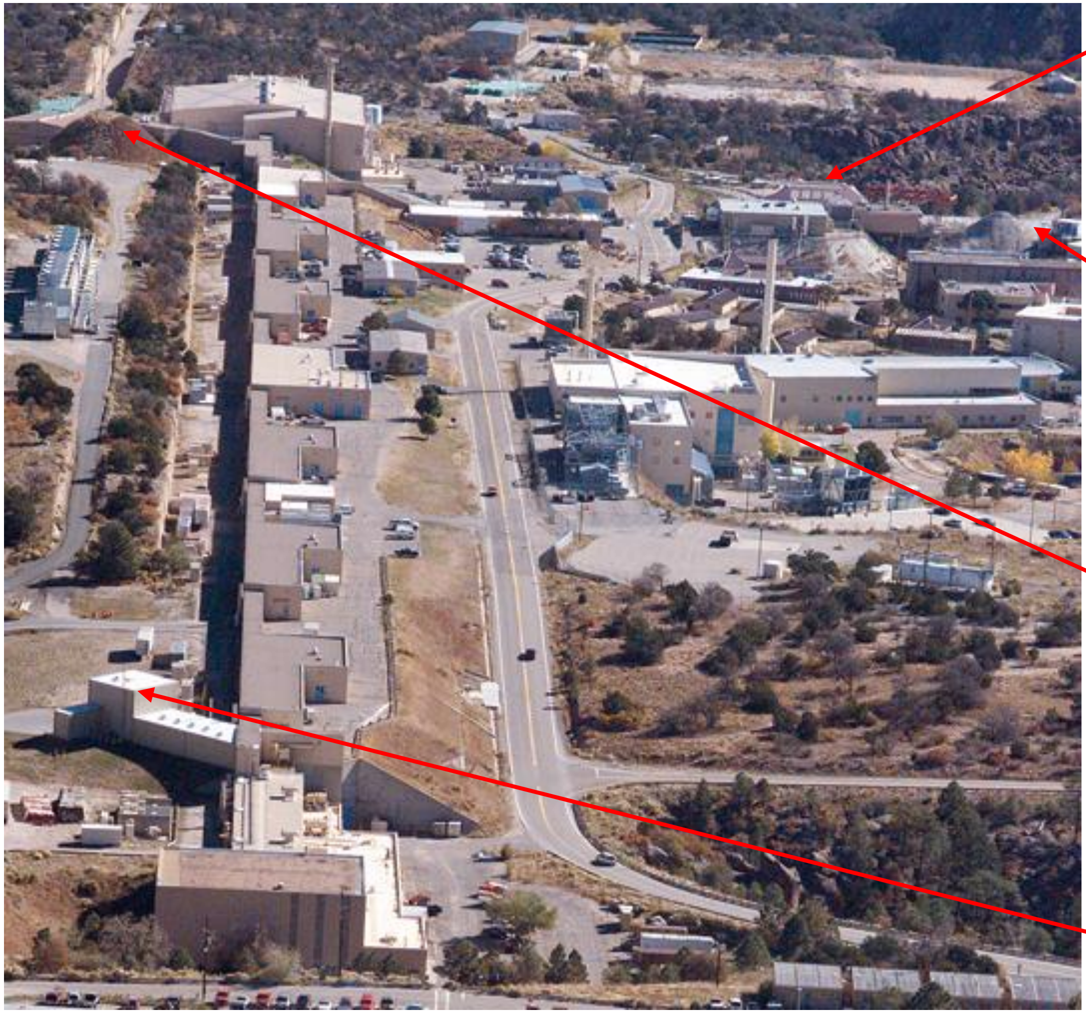

- Lujan Center
  - ***National security research***
  - ***Materials, bio-science, and nuclear physics***
  - ***National user facility***
- WNR
  - ***National security research***
  - ***Nuclear Physics***
  - ***Neutron Irradiation***
- Proton Radiography
  - ***National security research***
  - ***Dynamic Materials science,***
  - ***Hydrodynamics***
- Isotope Production Facility
  - ***Medical radioisotopes***

800 MeV pRad Facility at LANSCE

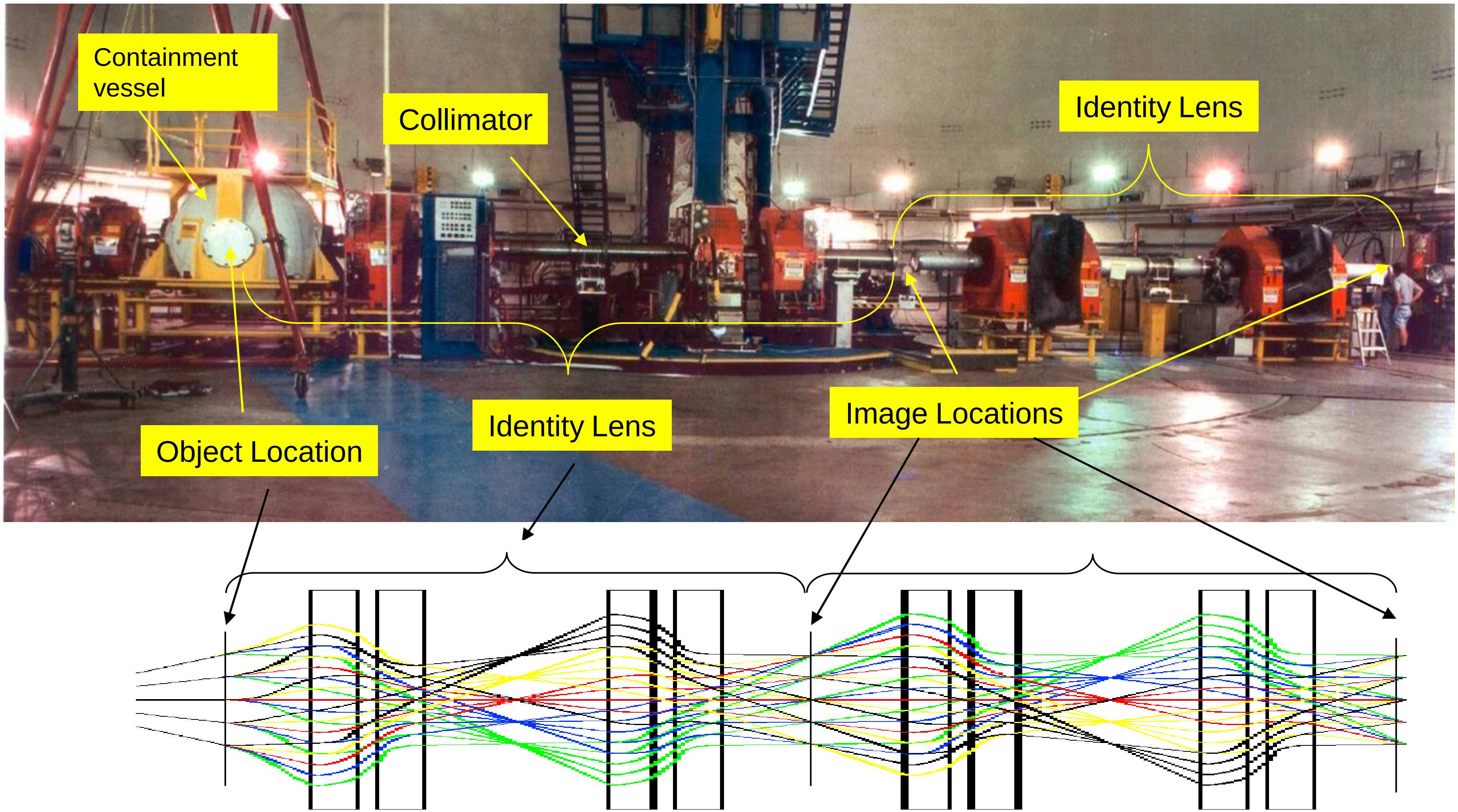

x3 Magnifier (PMQs)

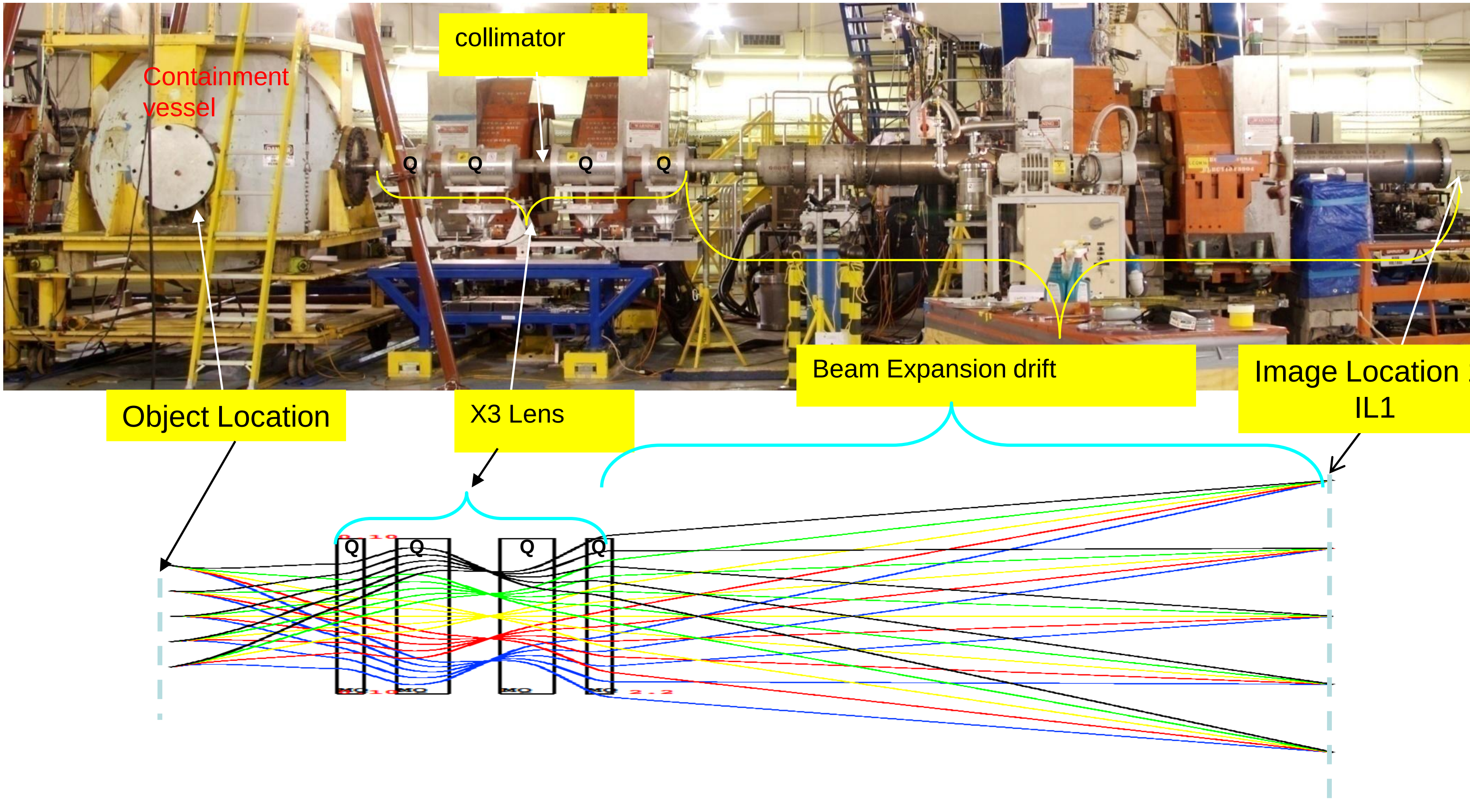

Made up of four 4” bore permanent magnet quads.

Temporal Resolution

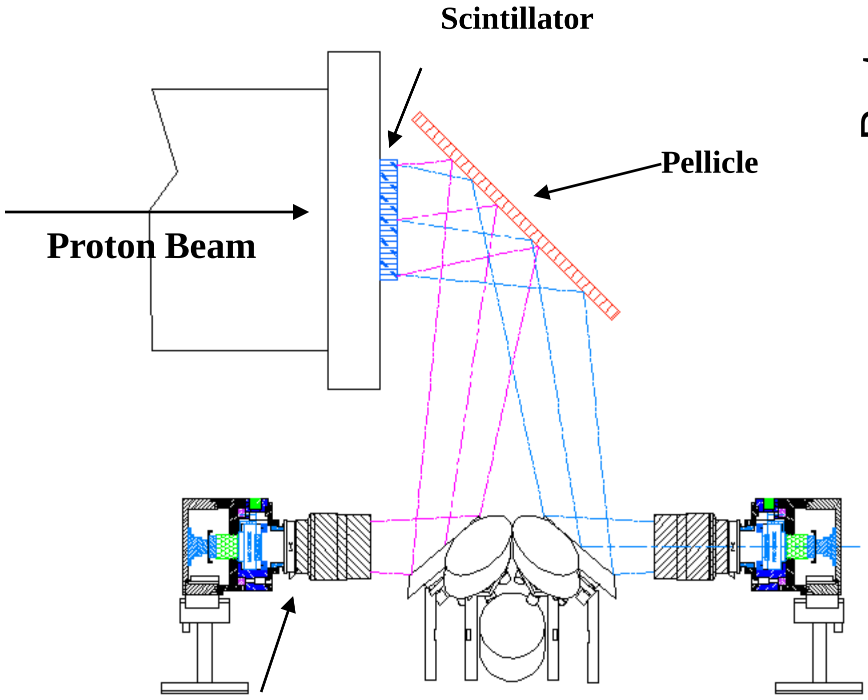

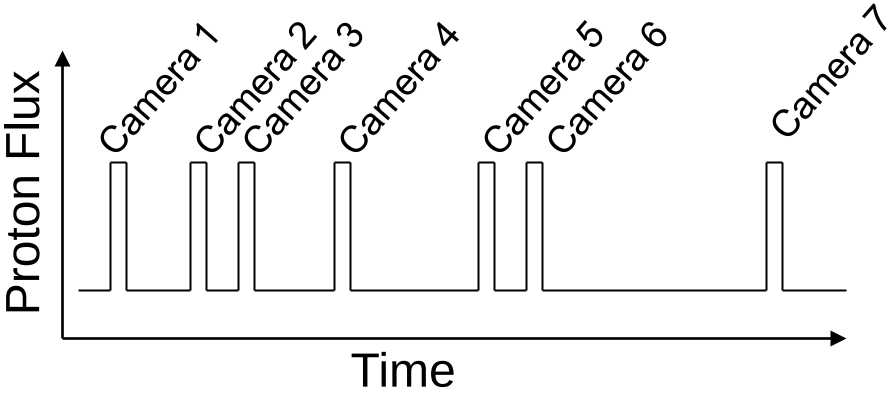

- 19 images at first station
- 22 images at second station
- Typically 60 ns exposure times

Failure Cone (Eric Ferm) (-I Lens)

Failure occurs at d=5.4 to 5.6mm

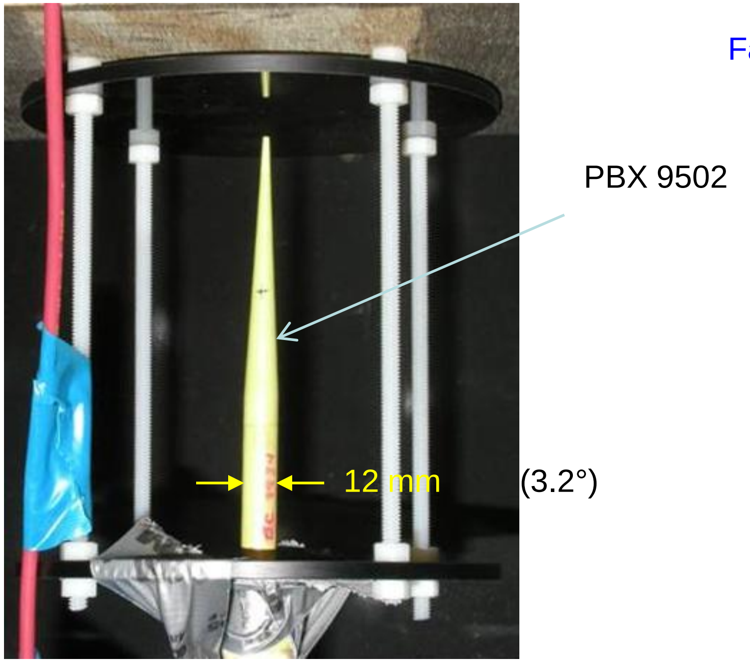

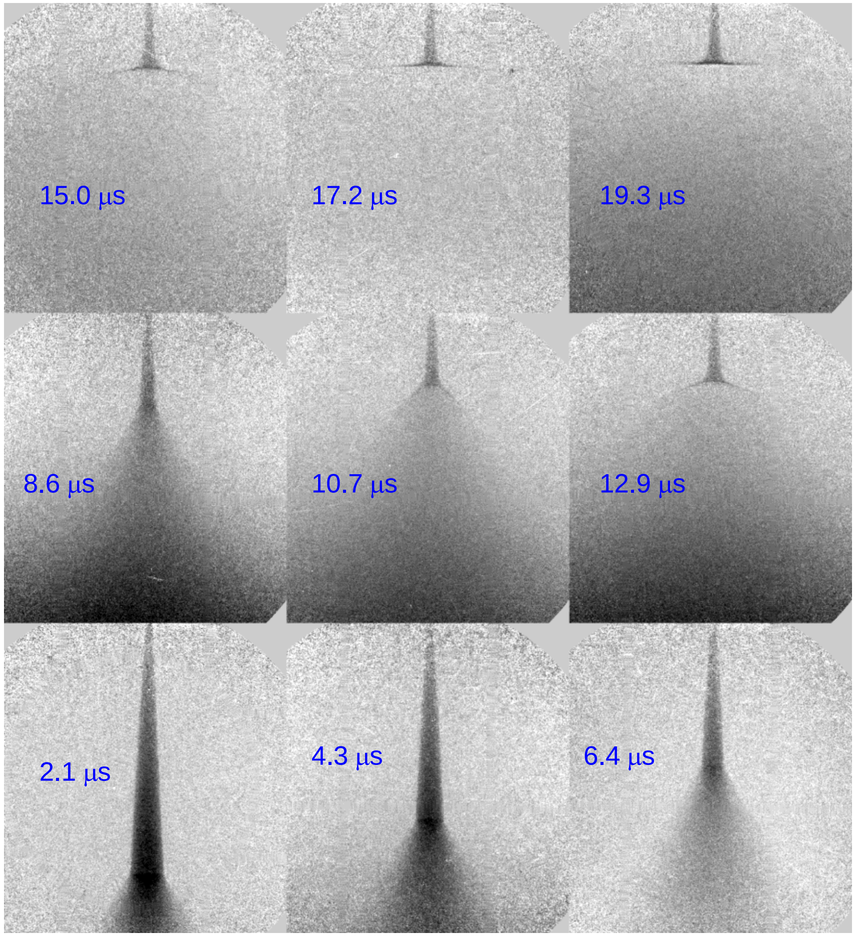

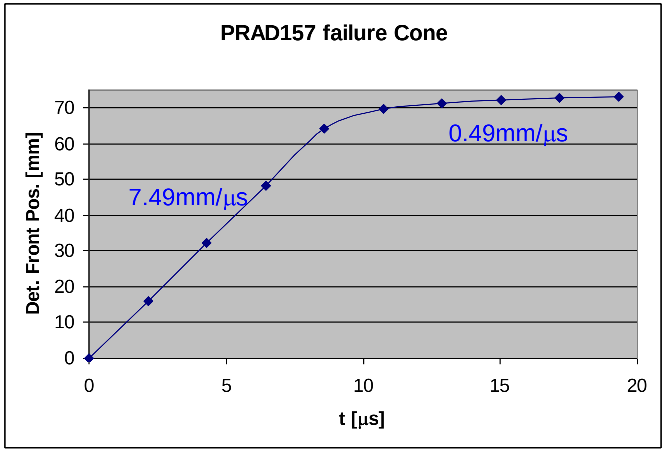

Tin RMI Shots (Example)

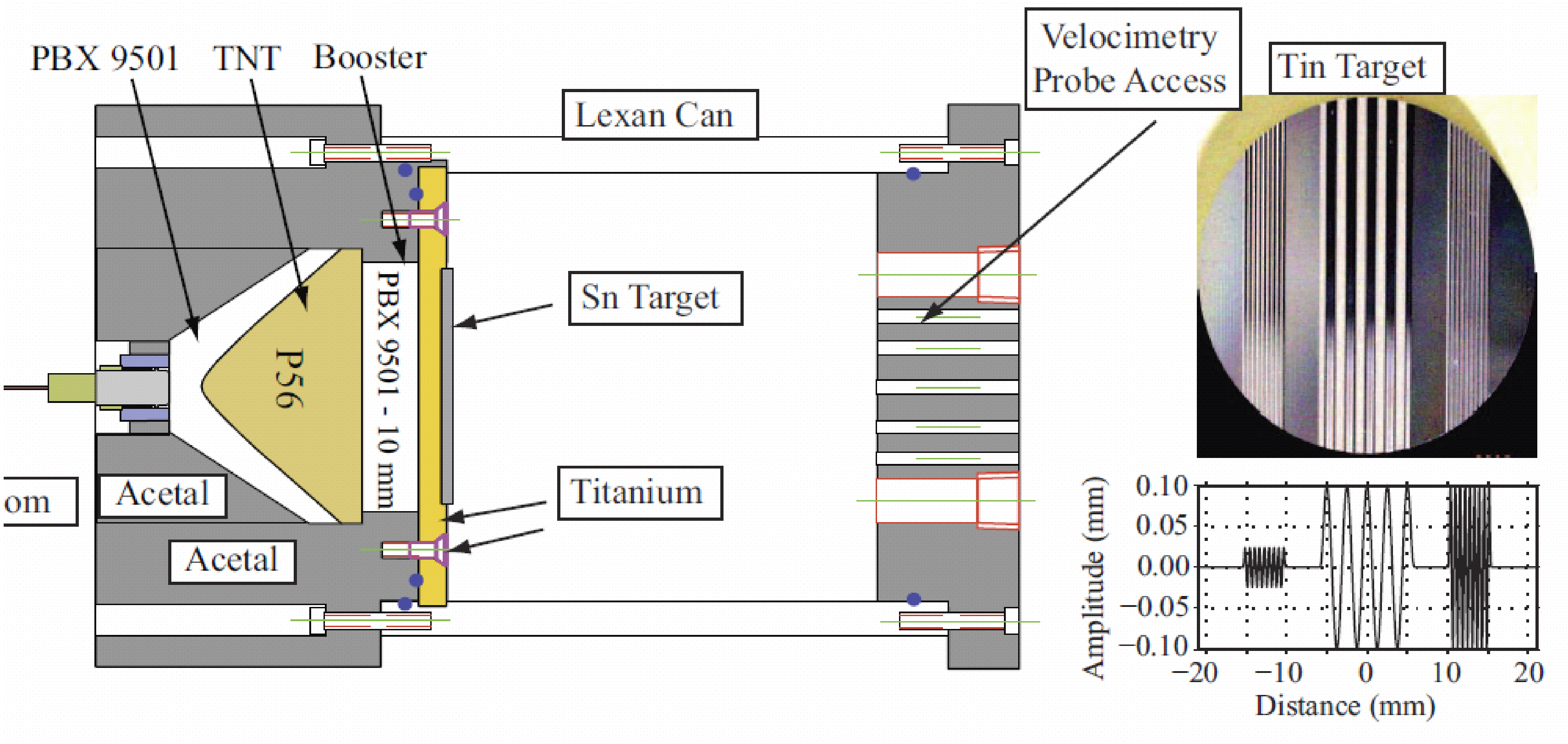

Richtmyer-Meshkov instability studies have provided critical data for the development of an ejecta model [W.T. Buttler, et. al]

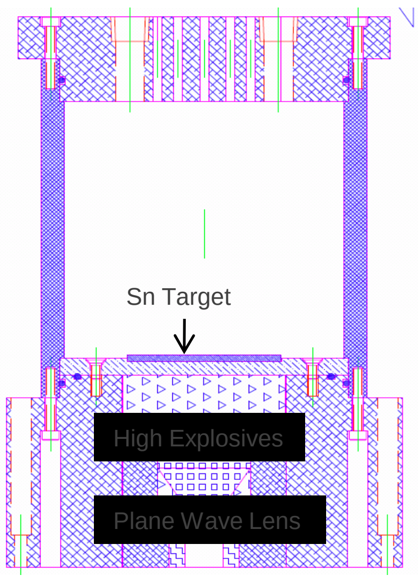

detonator

Initial Seeding Perturbation

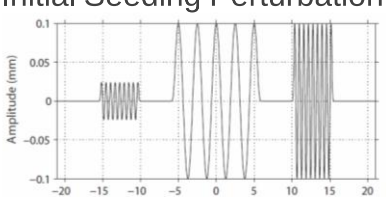

vacuum | 5 bar Xe | 5 bar He

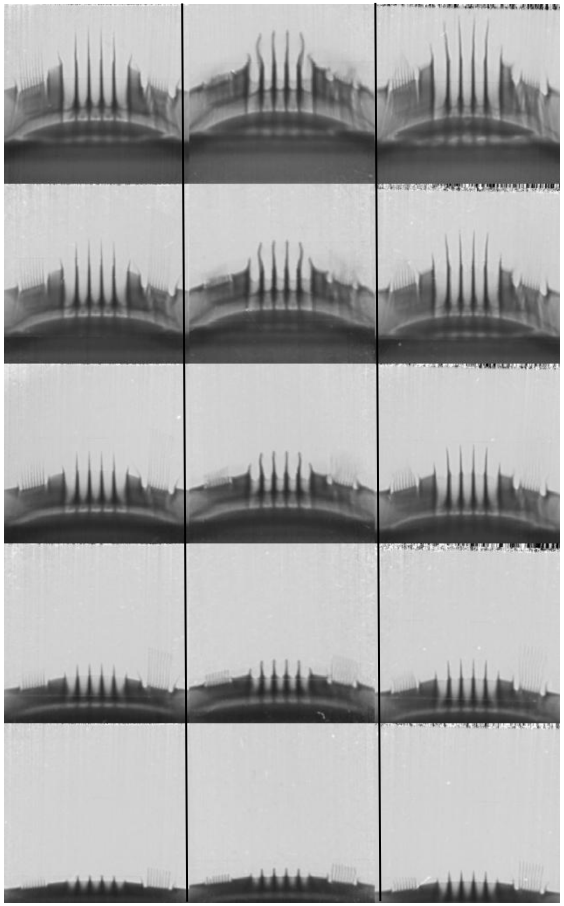

Photon Doppler Velocimetry

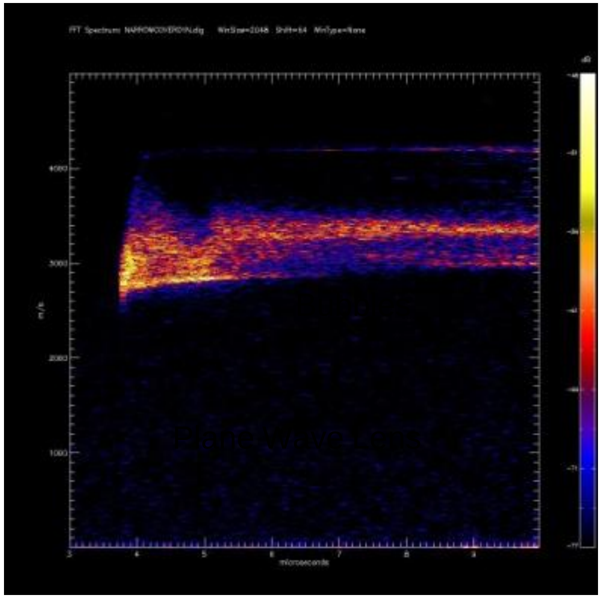

Continuous velocity record

RMI: [W.T. Buttler]

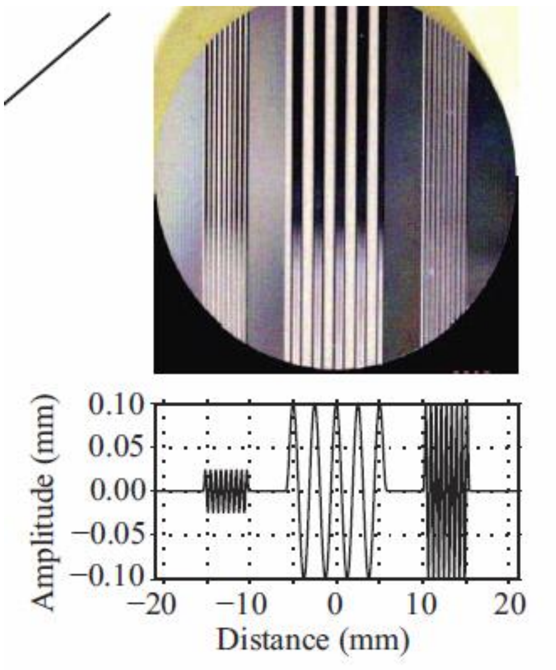

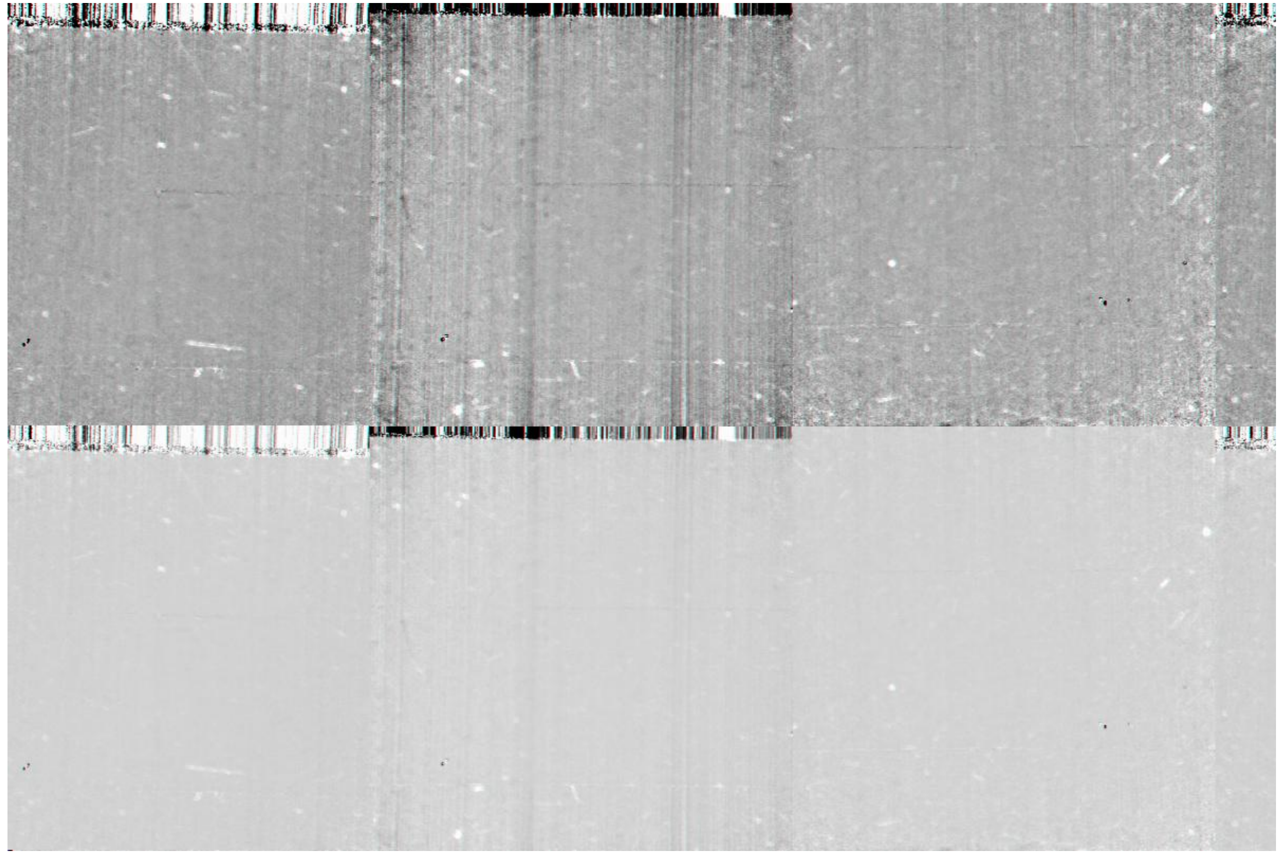

vacuum
vacuum

5 bars of Xe gas

5 bars of Ne gas

Dynamic metal-on-metal interface: Shock in HE Driver [Cline and Foley]

Frames separated by 0.8μs

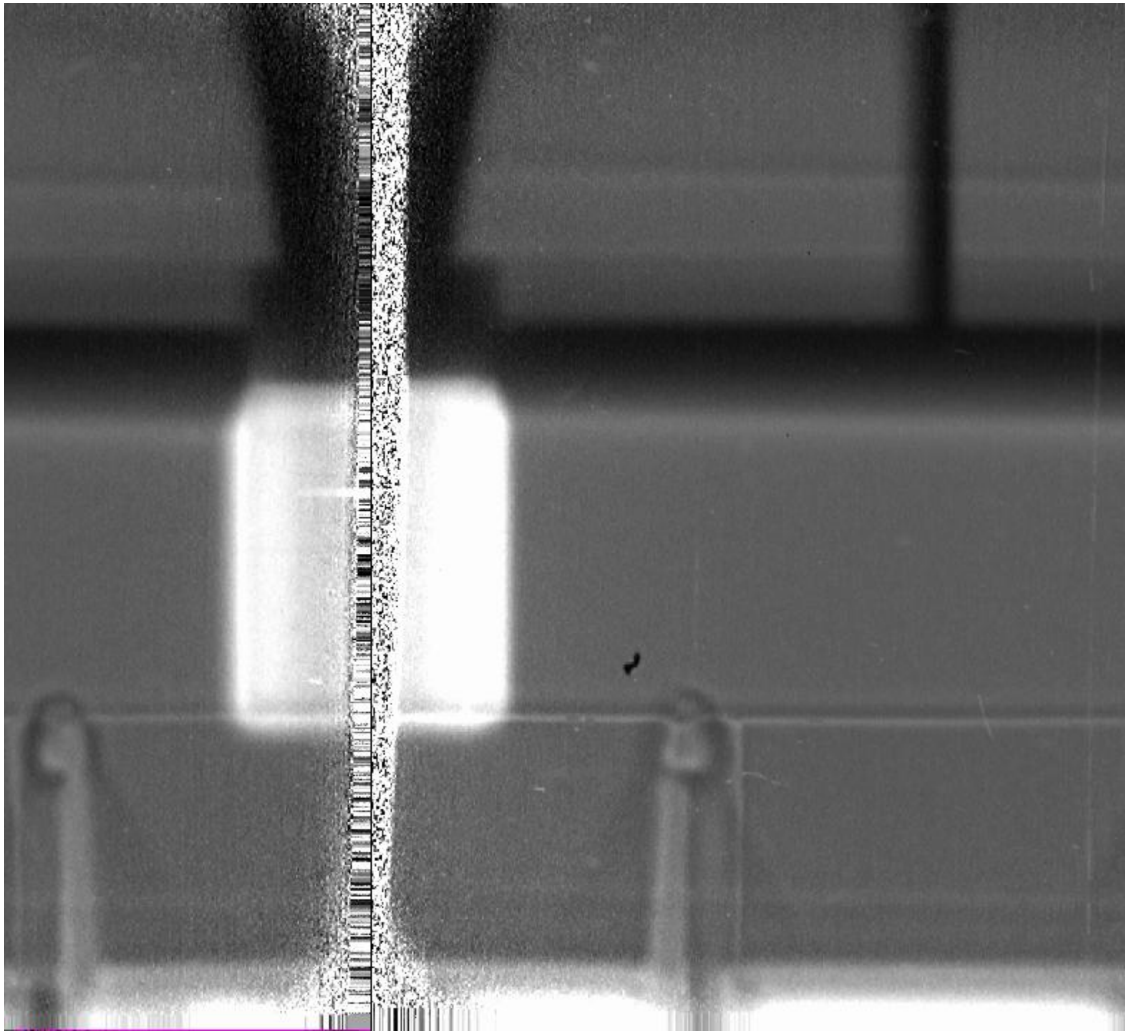

Hydrodynamic model validation of HE-driven metal plates flowing around a steel "T".

PBX9501 charge is used to drive a flyer a tantalum or tungsten flyer onto steel. The observed behavior of the metal ejecta flow is compared to hydrodynamic codes.

Cline Series: Hydrodynamic flow of Tungsten on Steel

[Cline and Foley]

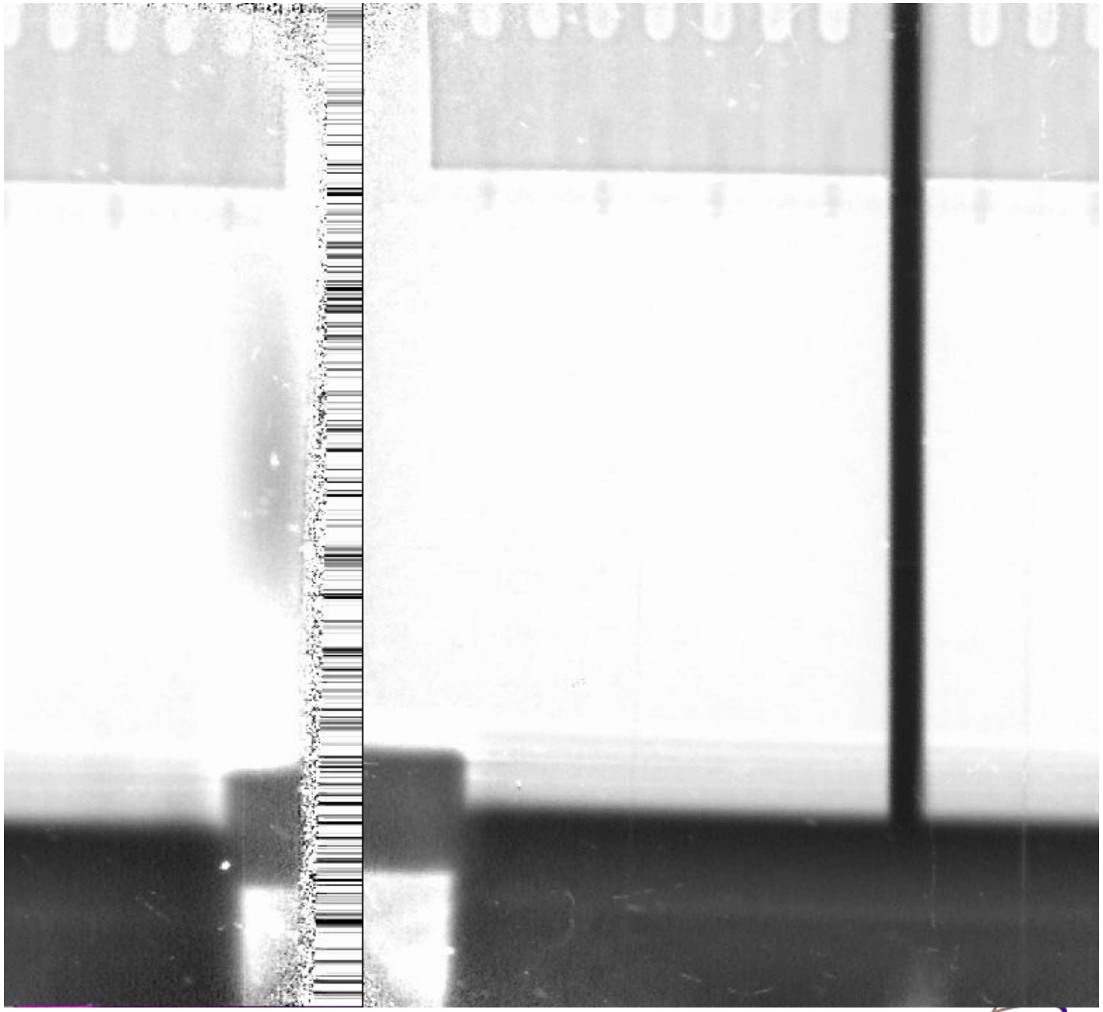

Cline Series: Metal Interface Interactions [Cline and Foley]

Energy degrader used to get simultaneous focus thru HE and thru vacuum

Prad0468

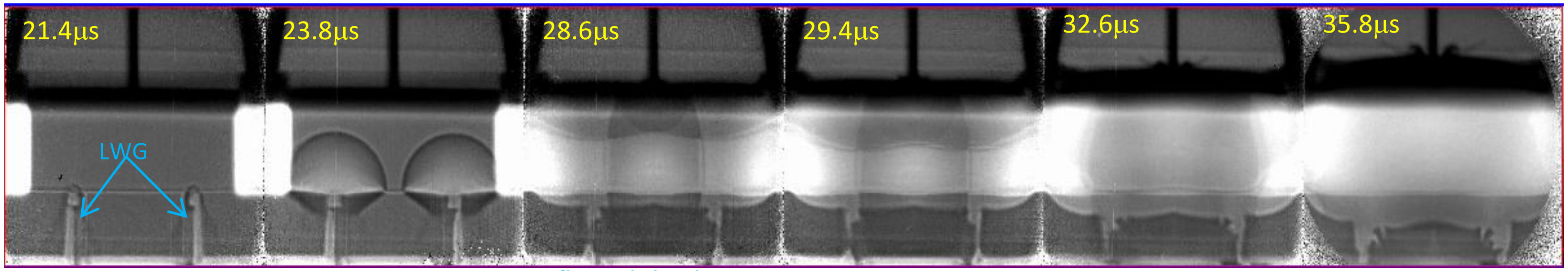

HE initiation | HE Det. Front | Reflected shock in HE byproducts and | Metal flow initiation | Fully formed Metal flow

Early Time images: HE (driver) detonation and shock waves

Prad0464

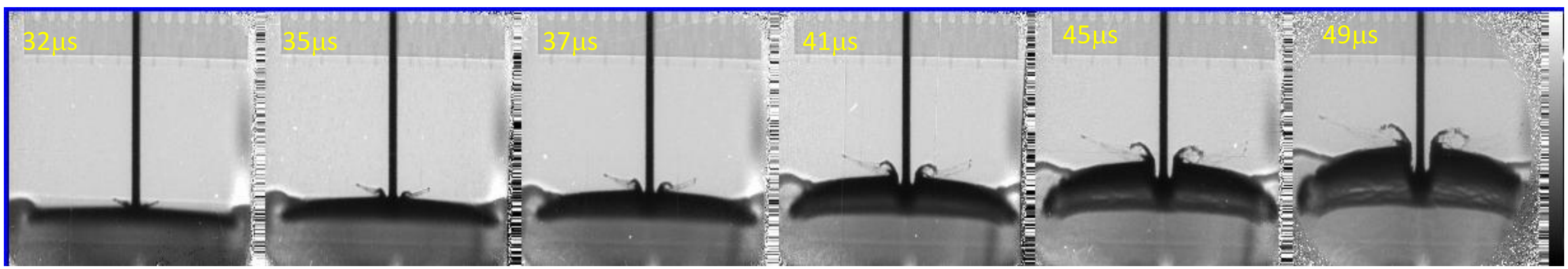

Tungsten on Steel

Prad0465

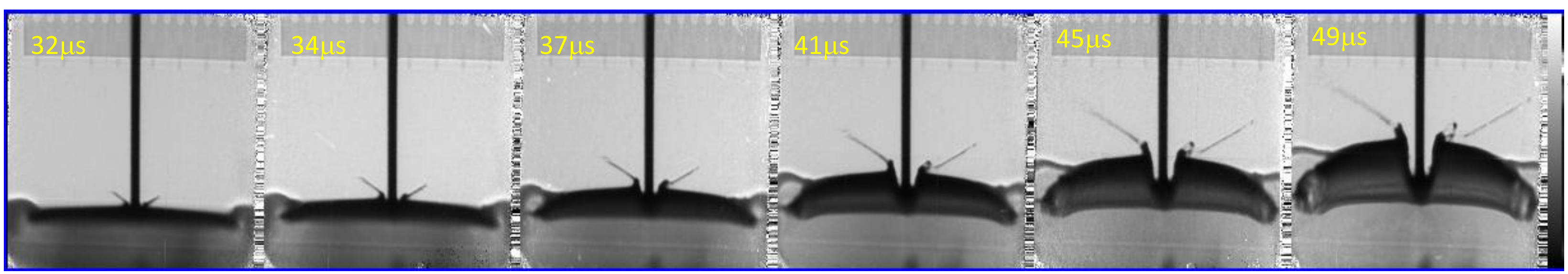

Tantalum on Steel

Demonstration of new EOS measurement capability with pRad

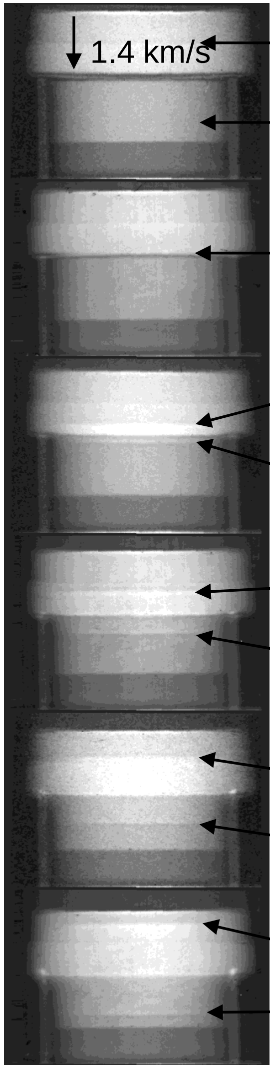

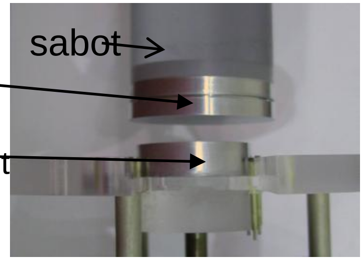

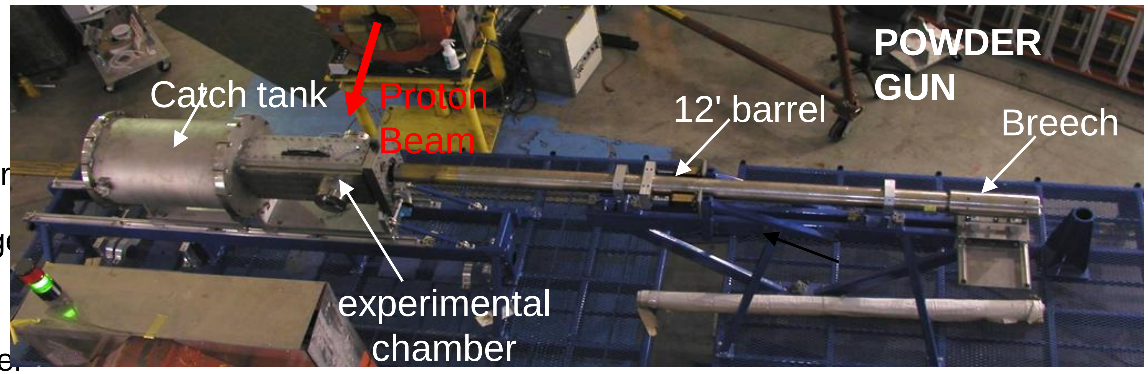

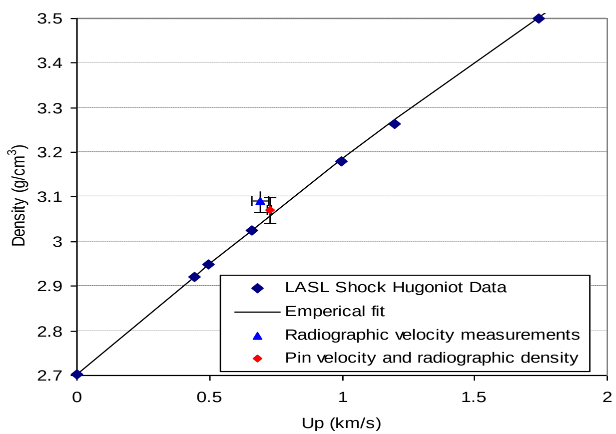

Two methods of measuring a point on shock Hugoniot per dynamic event:

- Radiographic measurement of density behind shock front.
- Simultaineous measurement of particle and shock velocity

Material Strength Experiments [R. Olson]

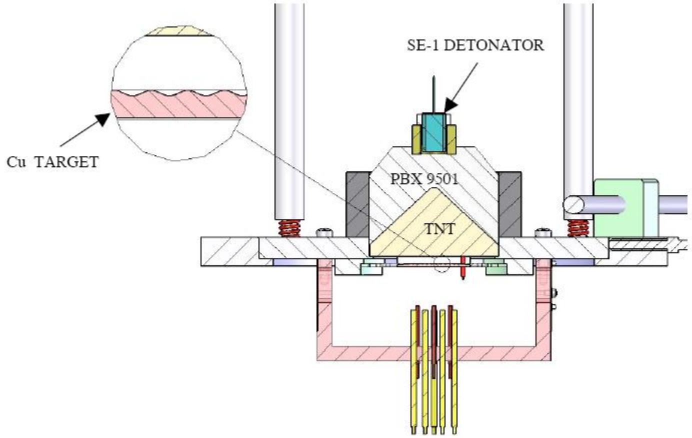

The technique utilizes a flat metal plate with perturbations of known wavelength and amplitude machined into one side of the plate. High explosive is used to generate shock-free, planar loading on the perturbed side of the plate and the amplitude of the Rayleigh-Taylor (R-T) unstable perturbations are measured from radiographs acquired as a function of time (see Fig. 1). The perturbation growth rate is directly related to the dynamic shear strength of the metal and thus can be compared directly to that predicted by various strength models via hydrodynamic calculations.

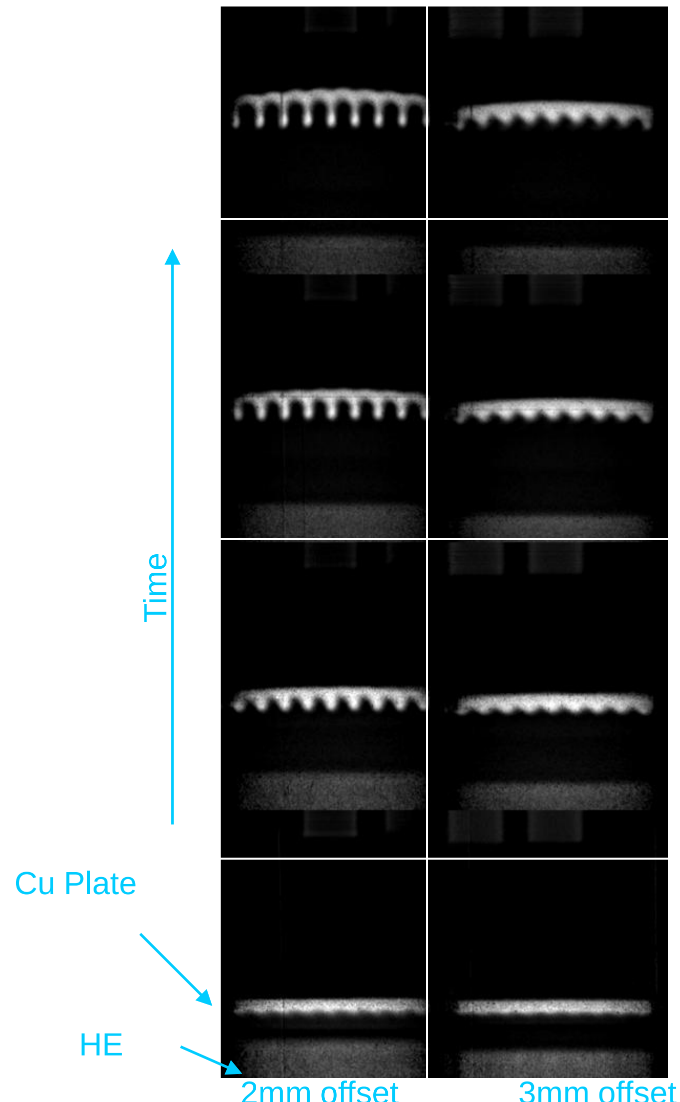

- Utilized improved resolution capability of new magnifier system.
- Six dynamic experiments performed to study instability growth versus drive pressure by varying HE standoff.
- Demonstrated shockless acceleration and reproducibility.

Set up: Tomography Surrogate Fuel Rods
(HfO_2 Pellets)

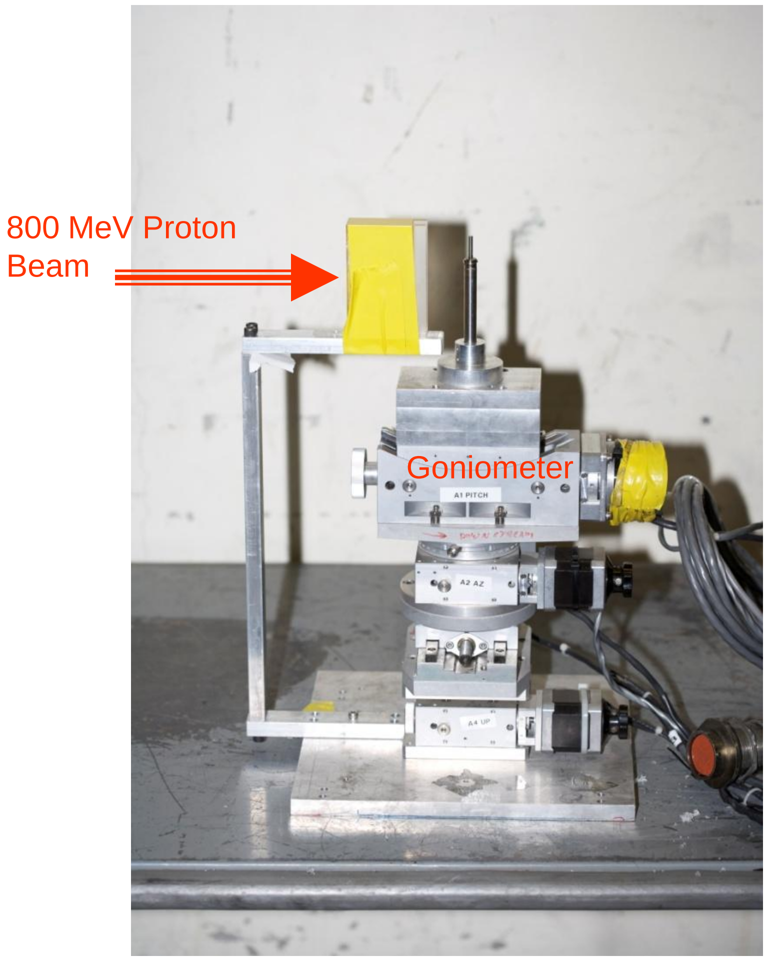

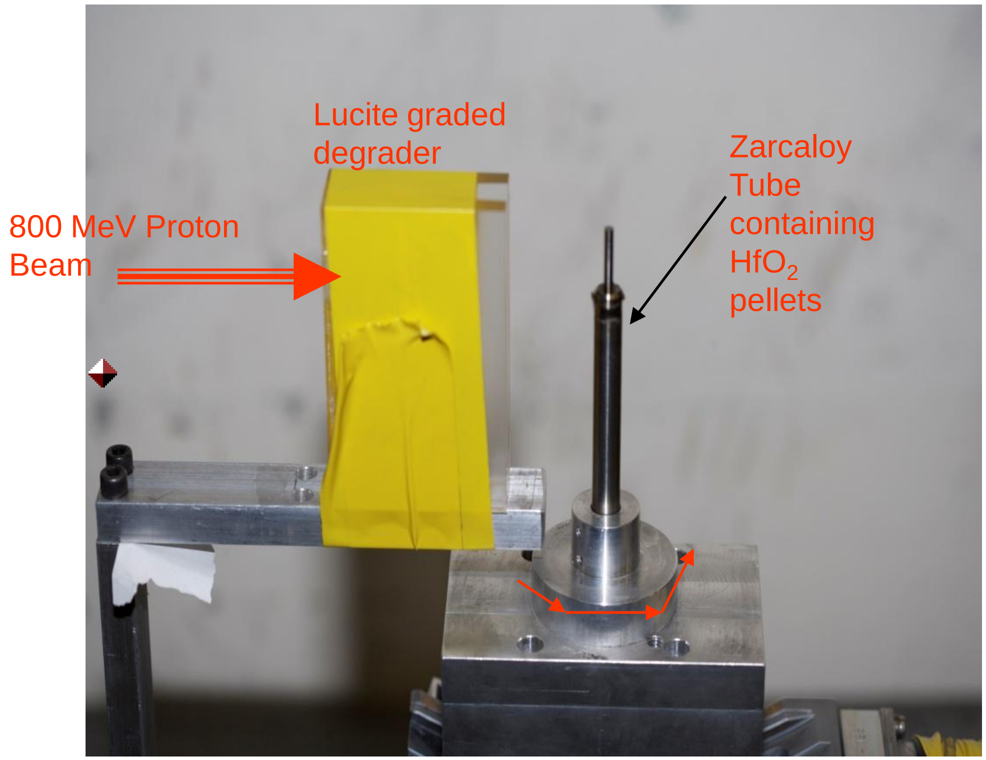

Zarcaloy tube was aligned on the graded degrader.
Radiograph pictures were taken at 181 rotational positions

CT Reconstructed Slices show Processing Defects in a pellet of HfO_2:

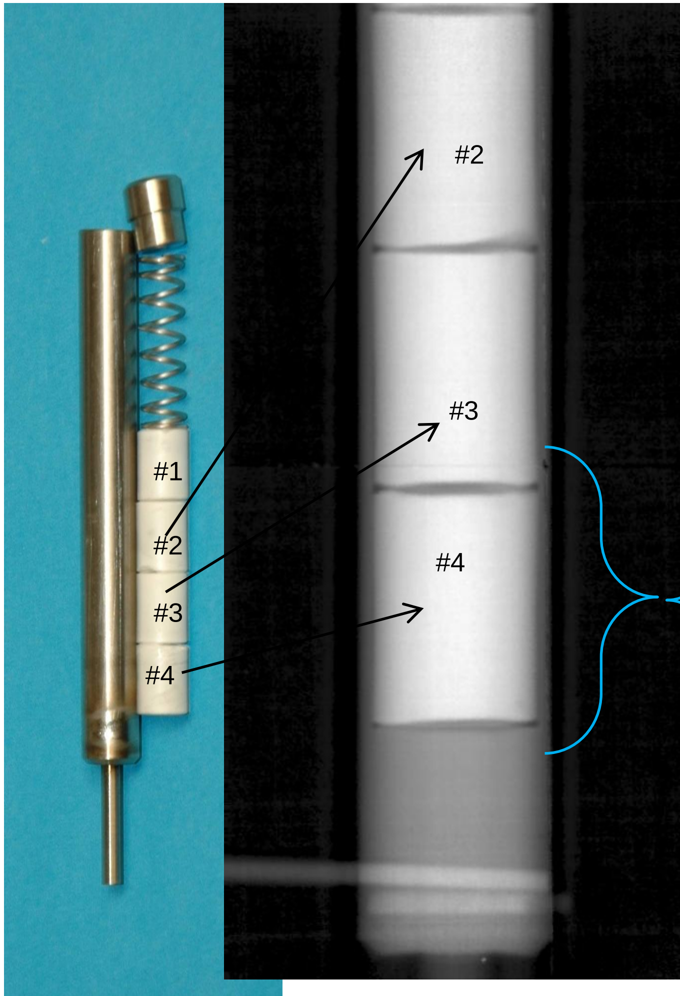

Reconstructed Areal Density of HfO_2 Pellets

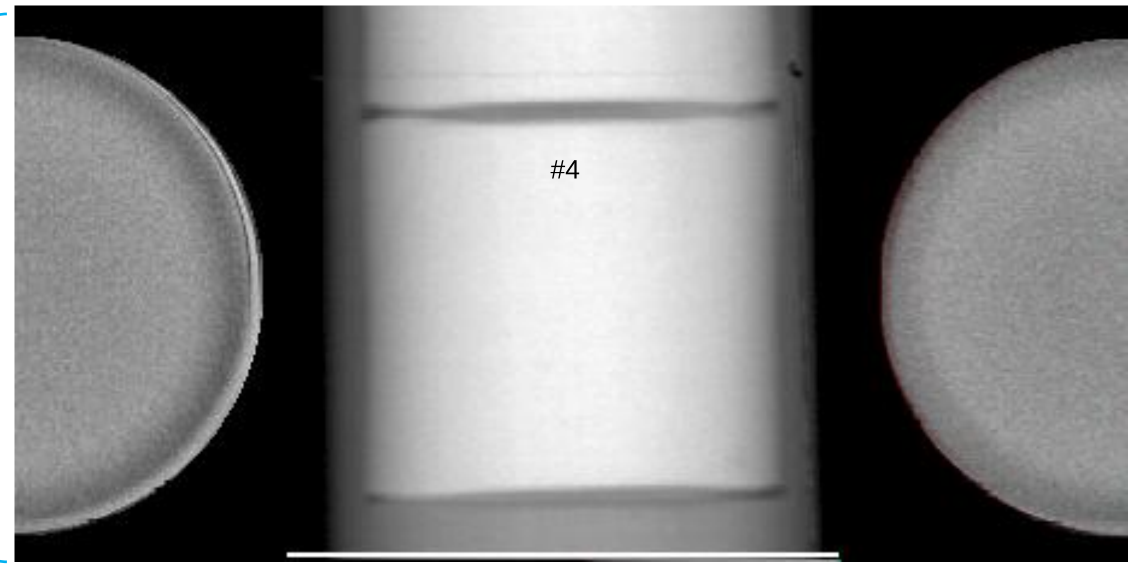

Metrology of a Defect in surrogate Fuel Pellet using CT slices

(Pellet #4, Slices 78 to 93, each 50 μm thick)

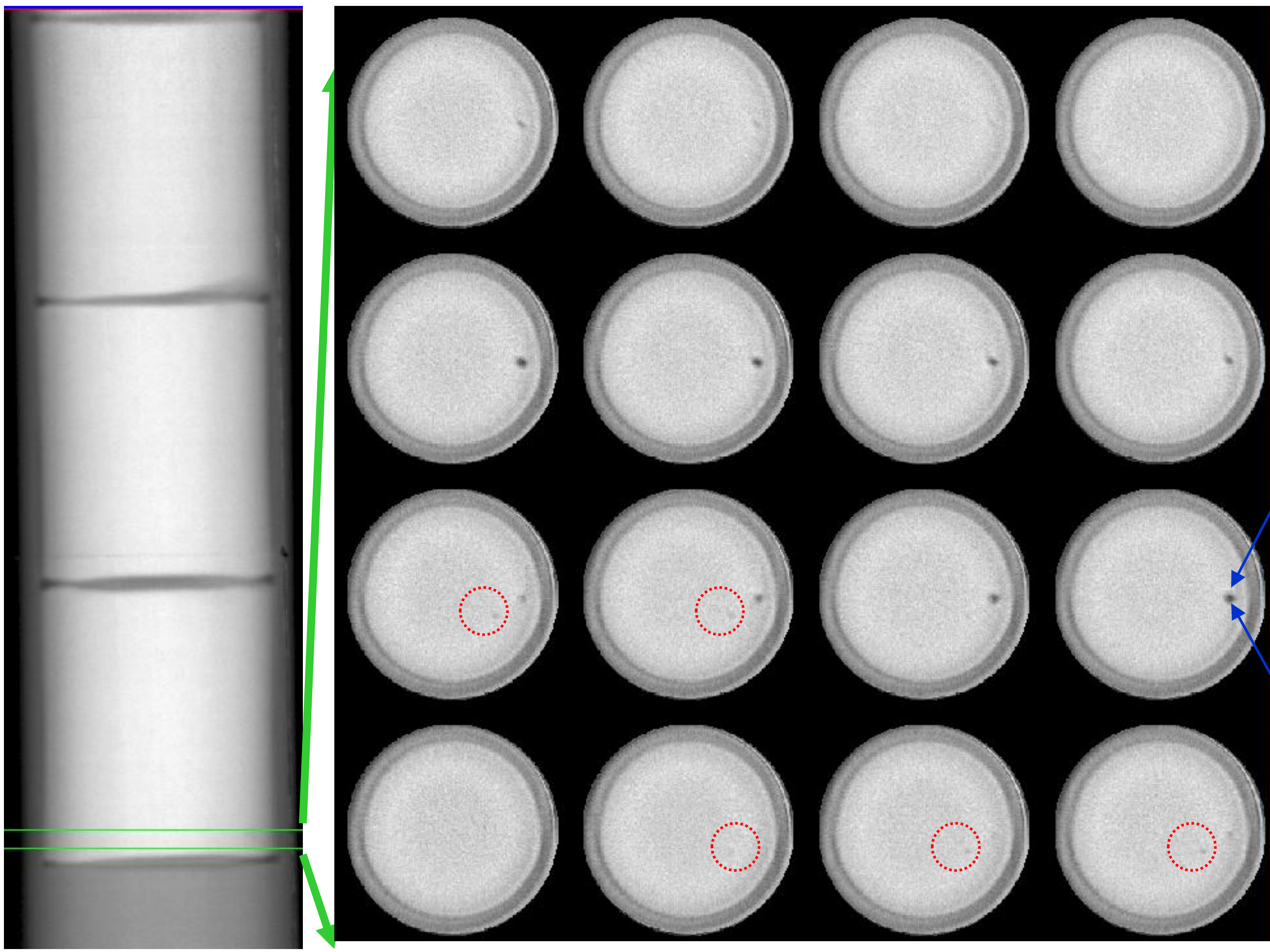

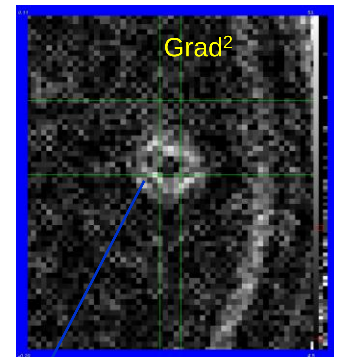

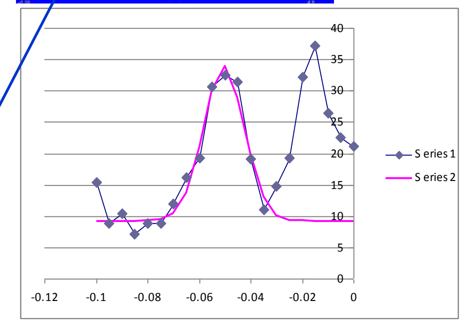

Resolution ~ 80 μm

Diameter$_{Inclusion}$ ~ 350 μm

Length$_{Inclusion}$ ~ 550 μm

Fainter 250 μm long by ~150 to 200 μm diameter inclusions are shown in the circles

Solid Flame Experiment at pRadSolid Flame @10 Hz

[Winkler, et al](movie005)

- Exothermic reaction of formation of refractory materials such as Ta_5Si_3, TiB_2, Ti_5Si_3, was initiated by using a heating filament on pressed samples of Ta and Si powder.
- The reaction front travels from the point of ignition; due to small density differences between the pre-reaction and post-reaction material, the progress of burn front was observed using pRad.
- Interesting data on a Ta_5Si_3 exhibiting unsteady and steady burn is presented. Inert mixture in the sample preparation apparently gives rise to unsteady burn.

Solid Flame @10 Hz

[Winkler, et al](movie005)

Images normalized to pre-burn pictures of a ~1 cm long tantalum scilicide $\mathbf{Ta_5Si_3}$

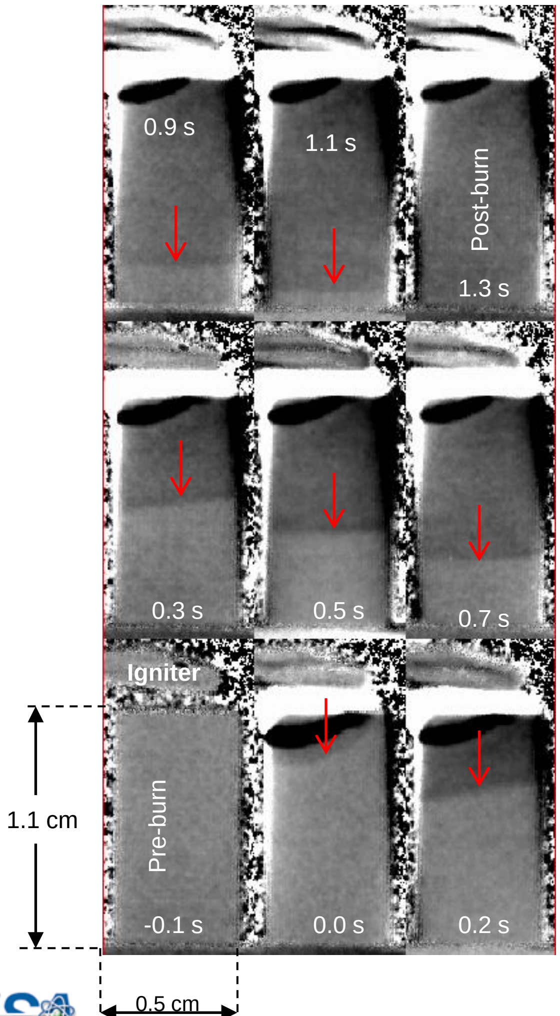

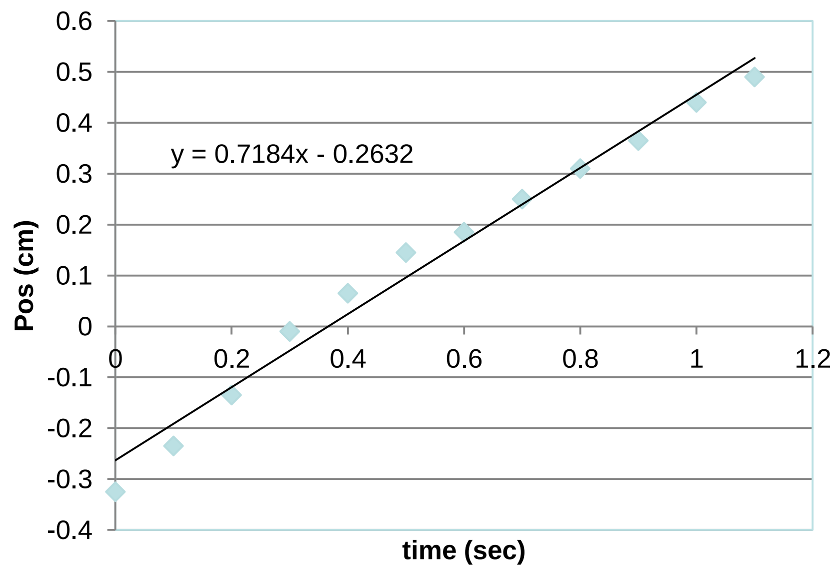

The burn progresses from top to bottom as indicated by the arrows. A fit to the approximate location of the flame front indicates that the burn proceeds at 0.7cm/sec. The density change due to the reaction is -5% to 6%

More detailed analysis is in progress

Metal Eutectics: (Clark, et. al)

Time-resolved imaging to study dynamic processes during melting and solidification of metal alloys

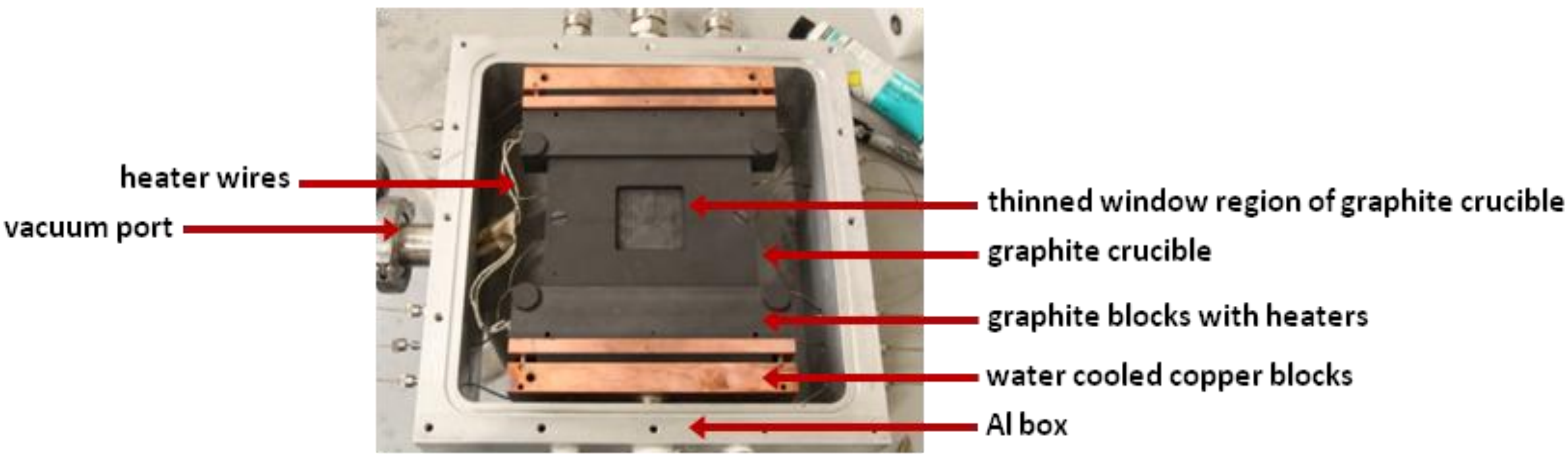

Crucible mounted in front of the x3 pRad magnifier. Various alloys were inserted iinside the graphite crucible and heated. Images were acquired during the liquifiction and solidification processes.

Mesoscale Priority Research Direction

In-situ Monitoring of Dynamic Phenomena during Phase Transformations

Proton radiography:

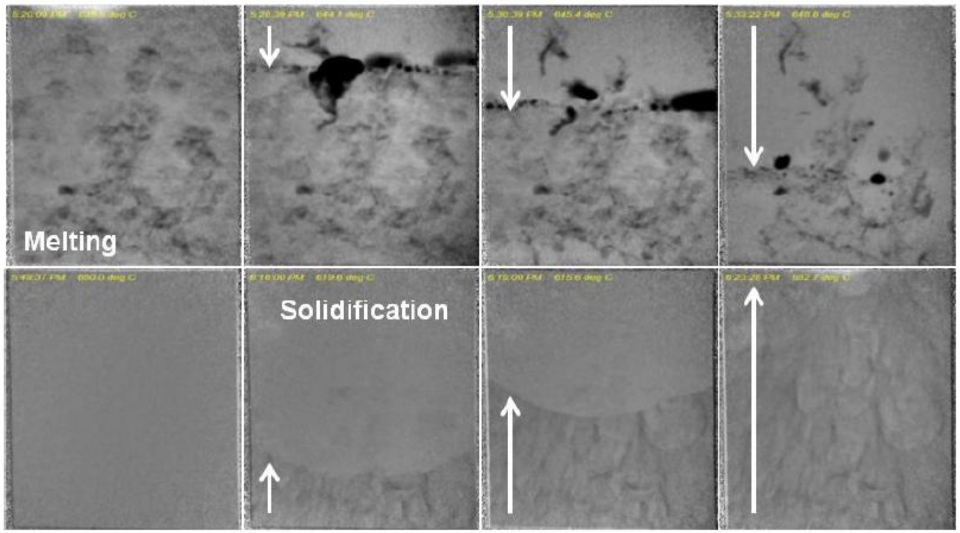

Al-In, 6 mm thick, nominally a 44 x 44 mm^2 field of view (August 2011)

Synchrotron x-ray radiography:

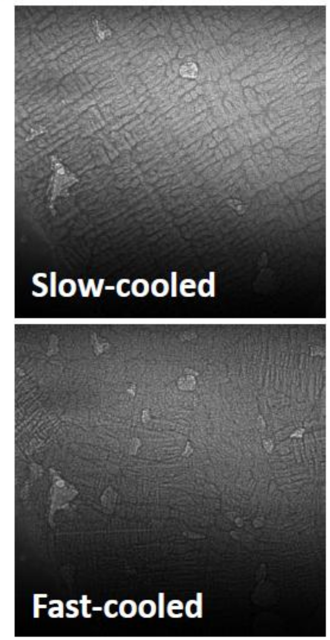

<2μm resolution

Al-Cu, 100 microns thick, nominally a 1. 4 x 1.4 mm^2 field of view (December 2011)

Microstructure relevant sampling:
Spatial and temporal resolution, field of view, sample size…

Use of the Advanced Photon Source, an Office of Science User Facility operated for the U.S. Department of Energy (DOE) Office of Science by Argonne National Laboratory, was supported by the U.S. DOE under Contract No. DE-AC02-06CH11357.

Contact: Amy Clarke (aclarke@lanl.gov) and Jason Cooley (cooley@lanl.gov); LANL

Resolution of Proton Radiography

1. **Object scattering** - introduced as the protons are scattered while traversing the object.
2. **Chromatic aberrations**- introduced as the protons pass through the magnetic lens imaging system.
3. **Detector blur**- introduced as the proton interacts with the proton-to-light converter and as the light is gated and collected with a camera system.

Assume detector development can keep up

Object Scattering

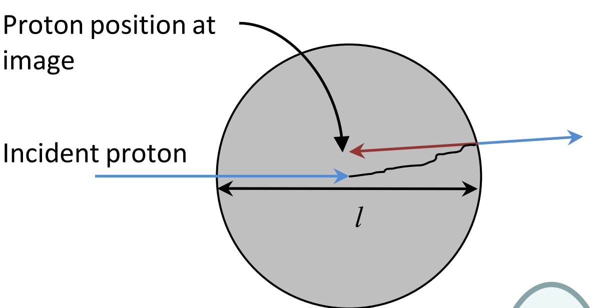

$$\sigma_o = \frac{1}{\sqrt{3}}\theta\frac{l}{2} = \frac{14.1}{\sqrt{6}}\frac{1}{P\beta}\sqrt{\frac{l^3}{x_o}} \propto \frac{l^{\frac{3}{2}}}{P}$$

Chromatic Aberrations

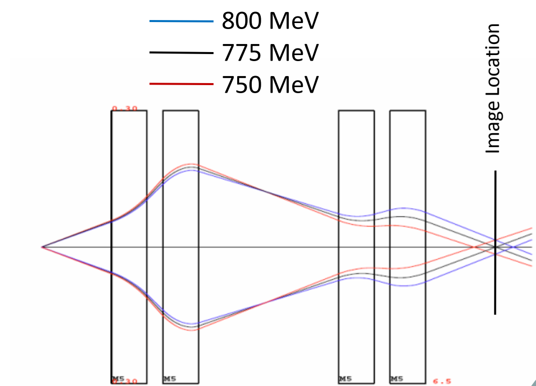

$$\sigma_c = l_c\theta\frac{\delta P}{P} = c\sqrt{P}\frac{\delta P}{P^2}\frac{14.1}{\beta}\sqrt{\frac{l}{x_o}} \propto \sqrt{\frac{l}{P^3}}$$

Detector Blur

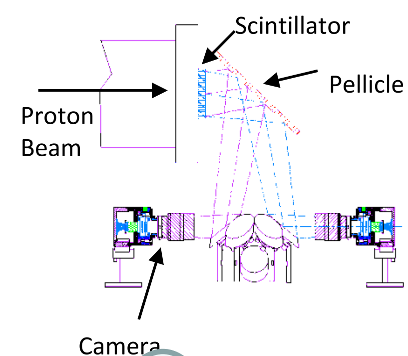

Scintillator

$$\sigma_s = \theta l_s \propto \frac{l_s\sqrt{l}}{P}$$

Camera

Resolution is independent of proton energy

Results of Scaling 800 MeV Resolution

Resolution: RMS of a Gaussian distribution (typically)

No Detector Blur

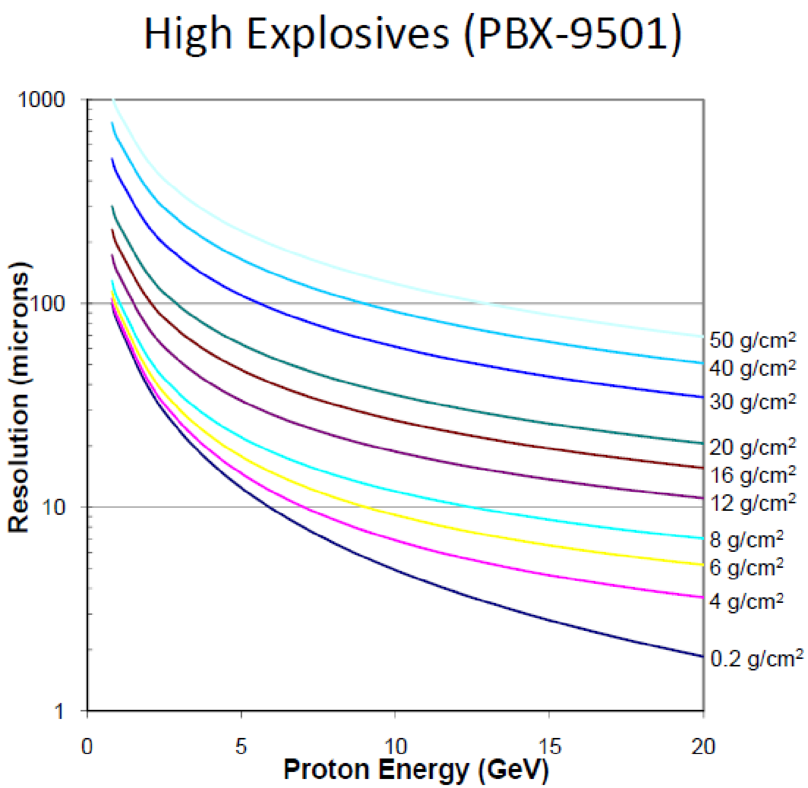

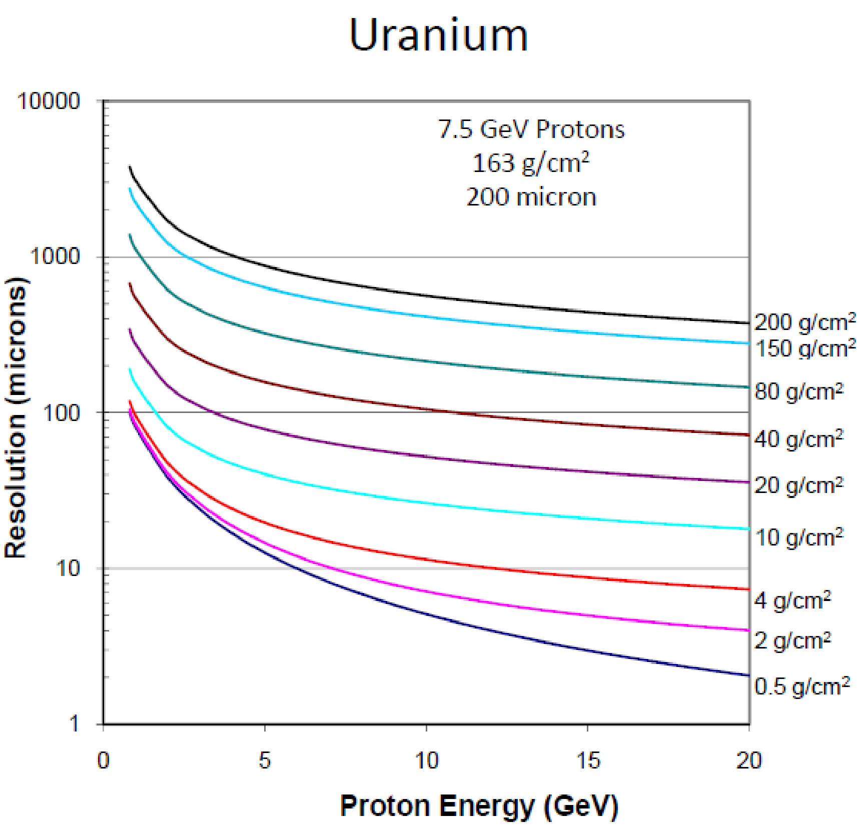

4 GeV Protons

25 - 350 μm resolution in HE
25 - 1000 μm resolution in Uranium

20 GeV Protons

2 - 100 μm resolution in HE
2 – 350 μm resolution in Uranium

Comparison of Scaling to a Measurement

Scaling is a factor of 2-3 conservative for this comparison

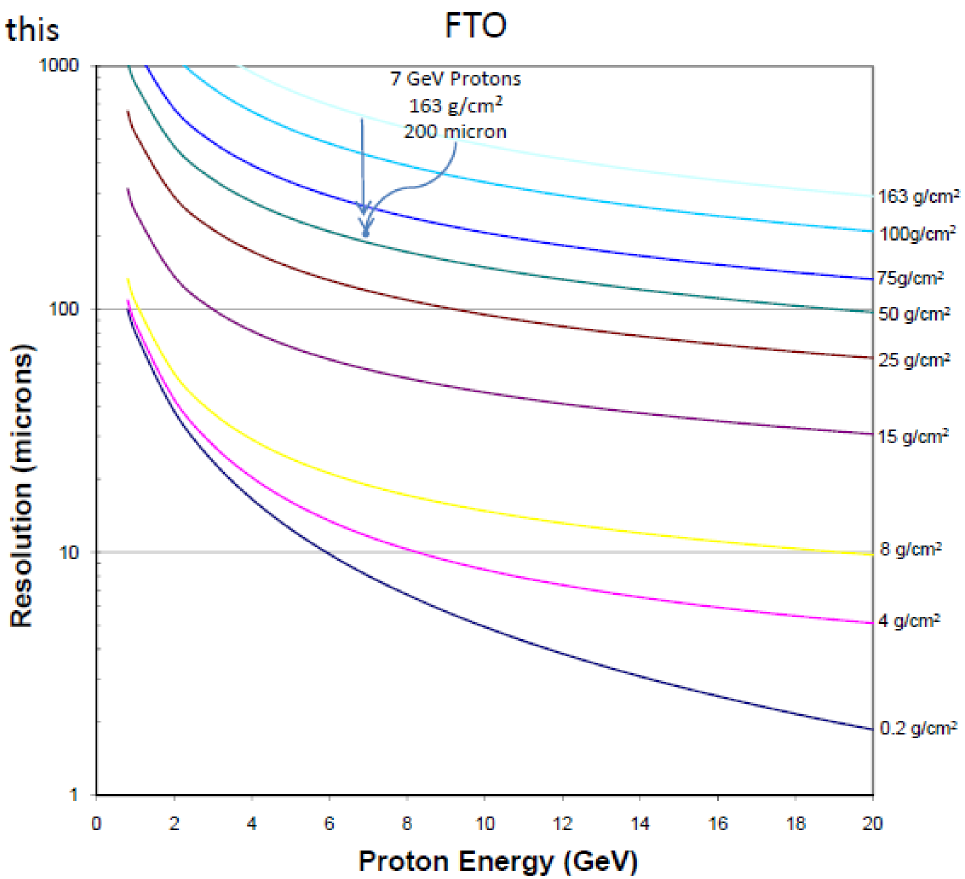

High Energy Magnifier

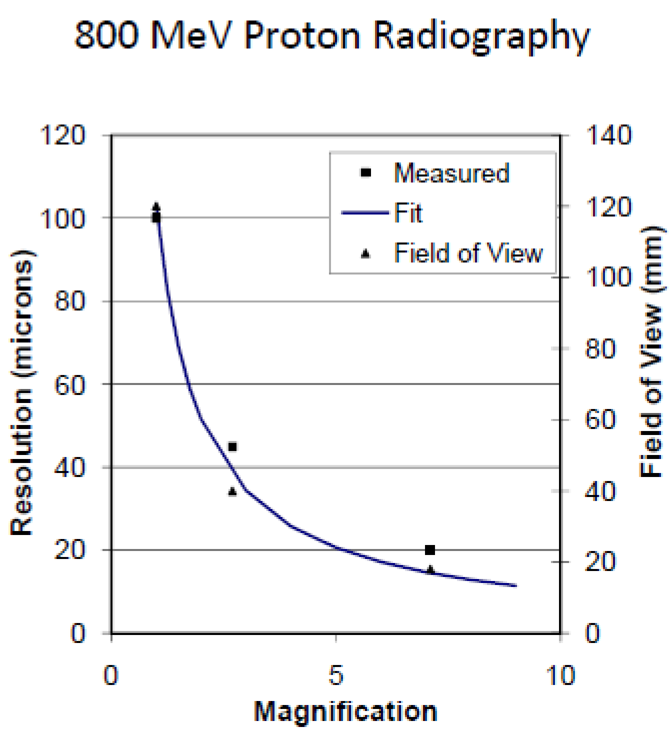

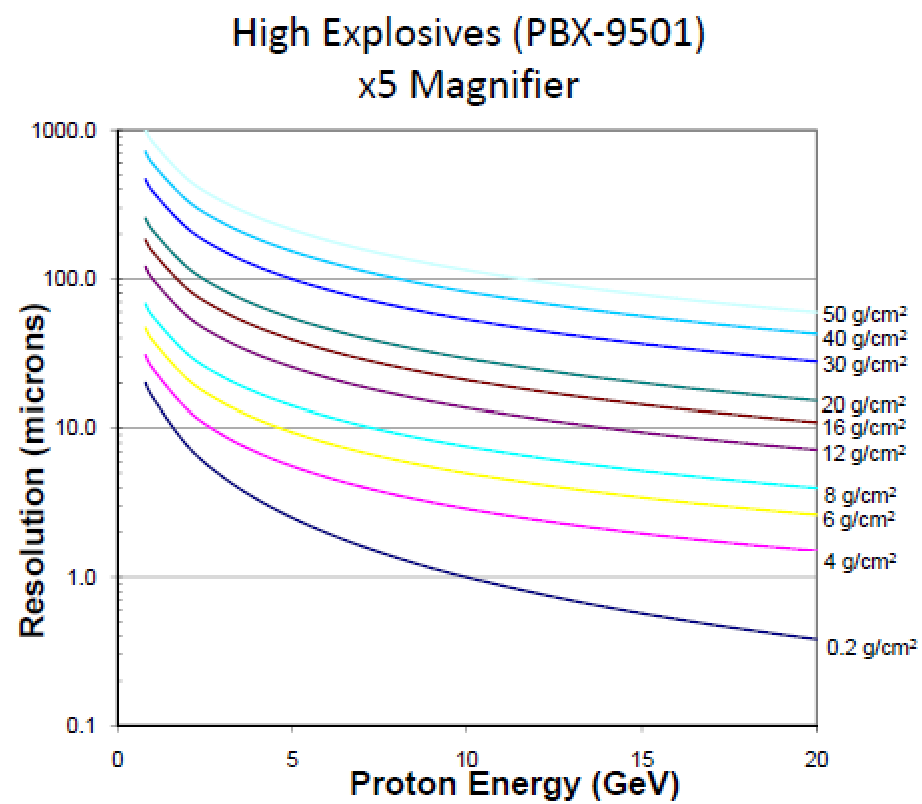

Magnification at high energy can result in high resolution (<1 μm) but small field of view (20 mm)

Conclusion

- 800 MeV proton radiography provides high quality dynamic in materials studies.
- Over 500 dynamic experiments have so far been carried out at the LANL pRad facility
- Use of pRad tomography for the study of nuclear fuel rods demonstrated.
- Gains in resolution realized through the development of magnifying lens systems.
- Groundwork for studies of high resolution prad started.
- Interest at Los Alamos to build a user community for access to 800 MeV proton radiography.

Supporting Slides

Full LANSCE System

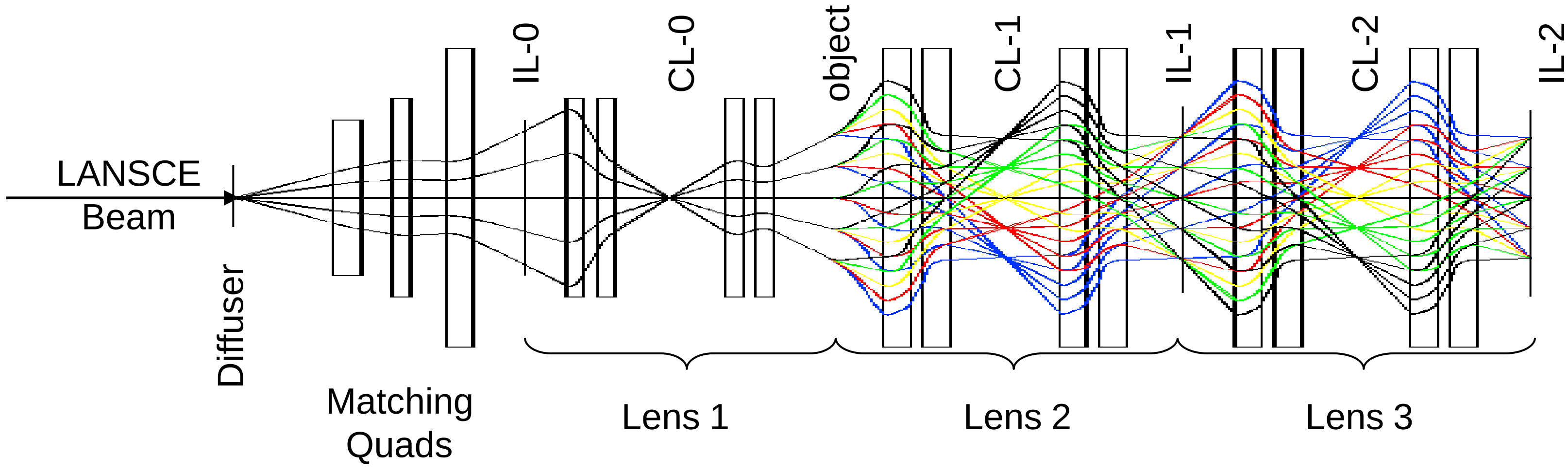

- Diffuser sets illumination pattern at object.
- Matching quads establish position-angle correlation
- CL-0 has a 9.0 mRad collimator
- CL-1 and CL-2 can independently have 5-20 mrad collimators
- Lens 0 used for beam monitoring
- IL-1 has seven single-shot camera systems
- IL-2 has five single-shot camera systems and a 9-frame framing camera
- 21 images per dynamic event at up to 21 different times.

x7 Magnifier

Made up of four 1” bore permanent magnet quads; Yet to be commissioned properly

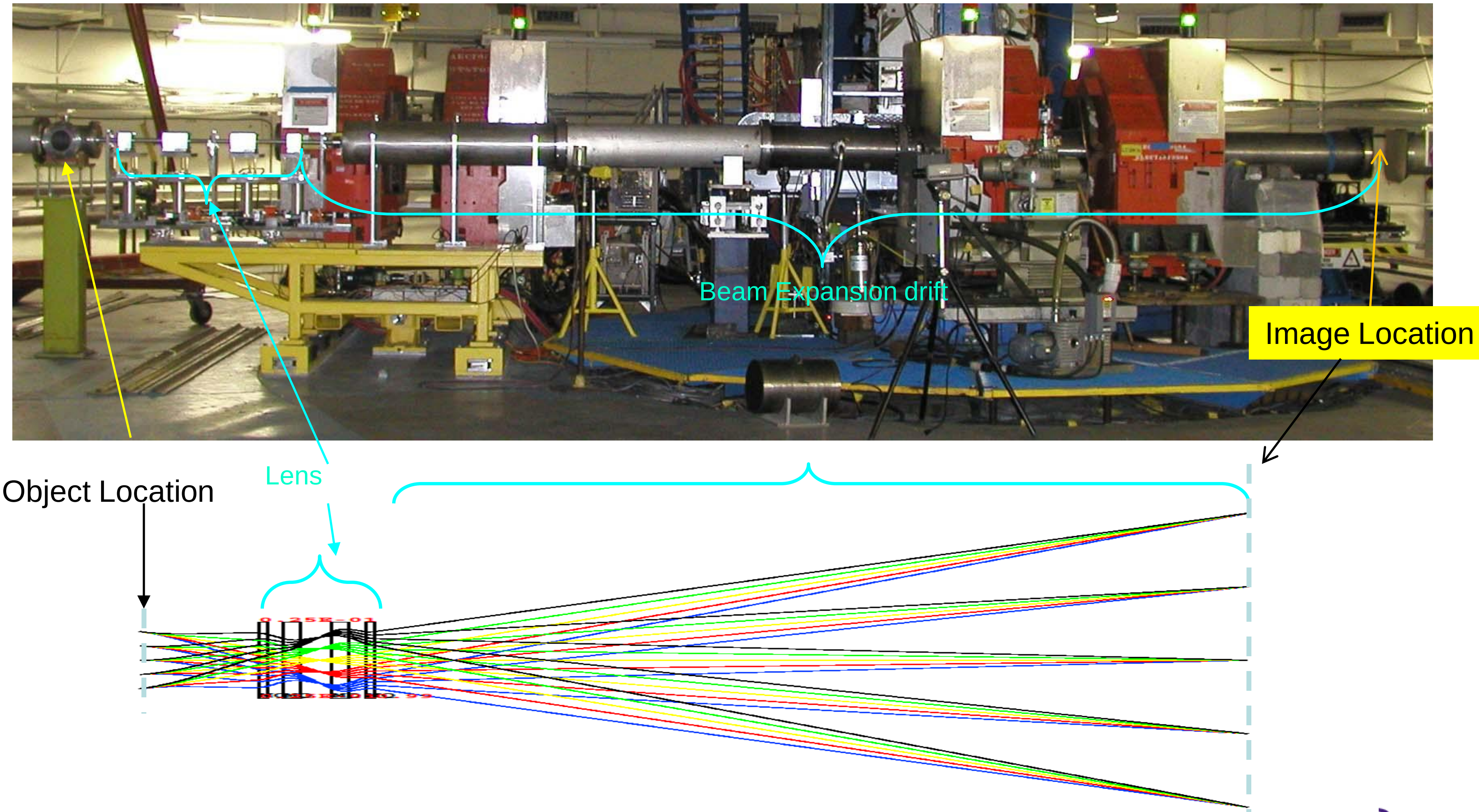

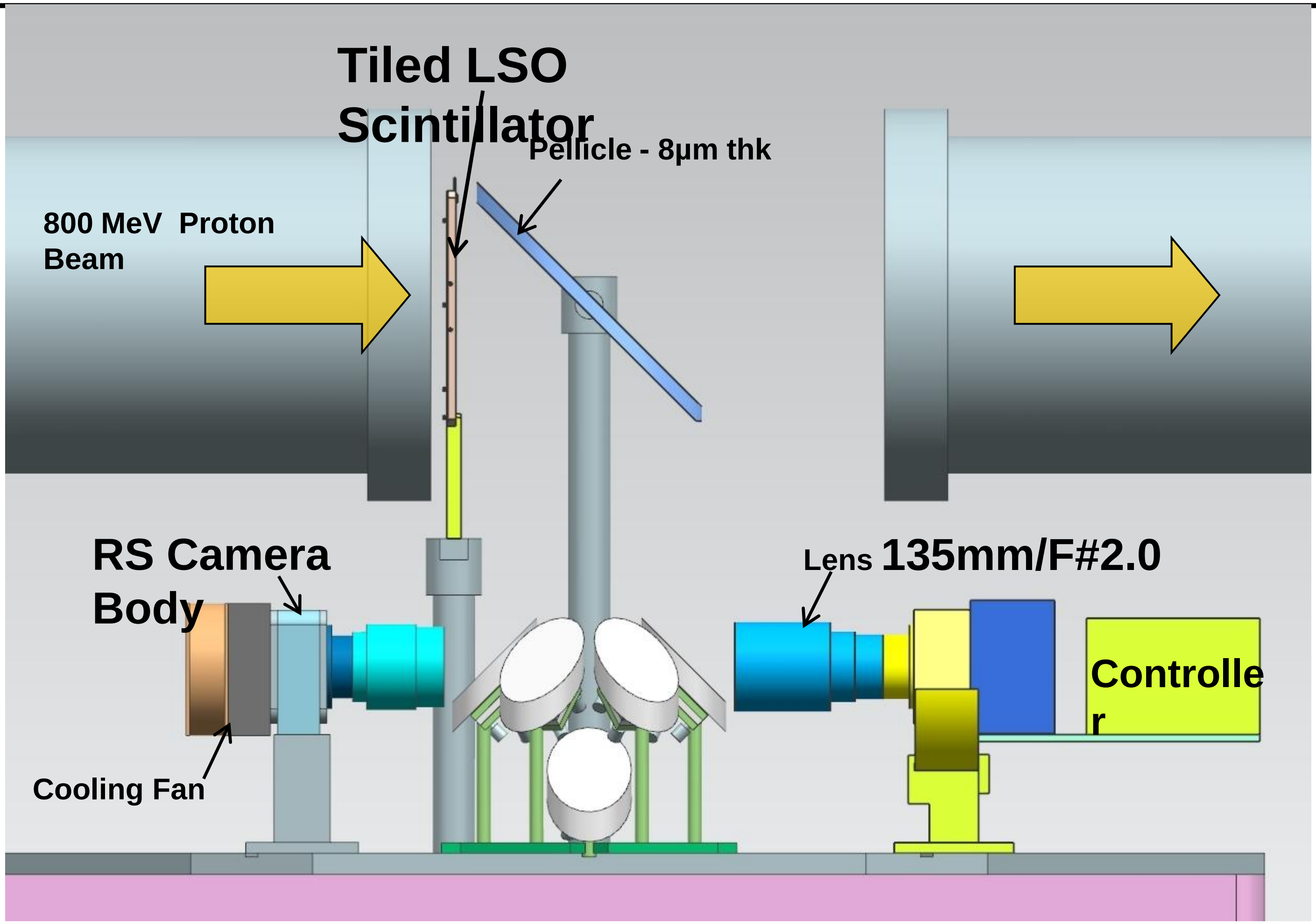

Tiled LSO Scintillator
Pellicle - 8µm thk
800 MeV Proton Beam
RS Camera Body
Lens 135mm/F#2.0
Controlle r
Cooling Fan

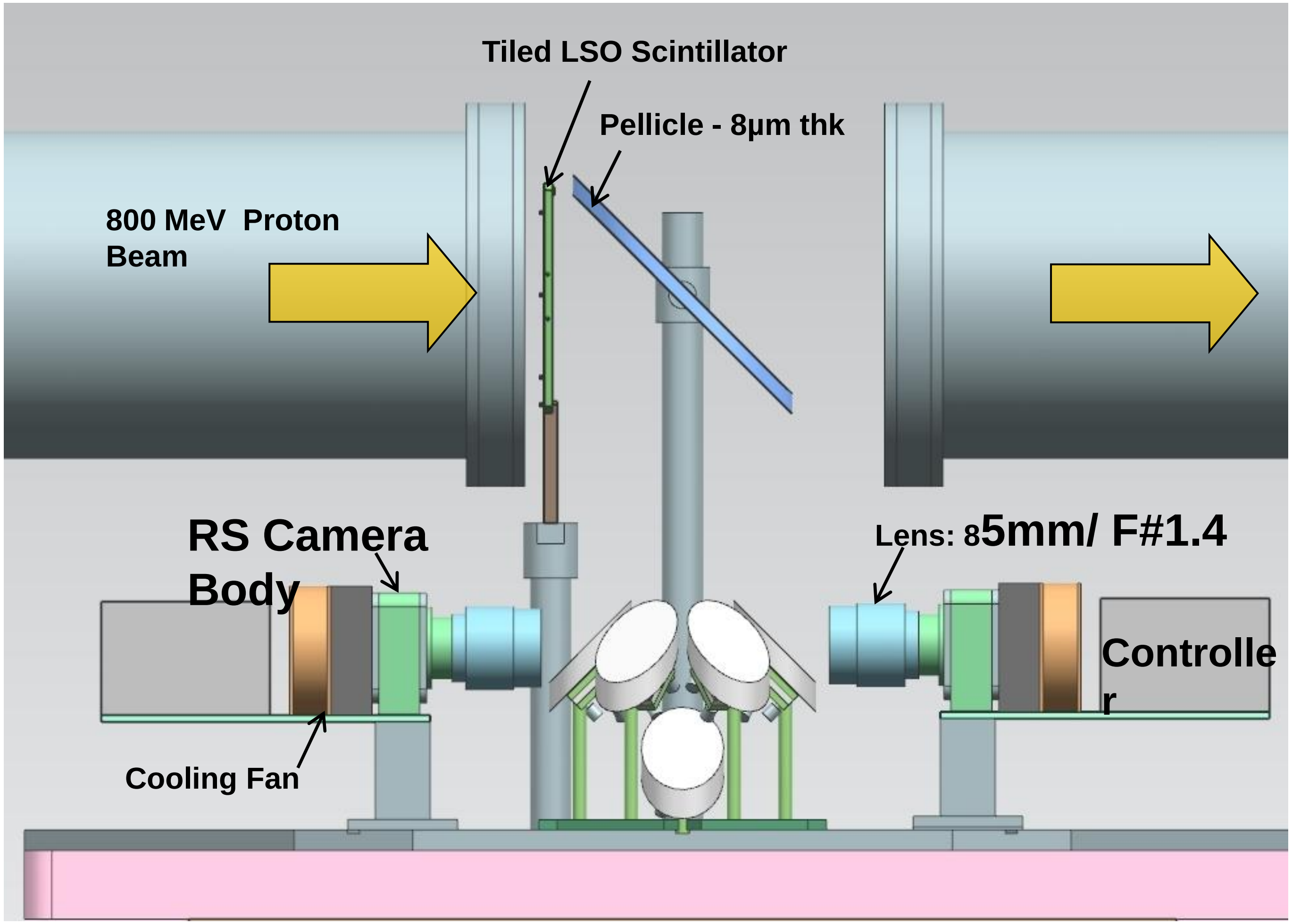
Tiled LSO Scintillator
Pellicle - 8μm thk
800 MeV Proton
Beam
RS Camera
Body
Lens: 85mm/ F#1.4
Controlle
r
Cooling Fan

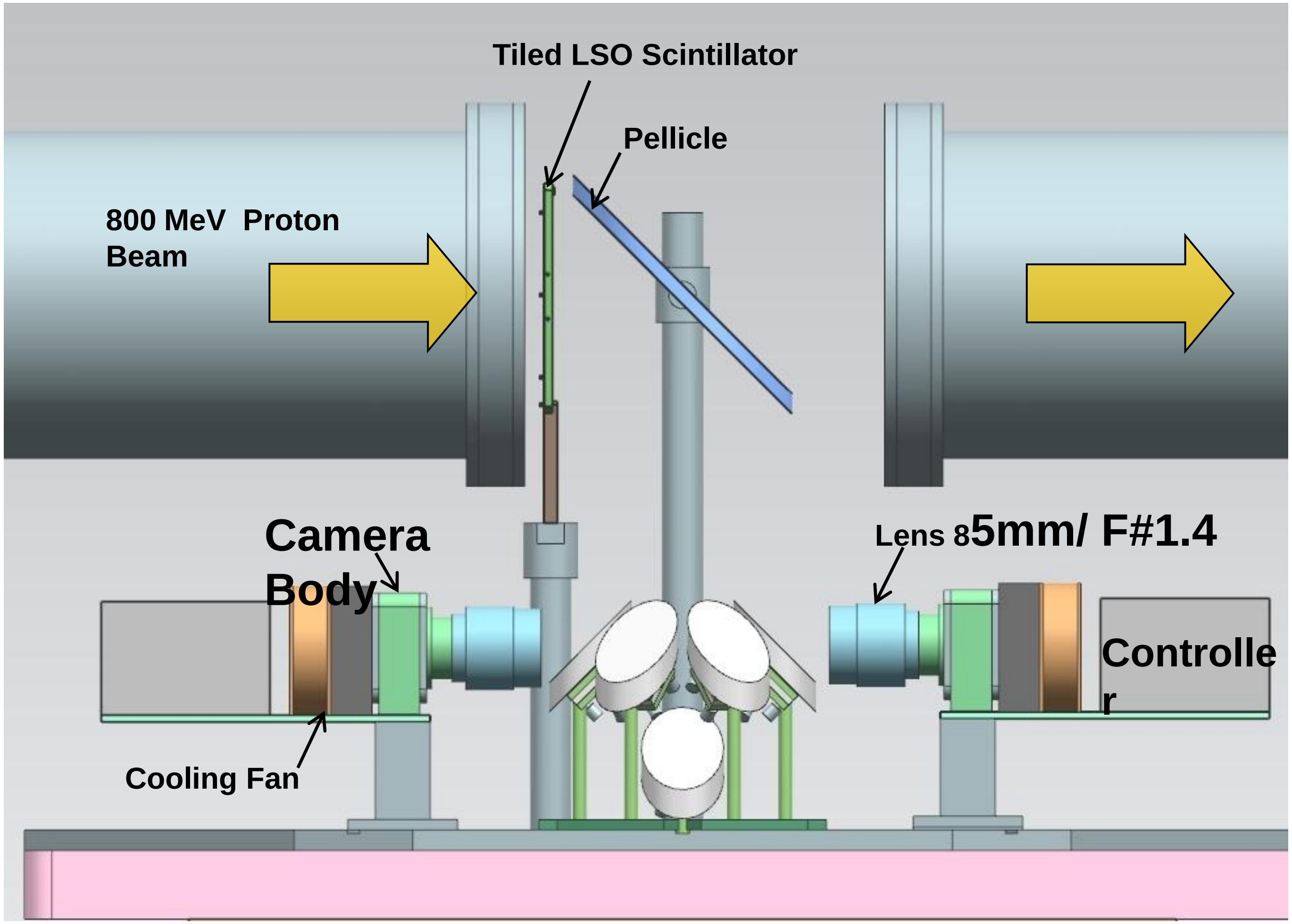
Tiled LSO Scintillator
Pellicle
800 MeV Proton Beam
Camera Body
Lens 85mm/ F#1.4
Controller
Cooling Fan

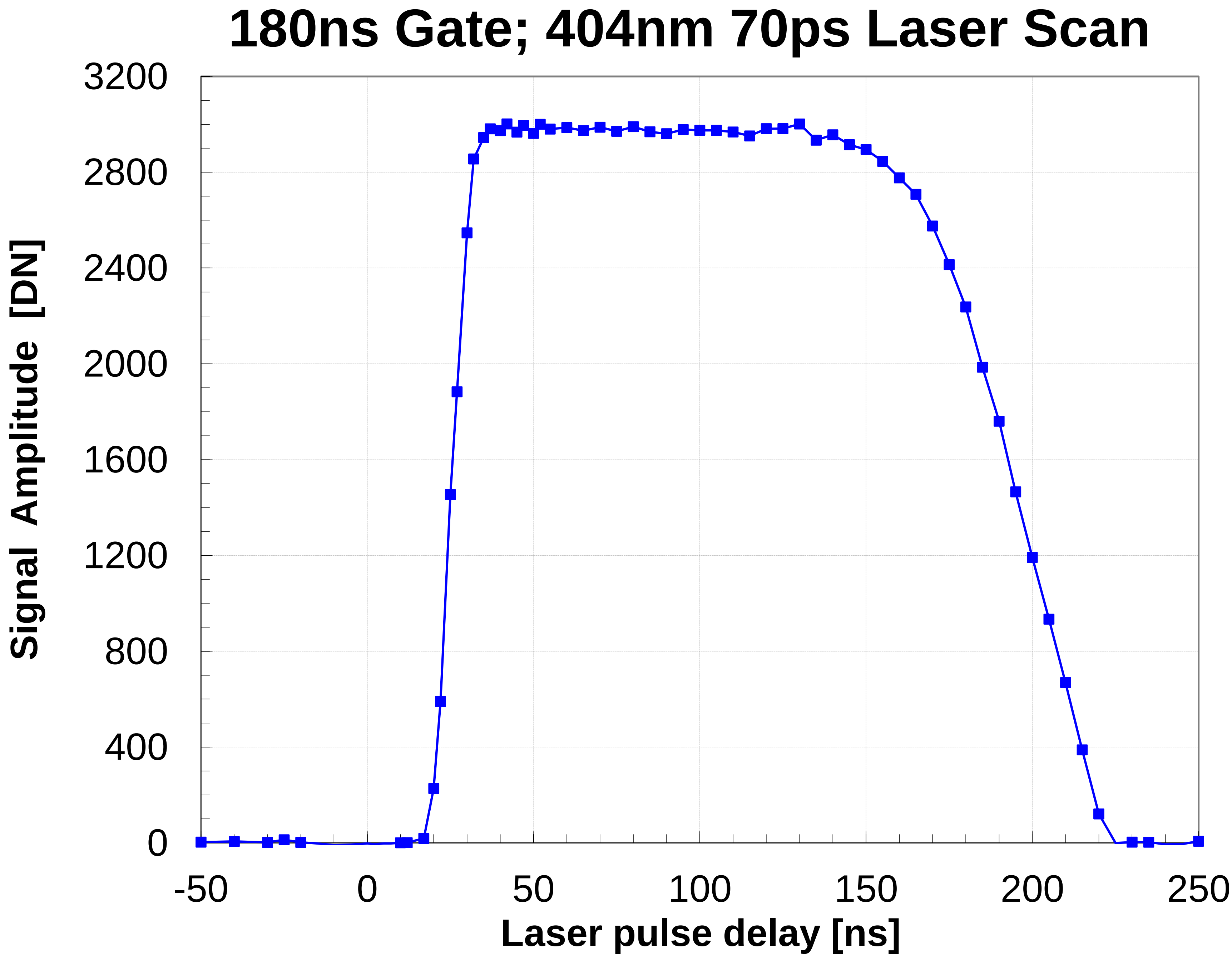
180ns Gate; 404nm 70ps Laser Scan
Signal Amplitude [DN]
3200
2800
2400
2000
1600
1200
800
400
0
-50
0
50
100
150
200
250
Laser pulse delay [ns]

Accurate Areal Density Reconstructions

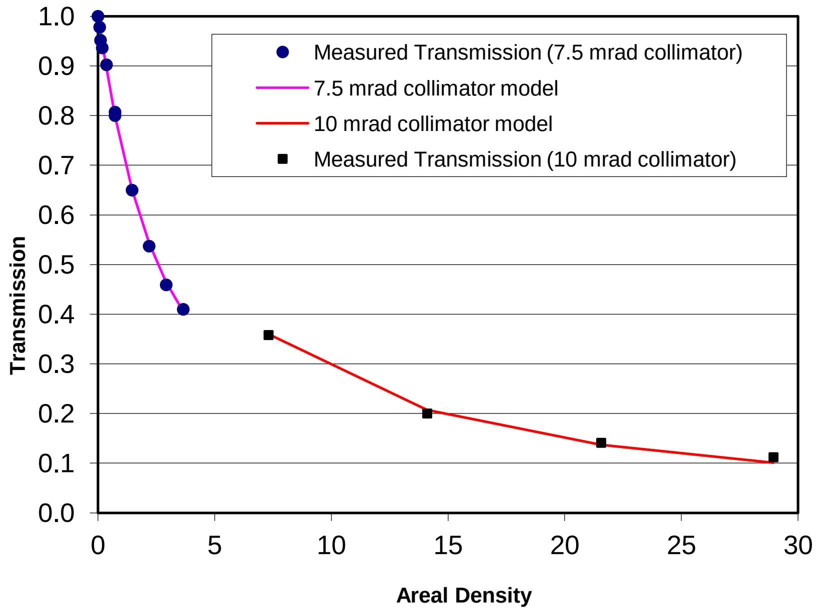

$$T = e^{-\left(x/\lambda_c + \left(\frac{\theta_c p \beta}{14.1 MeV} \right)^2 \frac{x_o}{2\left(x + x_f\right)} \right)}$$

Adjust parameters to fit transmission data:

- λ_c - nuclear collision length
- X_f – fixed radiation length (windows, beam angular spread)

Build a step wedge and adjust parameters to fit measured data

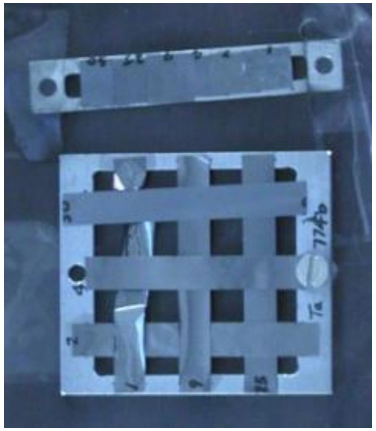

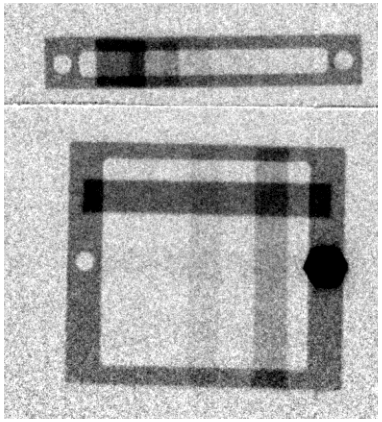

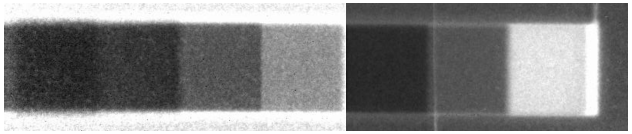

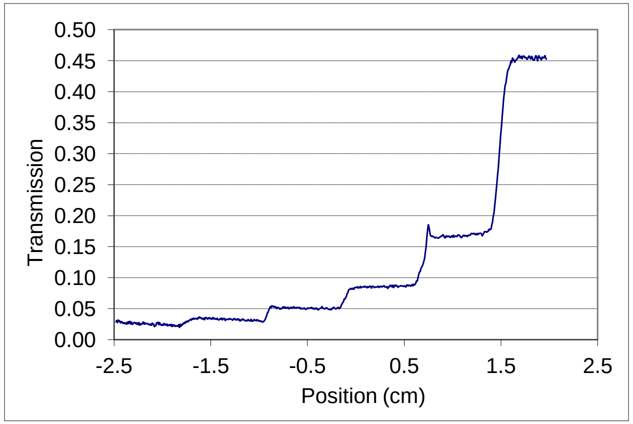

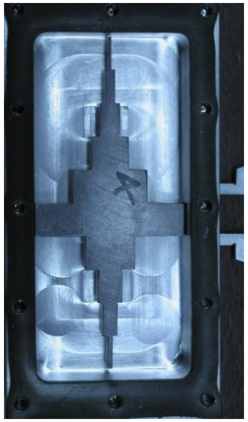

Magnetic Imaging Lens

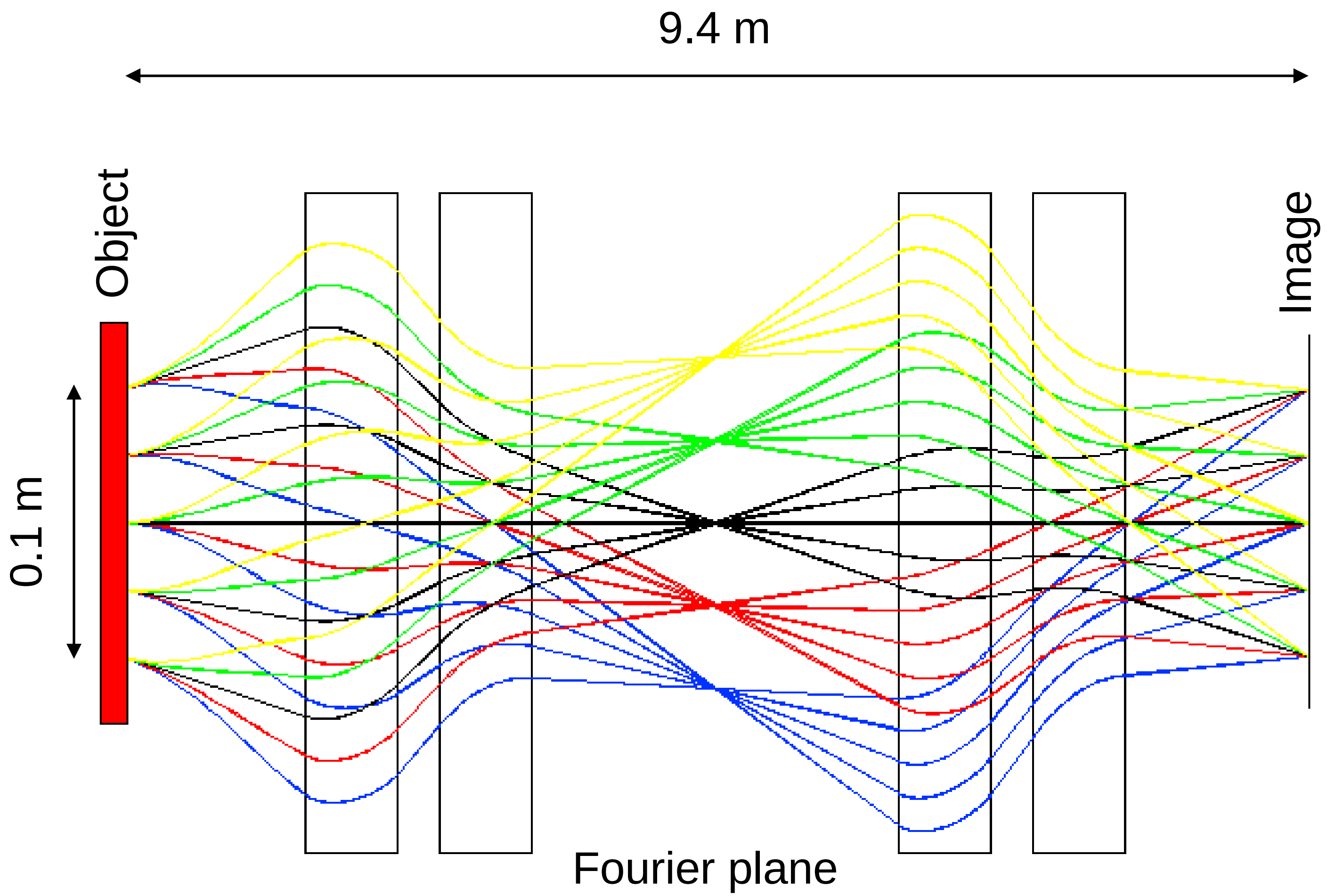

Quadrupole Identity Lens

Multiple Coulomb Scattering

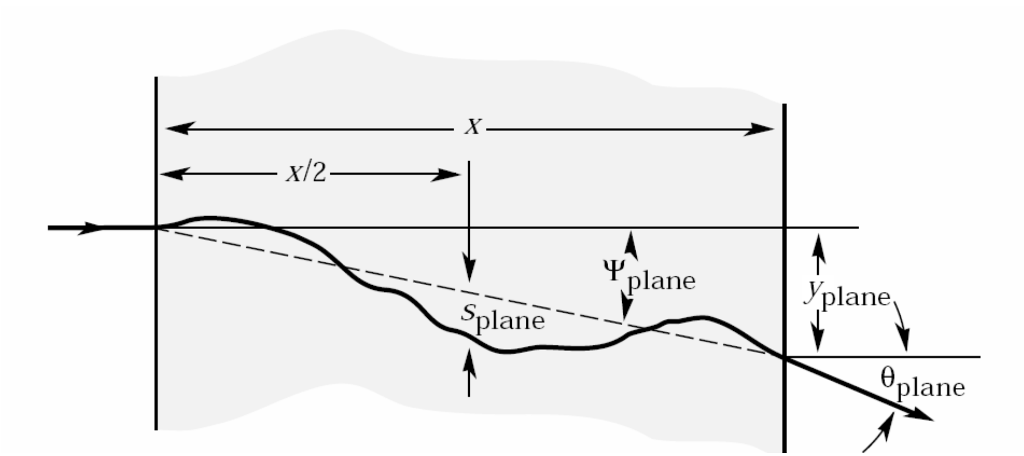

$$\theta_o = \frac{13.6MeV}{\beta p}\sqrt{x/X_o}\left[1+0.038\ln\left(x/X_o\right)\right] \; *$$

RMS Width

Full Width Half Maximum=2.35 θ_o

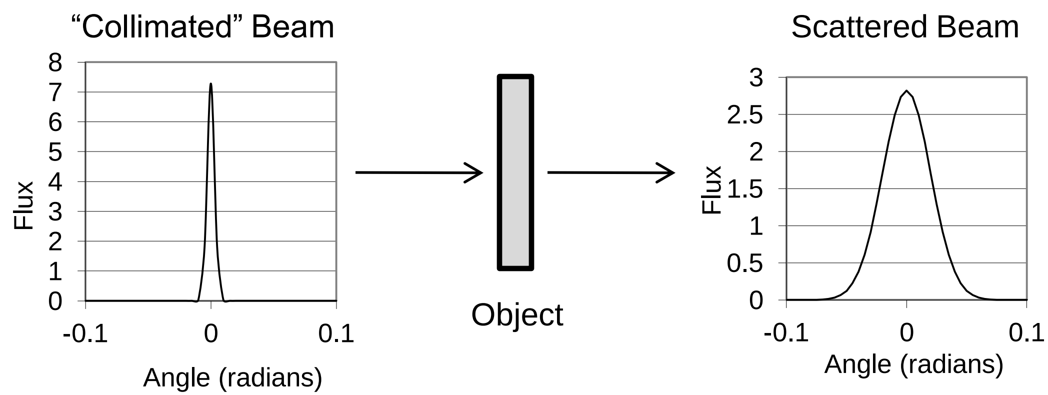

$$\theta_o = \frac{14.1MeV}{\beta p}\sqrt{x/X_o}$$

Typical LANL simplification

*C. Amsler et al., Physics Letters **B667**, 1 (2008)

Contrast from Multiple Coulomb Scattering

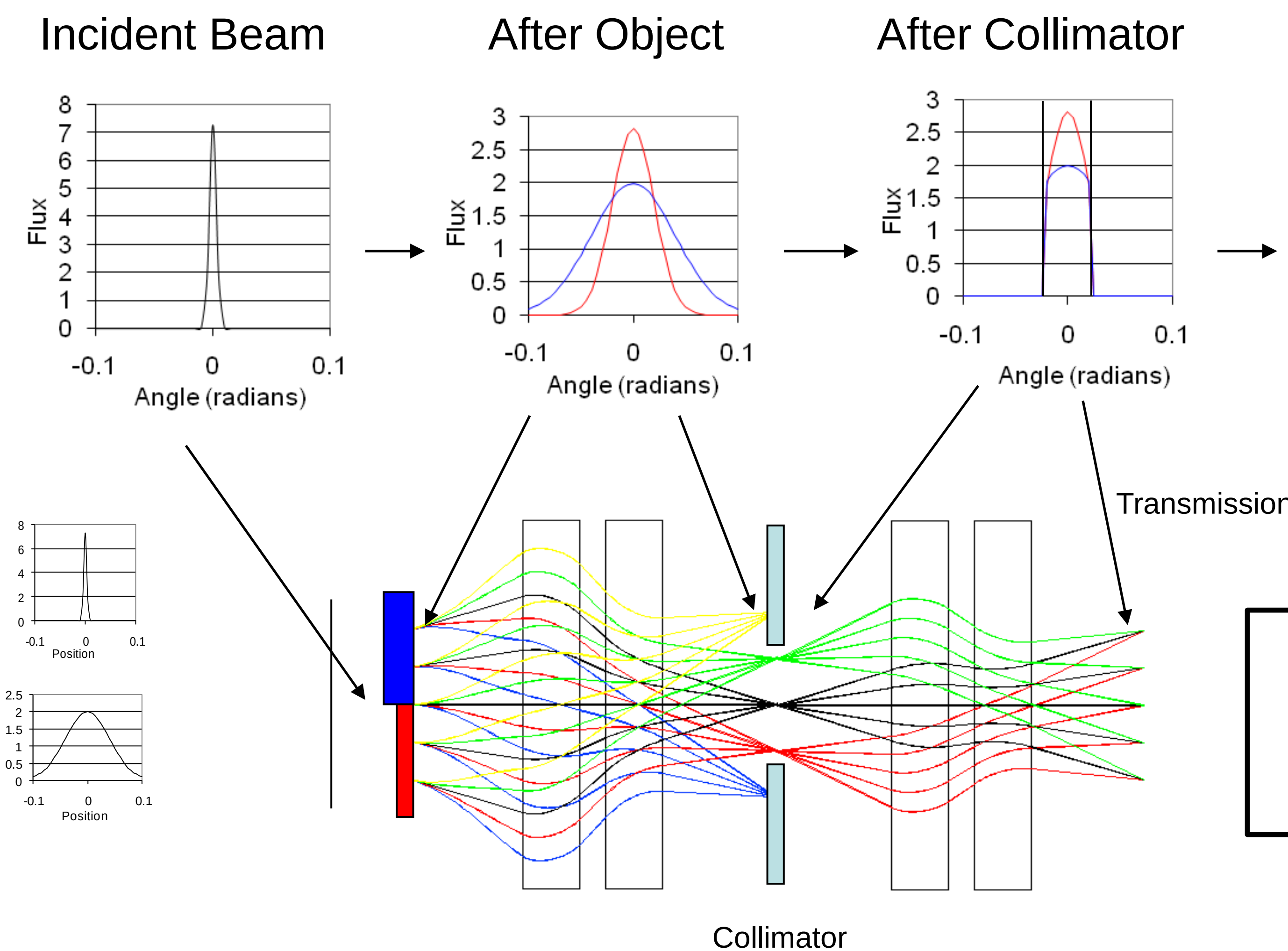

Measured transmission provides information of object thickness

Transmission

$$T_{MCS} = 1 - e^{-\theta_c^2 / 2\theta_o^2}$$

Nuclear Interactions

Angular distribution of 800 MeV proton nuclear elastic scattering from Iron.

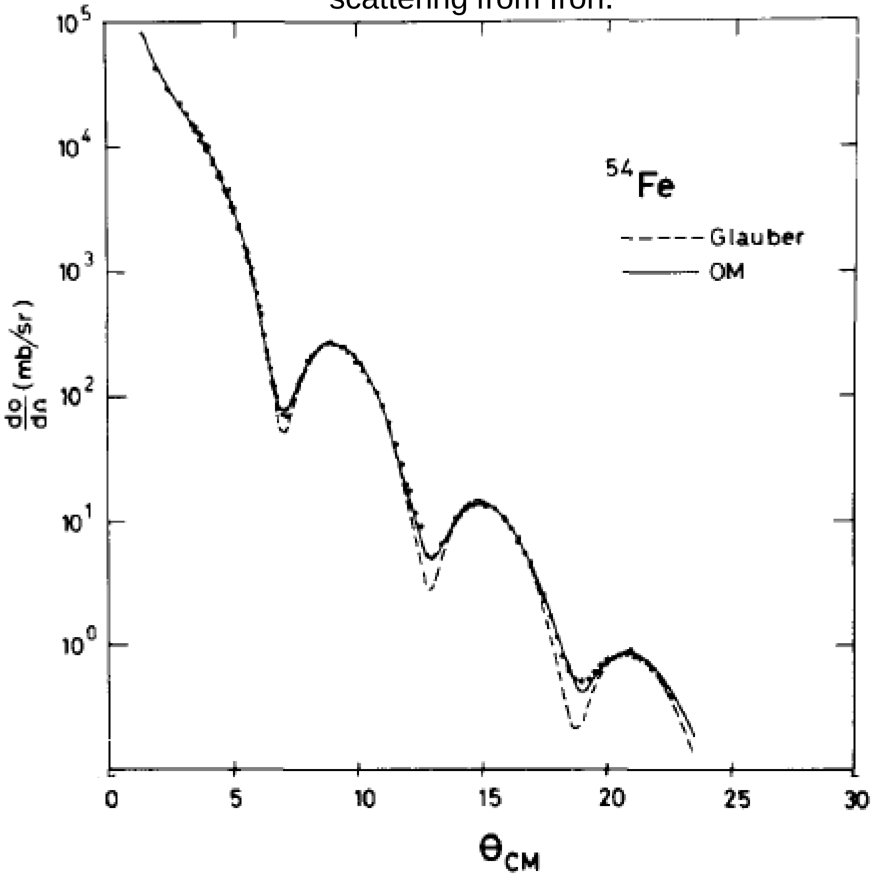

<u>Simple Approximation for Modeling Proton Radiography</u>

- Characteristic Nuclear Collision Length: λ_c
- Approximate that each interaction removes the proton from the acceptance of the imaging lens.
- Measure the collision Length at 800 MeV

The "true" nuclear interactions are more complicated than this simple assumption and these interactions are reasonably well understood. This can all be simulated, but it is typically not worth the effort for designing small scale experiments.

<u>Transmission</u>

$$T_{nuclear} = e^{-x/\lambda_C}$$

Particle Data Group:
http://pdg.lbl.gov/

A Useful Table

6. ATOMIC AND NUCLEAR PROPERTIES OF MATERIALS

Table 6.1 Abridged from `pdg.lbl.gov/AtomicNuclearProperties` by D. E. Groom (2007). See web pages for more detail about entries in this table including chemical formulae, and for several hundred other entries. Quantities in parentheses are for NTP (20° C and 1 atm), and square brackets indicate quantities evaluated at STP. Boiling points are at 1 atm. Refractive indices n are evaluated at the sodium D line blend (589.2 nm); values $\gg$1 in brackets are for $(n-1) \times 10^6$ (gases).

Material	Z	A	$\langle Z/A \rangle$	Nucl.coll. length λ_T {g cm^{-2}}	Nucl.inter. length λ_I {g cm^{-2}}	Rad.len. X_0 {g cm^{-2}}	$dE/dx\|_{\min}$ { MeV g^{-1}cm^2}	Density {g cm^{-3}} ({gℓ^{-1}})	Melting point (K)	Boiling point (K)	Refract. index (@ Na D)
H_2	1	1.00794(7)	0.99212	42.8	52.0	63.04	(4.103)	0.071(0.084)	13.81	20.28	1.11[132.]
D_2	1	2.01410177803(8)	0.49650	51.3	71.8	125.97	(2.053)	0.169(0.168)	18.7	23.65	1.11[138.]
He	2	4.002602(2)	0.49967	51.8	71.0	94.32	(1.937)	0.125(0.166)		4.220	1.02[35.0]
Li	3	6.941(2)	0.43221	52.2	71.3	82.78	1.639	0.534	453.6	1615.	
Be	4	9.012182(3)	0.44384	55.3	77.8	65.19	1.595	1.848	1560.	2744.	
C diamond	6	12.0107(8)	0.49955	59.2	85.8	42.70	1.725	3.520			2.42
C graphite	6	12.0107(8)	0.49955	59.2	85.8	42.70	1.742	2.210			
N_2	7	14.0067(2)	0.49976	61.1	89.7	37.99	(1.825)	0.807(1.165)	63.15	77.29	1.20[298.]
O_2	8	15.9994(3)	0.50002	61.3	90.2	34.24	(1.801)	1.141(1.332)	54.36	90.20	1.22[271.]
F_2	9	18.9984032(5)	0.47372	65.0	97.4	32.93	(1.676)	1.507(1.580)	53.53	85.03	[195.]
Ne	10	20.1797(6)	0.49555	65.7	99.0	28.93	(1.724)	1.204(0.839)	24.56	27.07	1.09[67.1]
Al	13	26.9815386(8)	0.48181	69.7	107.2	24.01	1.615	2.699	933.5	2792.	
Si	14	28.0855(3)	0.49848	70.2	108.4	21.82	1.664	2.329	1687.	3538.	3.95
Cl_2	17	35.453(2)	0.47951	73.8	115.7	19.28	(1.630)	1.574(2.980)	171.6	239.1	[773.]
Ar	18	39.948(1)	0.45059	75.7	119.7	19.55	(1.519)	1.396(1.662)	83.81	87.26	1.23[281.]
Ti	22	47.867(1)	0.45961	78.8	126.2	16.16	1.477	4.540	1941.	3560.	
Fe	26	55.845(2)	0.46557	81.7	132.1	13.84	1.451	7.874	1811.	3134.	
Cu	29	63.546(3)	0.45636	84.2	137.3	12.86	1.403	8.960	1358.	2835.	
Ge	32	72.64(1)	0.44053	86.9	143.0	12.25	1.370	5.323	1211.	3106.	
Sn	50	118.710(7)	0.42119	98.2	166.7	8.82	1.263	7.310	505.1	2875.	
Xe	54	131.293(6)	0.41129	100.8	172.1	8.48	(1.255)	2.953(5.483)	161.4	165.1	1.39[701.]
W	74	183.84(1)	0.40252	110.4	191.9	6.76	1.145	19.300	3695.	5828.	
Pt	78	195.084(9)	0.39983	112.2	195.7	6.54	1.128	21.450	2042.	4098.	
Au	79	196.966569(4)	0.40108	112.5	196.3	6.46	1.134	19.320	1337.	3129.	
Pb	82	207.2(1)	0.39575	114.1	199.6	6.37	1.122	11.350	600.6	2022.	
U	92	[238.02891(3)]	0.38651	118.6	209.0	6.00	1.081	18.950	1408.	4404.	
Air (dry, 1 atm)			0.49919	61.3	90.1	36.62	(1.815)	(1.205)		78.80	
Shielding concrete			0.50274	65.1	97.5	26.57	1.711	2.300			
Borosilicate glass (Pyrex)			0.49707	64.6	96.5	28.17	1.696	2.230			
Lead glass			0.42101	95.9	158.0	7.87	1.255	6.220			
Standard rock			0.50000	66.8	101.3	26.54	1.688	2.650			
Methane (CH_4)			0.62334	54.0	73.8	46.47	(2.417)	(0.667)	90.68	111.7	[444.]
Ethane (C_2H_6)			0.59861	55.0	75.9	45.66	(2.304)	(1.263)	90.36	184.5	
Propane (C_3H_8)			0.58962	55.3	76.7	45.37	(2.262)	0.493(1.868)	85.52	231.0	
Butane (C_4H_{10})			0.59497	55.5	77.1	45.23	(2.278)	(2.489)	134.9	272.6	
Octane (C_8H_{18})			0.57778	55.8	77.8	45.00	2.123	0.703	214.4	398.8	
Paraffin ($CH_3(CH_2)_{n\approx 23}CH_3$)			0.57275	56.0	78.3	44.85	2.088	0.930			
Nylon (type 6, 6/6)			0.54790	57.5	81.6	41.92	1.973	1.18			
Polycarbonate (Lexan)			0.52697	58.3	83.6	41.50	1.886	1.20			
Polyethylene ($[CH_2CH_2]_n$)			0.57034	56.1	78.5	44.77	2.079	0.89			
Polyethylene terephthalate (Mylar)			0.52037	58.9	84.9	39.95	1.848	1.40			
Polyimide film (Kapton)			0.51264	59.2	85.5	40.58	1.820	1.42			
Polymethylmethacrylate (acrylic)			0.53937	58.1	82.8	40.55	1.929	1.19			1.49
Polypropylene			0.55998	56.1	78.5	44.77	2.041	0.90			
Polystyrene ($[C_6H_5CHCH_2]_n$)			0.53768	57.5	81.7	43.79	1.936	1.06			1.59
Polytetrafluoroethylene (Teflon)			0.47992	63.5	94.4	34.84	1.671	2.20			
Polyvinyltoluene			0.54141	57.3	81.3	43.90	1.956	1.03			1.58
Aluminum oxide (sapphire)			0.49038	65.5	98.4	27.94	1.647	3.970	2327.	3273.	1.77
Barium flouride (BaF_2)			0.42207	90.8	149.0	9.91	1.303	4.893	1641.	2533.	1.47
Bismuth germanate (BGO)			0.42065	96.2	159.1	7.97	1.251	7.130	1317.		2.15
Carbon dioxide gas (CO_2)			0.49989	60.7	88.9	36.20	1.819	(1.842)			[449.]
Solid carbon dioxide (dry ice)			0.49989	60.7	88.9	36.20	1.787	1.563	Sublimes at 194.7 K		
Cesium iodide (CsI)			0.41569	100.6	171.5	8.39	1.243	4.510	894.2	1553.	1.79
Lithium fluoride (LiF)			0.46262	61.0	88.7	39.26	1.614	2.635	1121.	1946.	1.39
Lithium hydride (LiH)			0.50321	50.8	68.1	79.62	1.897	0.820	965.		
Lead tungstate ($PbWO_4$)			0.41315	100.6	168.3	7.39	1.229	8.300	1403.		2.20
Silicon dioxide (SiO_2, fused quartz)			0.49930	65.2	97.8	27.05	1.699	2.200	1986.	3223.	1.46
Sodium chloride (NaCl)			0.55509	71.2	110.1	21.91	1.847	2.170	1075.	1738.	1.54
Sodium iodide (NaI)			0.42697	93.1	154.6	9.49	1.305	3.667	933.2	1577.	1.77
Water (H_2O)			0.55509	58.5	83.3	36.08	1.992	1.000(0.756)	273.1	373.1	1.33
Silica aerogel			0.50093	65.0	97.3	27.25	1.740	0.200	(0.03 H_2O, 0.97 SiO_2)		

When is an object too thick?

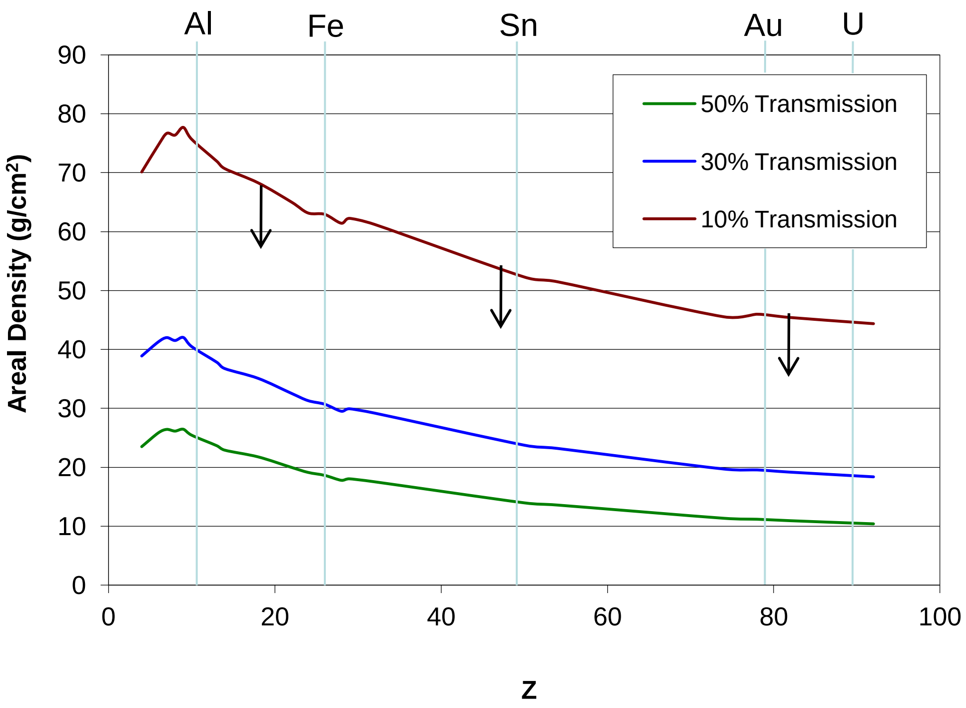

Areal density contours of constant transmission as a function of atomic number.

10% is near the lower limit of reasonable transmission.

Simple Figure of Merit Comparison

$$FOM = Dose/\sigma^2$$

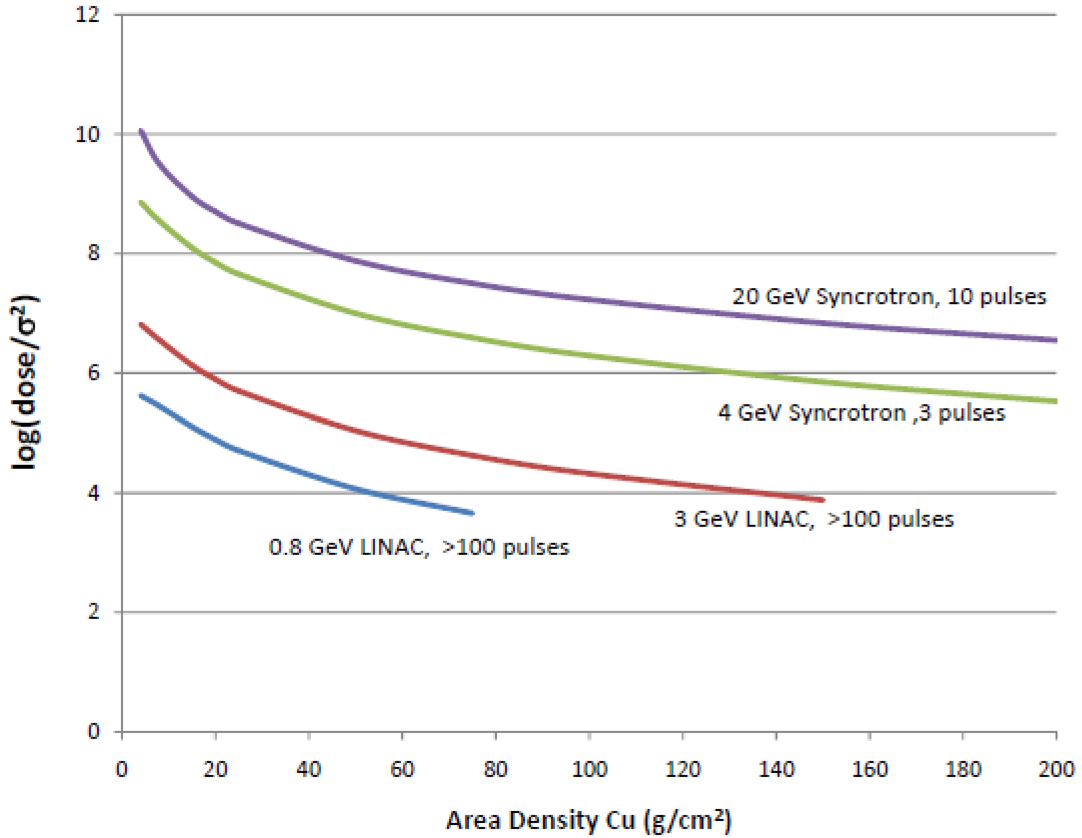

Dynamic Range of 800 MeV Proton Radiography

$$FOM = \frac{\Delta N / \sqrt{N}}{\Delta l / l} = \frac{l}{\sqrt{T}} \frac{dT}{dl}$$

Signal to noise

Fractional change in thickness

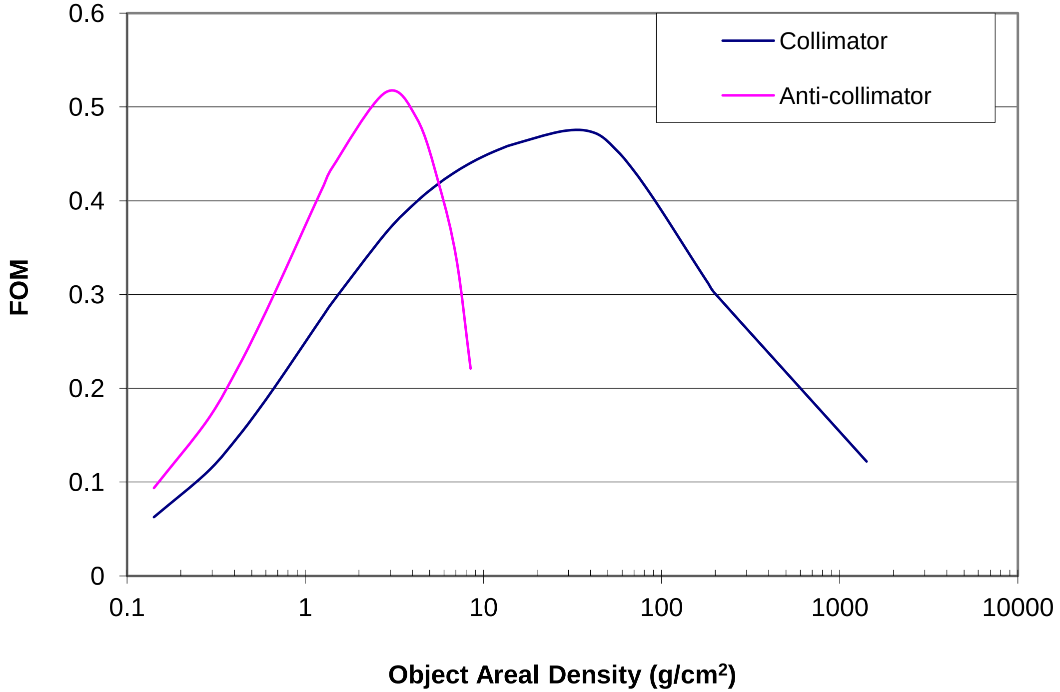

- 800 MeV proton radiography ranges from 1 g/cm^2 up to 70 g/cm^2 of iron

Chromatic Aberration and Resolution

Identity Lens

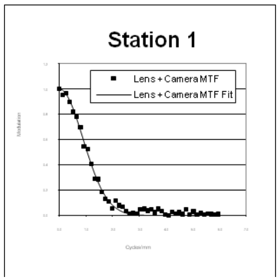

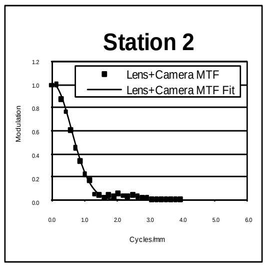

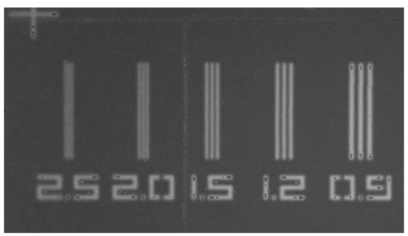

- 12 inch lens
- Station 1: 178 μm
- Station 2: 280 μm
- Gaussian blur function.
- 120 mm field of view

X3 Magnifier

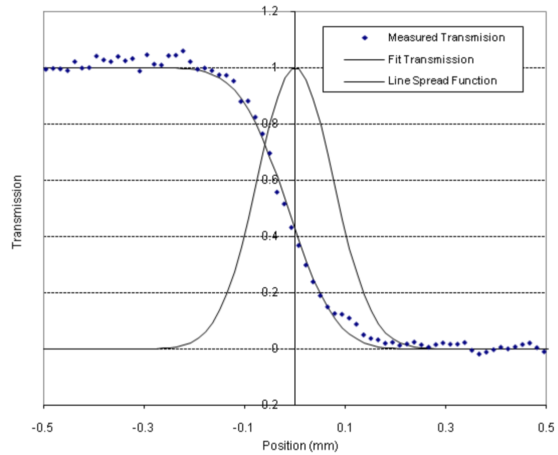

2.5 lp/mm

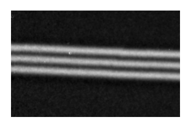

- 4 inch lens
- Station 1: 65 μm
- Gaussian blur function.
- 44 mm field of view

X7 Lens

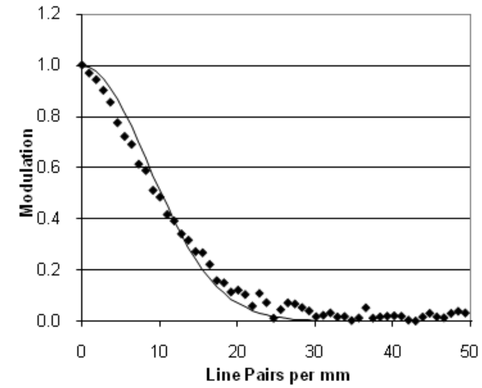

- 1 inch lens
- Station 1: 30 μm
- Gaussian blur function.
- 17 mm field of view

Radiographic Analysis

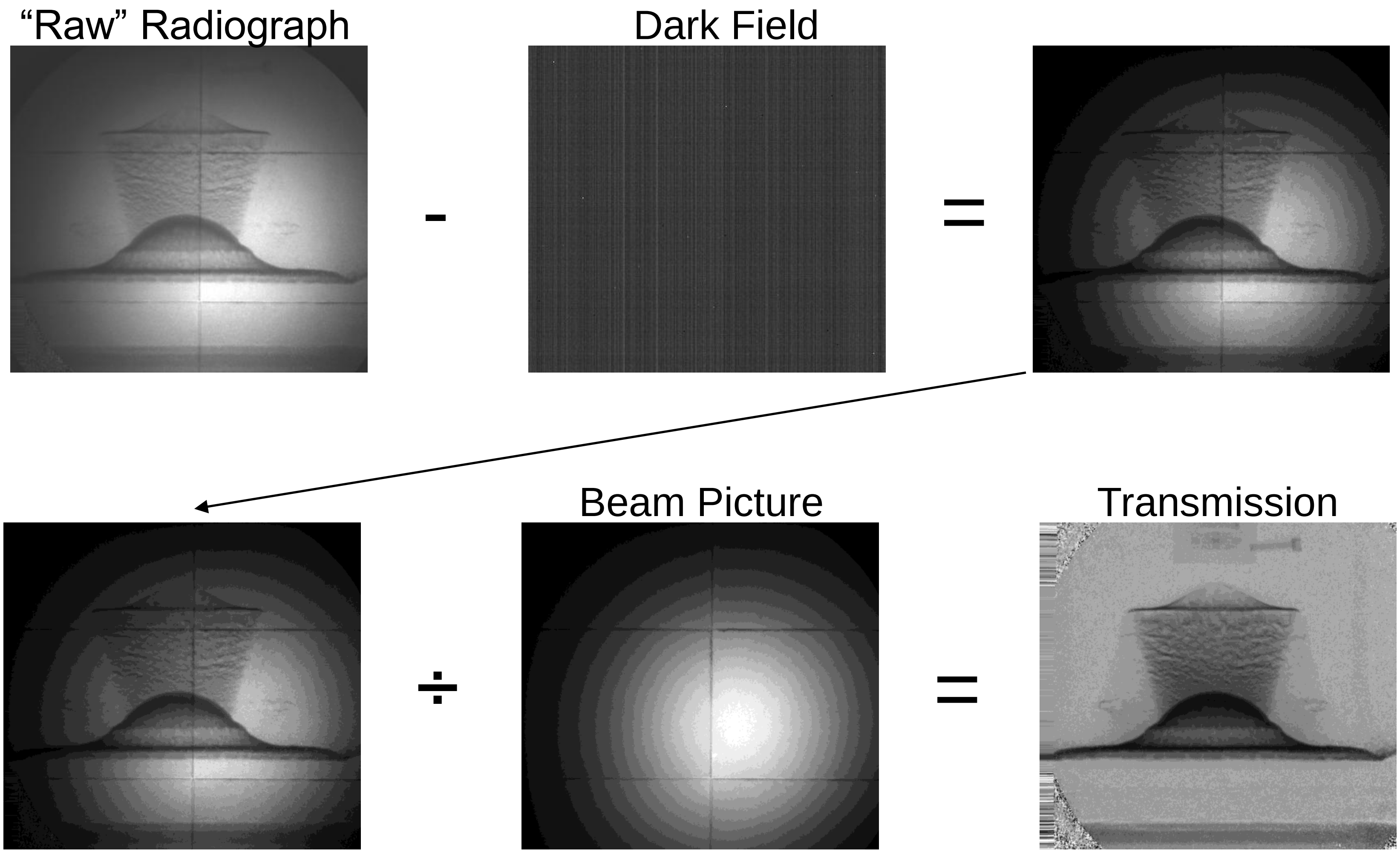

Bethe-Bloch Energy Loss for 800 MeV Protons

$$-\frac{dE}{dx} = Kz^2 \frac{Z}{A}\frac{1}{\beta^2}\left[\frac{1}{2}\ln\frac{2m_e c^2\beta^2\gamma^2 T_{\max}}{I^2} - \beta^2\right] \approx 1.5\frac{MeV}{g/cm^2}$$

$$K = 4\pi N_A r_e^2 m_e c^2 = 0.307\frac{MeV}{g/cm^2}$$

$$T_{\max} = \frac{2m_e c^2\beta^2\gamma^2}{1+2\gamma m_e/M + \left(m_e/M\right)^2}$$

C. Amsler et al., Physics Letters **B667**, 1 (2008)

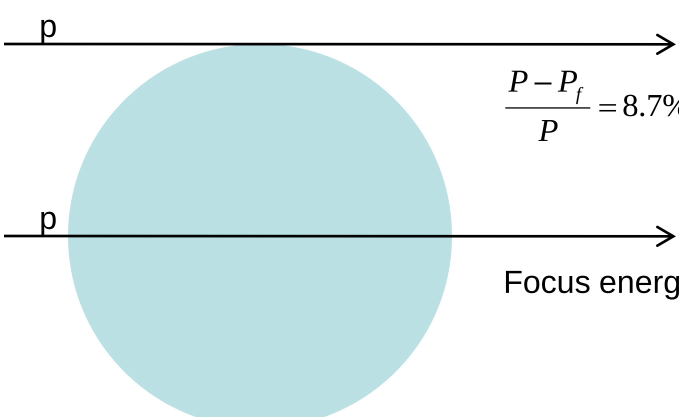

$$\frac{P-P_f}{P} = 8.7\%$$

Focus energy

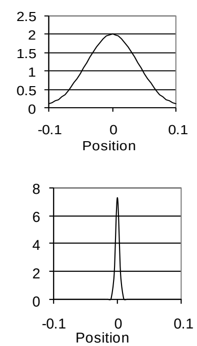

Line spread function

Identity Lens $\frac{P-P_f}{P} = 8.7\%$

copper

Density Reconstruction

Invert to calculate Areal Density

$$T = e^{-x/\lambda}\left(1 - e^{-\left(\frac{\theta_c p\beta}{14.1\,MeV}\right)^2 \frac{x_o}{2x}}\right)$$

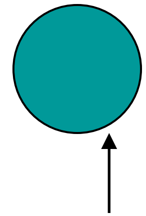

Use assumption of cylindrical symmetry to determine volume density (Abel inversion)

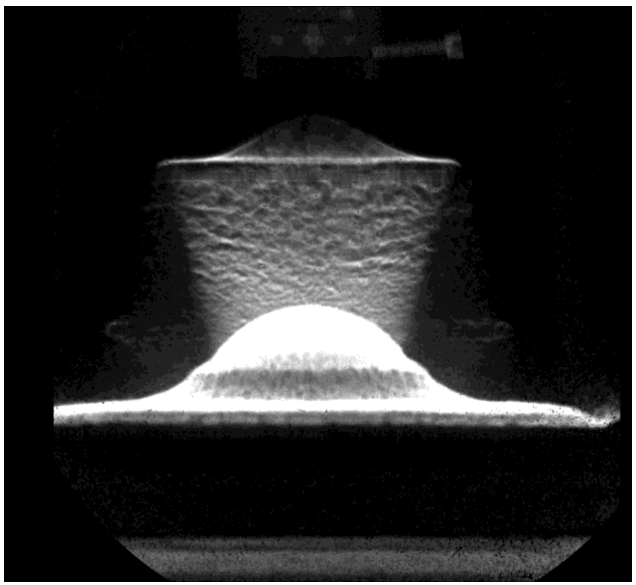

Areal Density (g/cm^2)

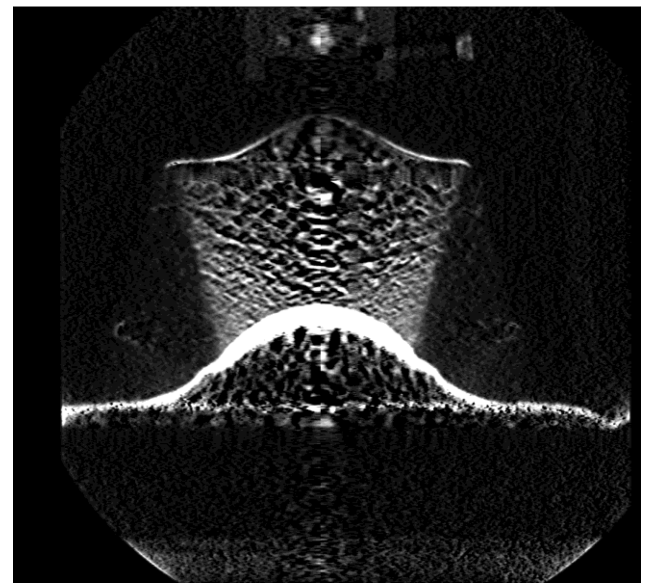

Volume Density (g/cm^3)

Multi-Frame Radiographic Movies

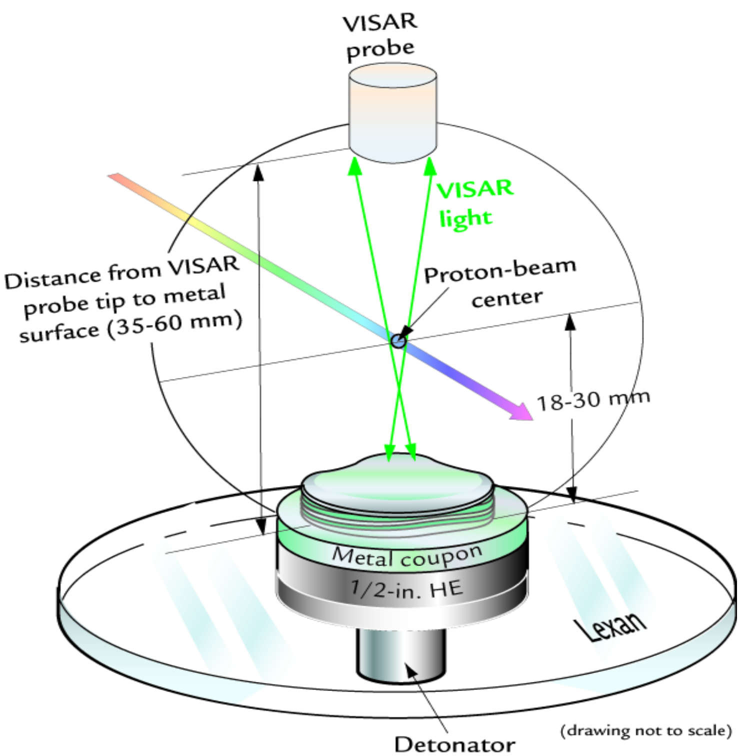

Measurements of Object Scattering Blur

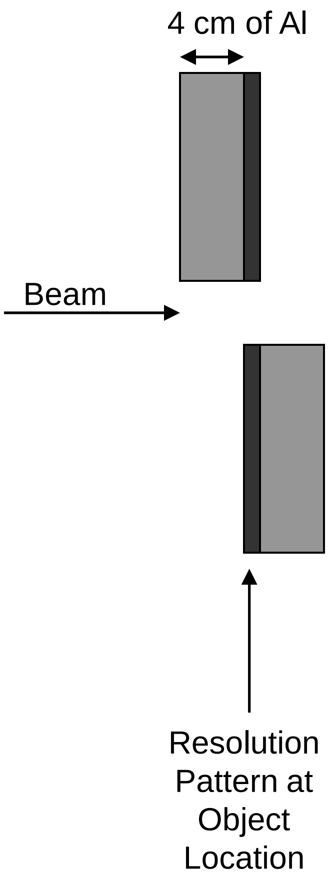

2.5 lp/mm

Sigma=0.061 mm

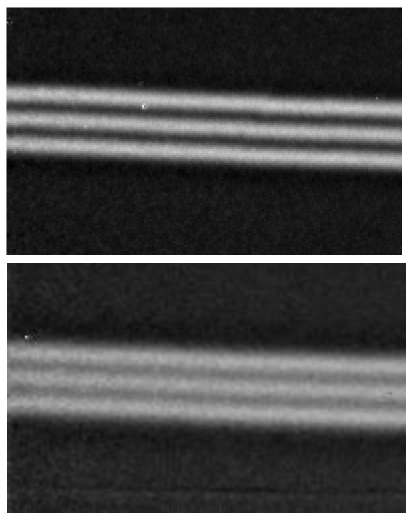

Sigma=0.150 mm

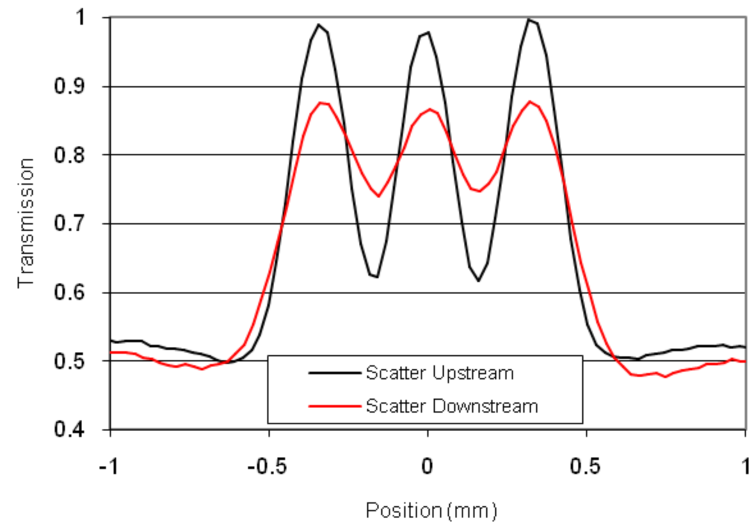

$$\sigma_o = \frac{1}{\sqrt{3}}\theta\frac{l}{2} = \frac{14.1}{\sqrt{6}}\frac{1}{P\beta}\sqrt{\frac{l^3}{x_o}} \propto \frac{l^{\frac{3}{2}}}{P}$$

Correcting Second Order Chromatic Aberrations

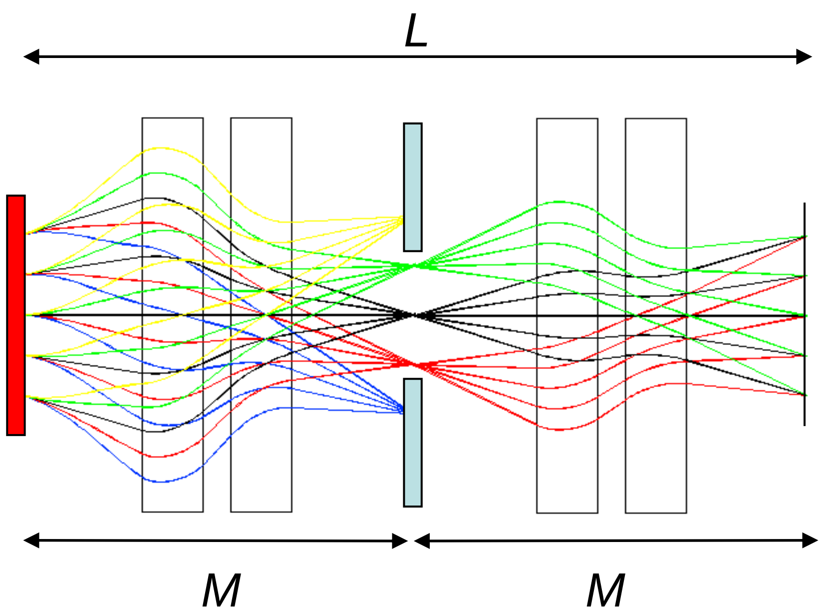

x_o, x_o'	- position and angle at object
x_{fp}	- position at midpoint of lens
x_i	- position and angle at image
δ	- $\Delta p/p$
M	- Transport matrix for doublet
L	- First order Transport matrix
T	- Second order Transport tensor

$$L = M^2 = -I$$

Form identity lens from identical doublets

Resolution

$$x_i = L_{11}x_o + L_{12}x_o' + T_{116}x_o\delta + T_{126}x_o'\delta$$

$$x_i = -x_o + T_{116}x_o\delta + T_{126}(wx_o + \phi)\delta$$

$$w = {-T_{116}} \big/ {T_{126}} = {-M_{11}} \big/ {M_{12}}$$

$$w = {-M_{11}} \big/ {M_{12}}$$

$$\Delta x_i = T_{126}\phi\delta$$

Dominates Blur

Inject beam with position-angle correlation to form Fourier plane at center of lens.

Fourier Plane

$$x_{fp} = M_{11}x_o + M_{12}x_o'$$

$$x_o' = wx_o + \phi$$

$$x_{fp} = M_{11}x_o + M_{12}\left(wx_o + \phi\right)$$

$$w = {-M_{11}} \big/ {M_{12}}$$

$$x_{fp} = M_{12}\phi$$

Same position-angle correlation which forms a Fourier plane at the center of the lens also cancels second order chromatic terms.

Chromatic Aberrations

Off-focus protons by lower momentum

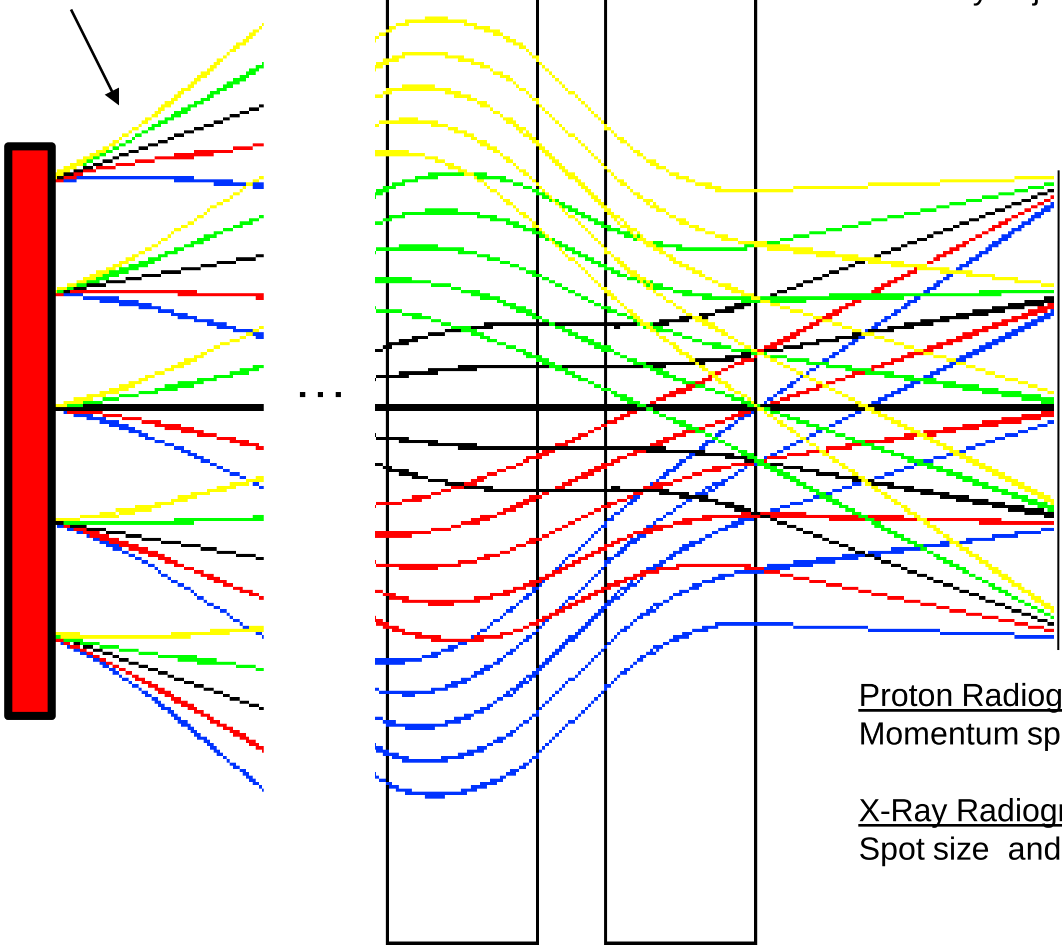

Black lines are the initial trajectories of the protons. Colored lines are trajectories of protons scattered by object.

$$\Delta x = L_c \phi \frac{\Delta p}{p}$$

Δx	-	Resolution
L_c	-	Chromatic Length
φ	-	Scattering angle
p	-	Momentum

<u>Proton Radiography:</u>
Momentum spread and chromatic length determine the resolution

<u>X-Ray Radiography:</u>
Spot size and magnification determine the resolution.

Chromatic Blur ⟶ Limbing

Focus on high energy protons

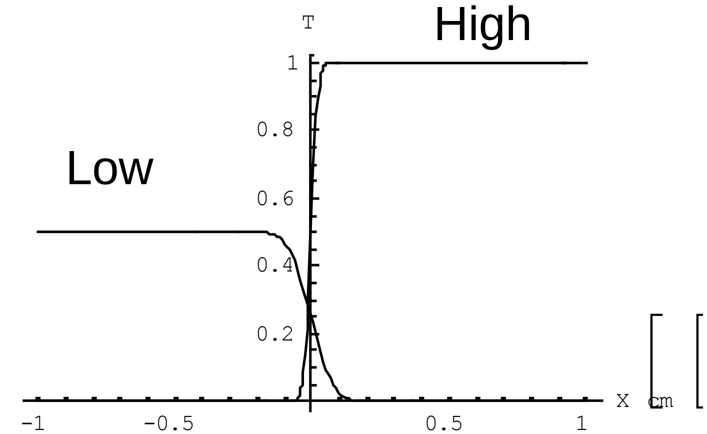

Limb: To outline in clear sharp detail

Like phase-contrast radiography:

- Useful to enhance edges
- Problem for density reconstruction

Resolution proportional to energy offset

$$\sigma = \theta l_c \frac{E - E_f}{E_f}$$

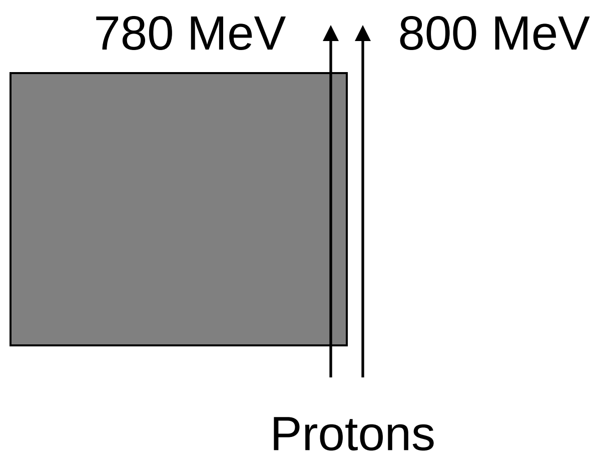

Low + High

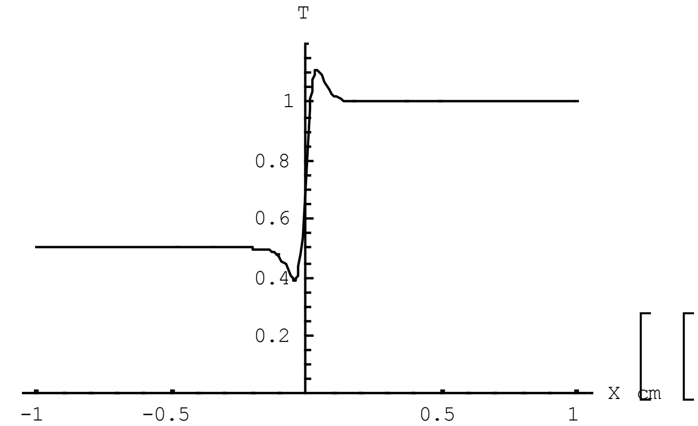

Example: Focused on high energy protons

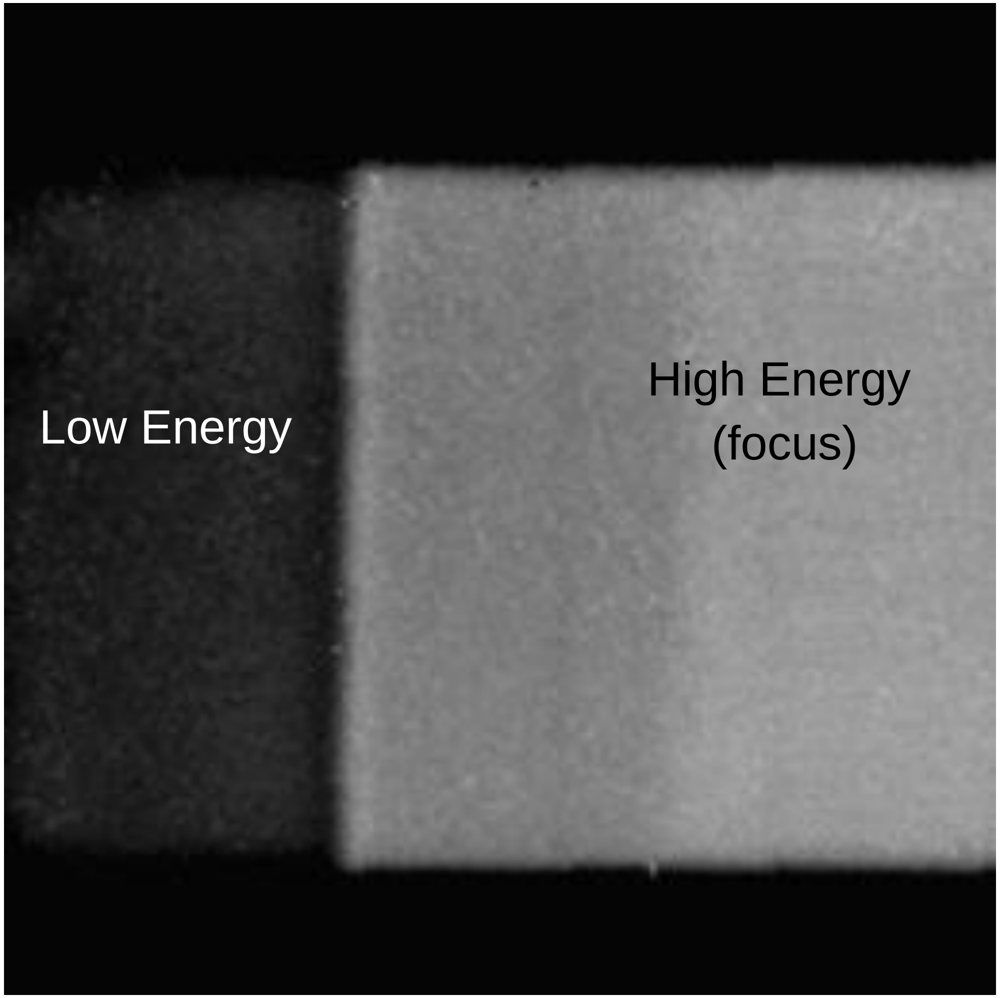

Focus on high energy protons

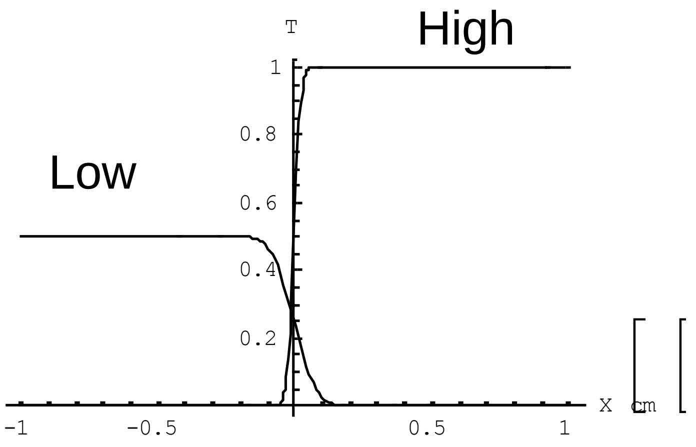

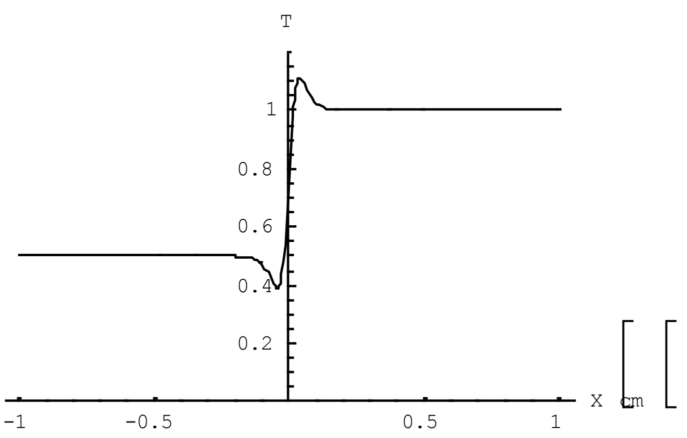

800 MeV x3 Magnifying Imaging Lens

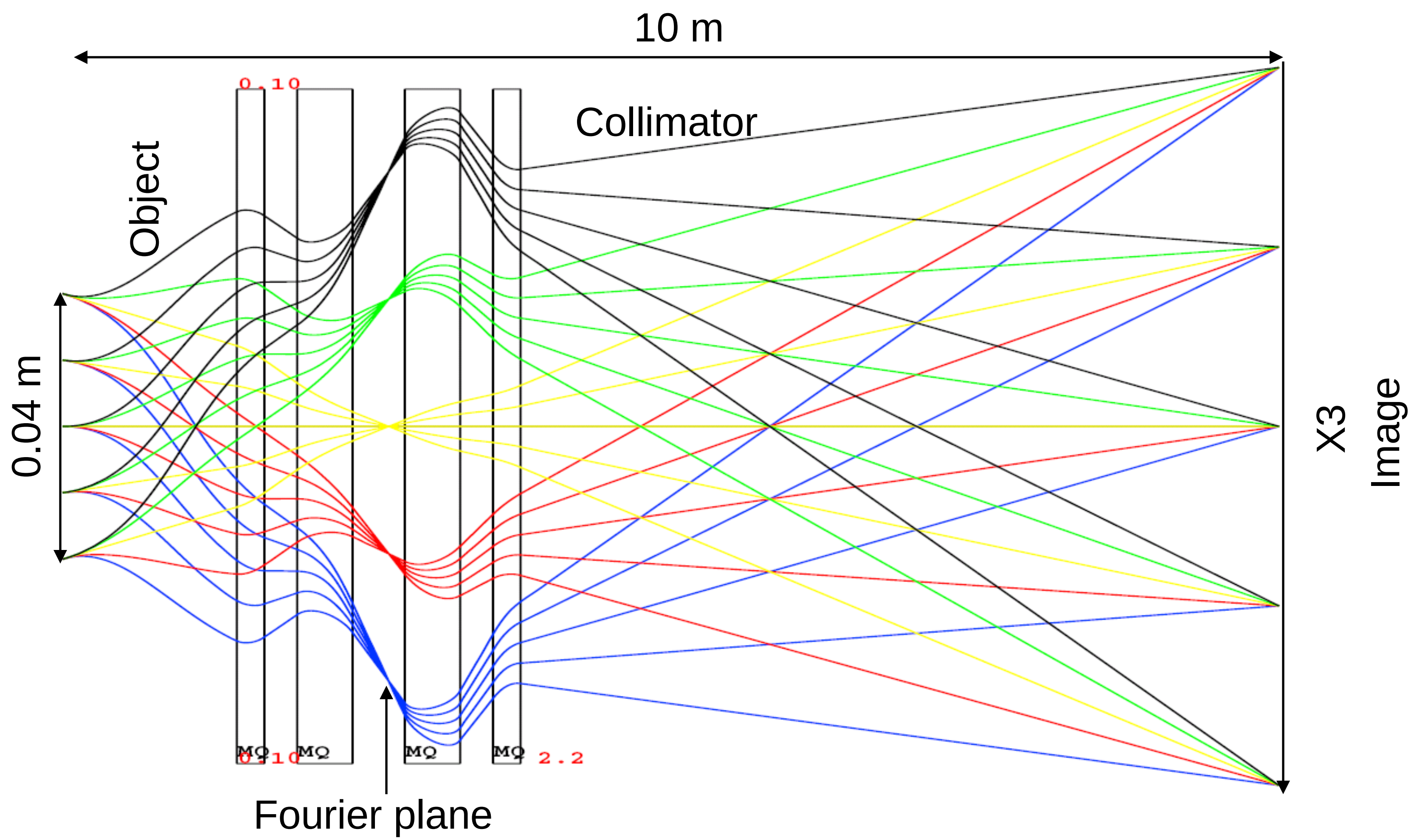

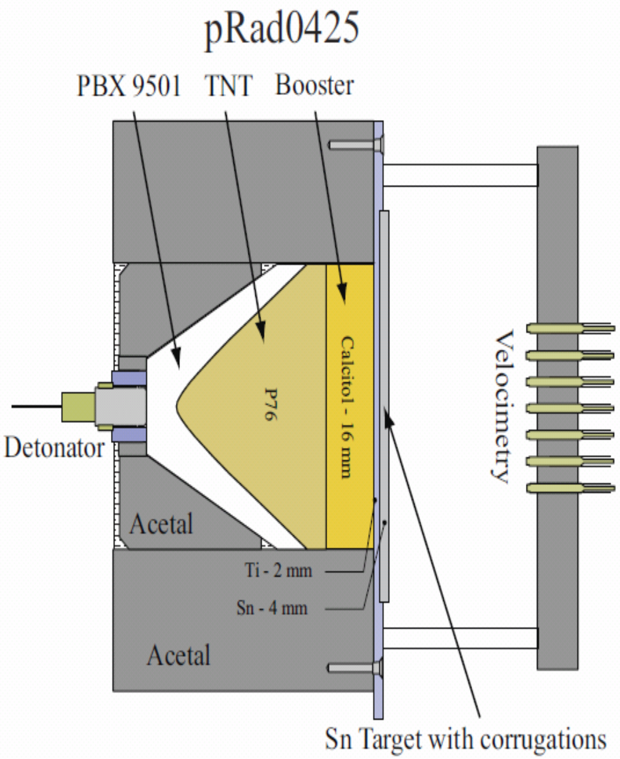
pRad0425
PBX 9501
TNT
Booster
P76
Calcitol - 16 mm
Velocimetry
Detonator
Acetal
Ti - 2 mm
Sn - 4 mm
Acetal
Sn Target with corrugations

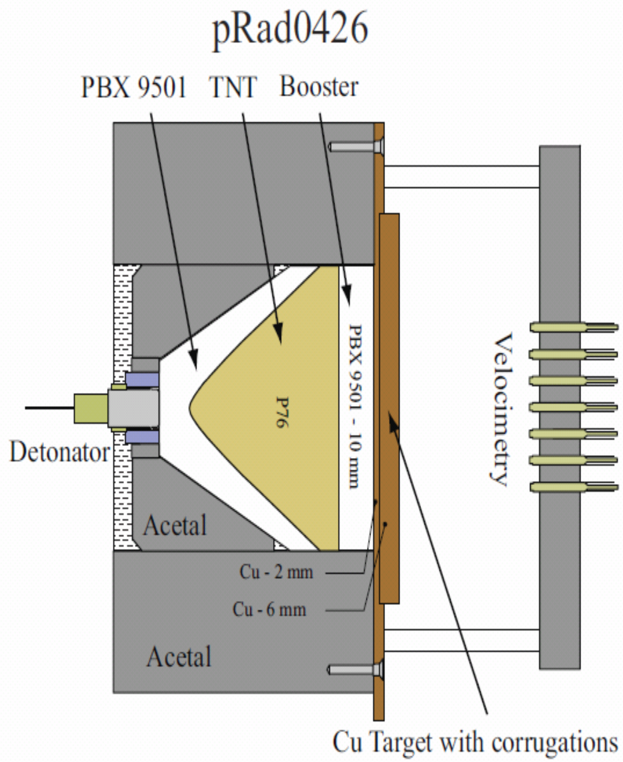
pRad0426
PBX 9501
TNT
Booster
P76
PBX 9501 - 10 mm
Velocimetry
Detonator
Acetal
Cu - 2 mm
Cu - 6 mm
Acetal
Cu Target with corrugations

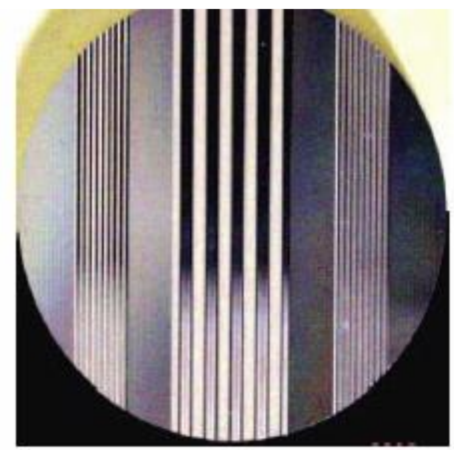

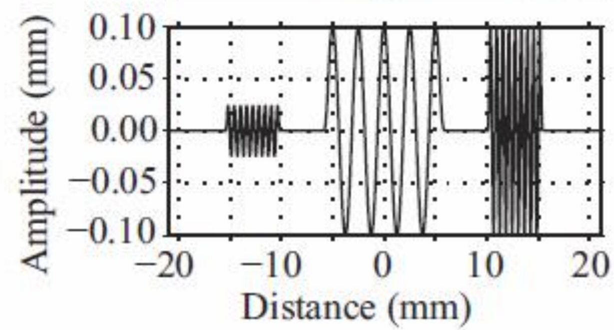
Amplitude (mm)
0.10
0.05
0.00
−0.05
−0.10
−20
−10
0
10
20
Distance (mm)

Solid-Solid Phase Transition in Iron

Dramatic Improvement in Resolution is allowing us to make new measurements like this solid-solid phase transition in iron. We are performing experiments with the magnifier to study solid-solid phase transitions in cerium this week.

Identity Lens $\frac{\Delta P}{P} = 8.7\%$

copper

X3 Magnifying Lens $\frac{\Delta P}{P} = 8.1\%$

Iron

Resolution improvement equivalent to an energy increase from 800 MeV to 2 GeV (in terms of chromatic blur)

Material Strength Experiments

PTW fit to Hopkinson-Bar data*

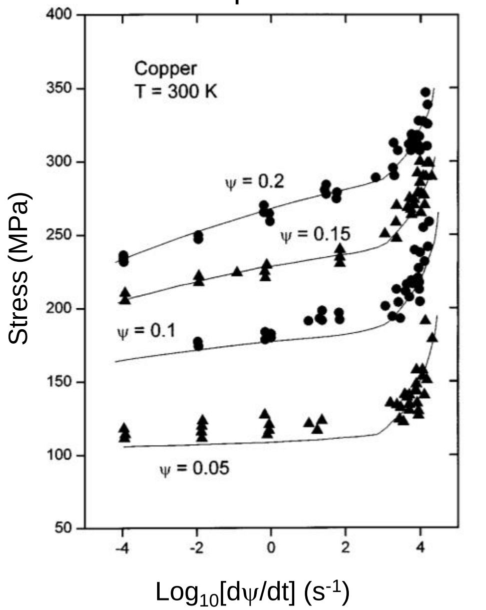

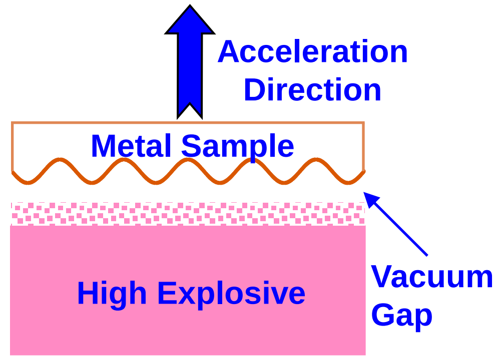

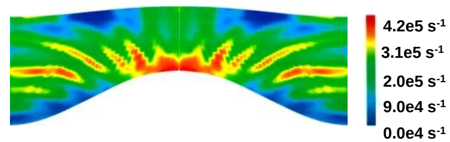

Calculated Strain Rate

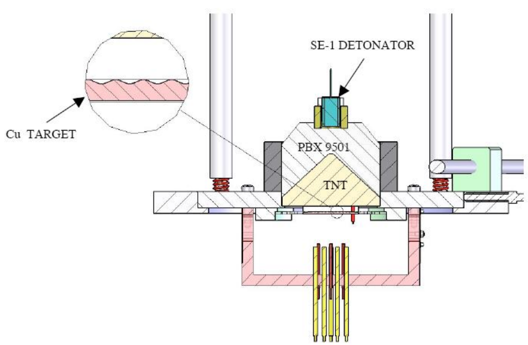

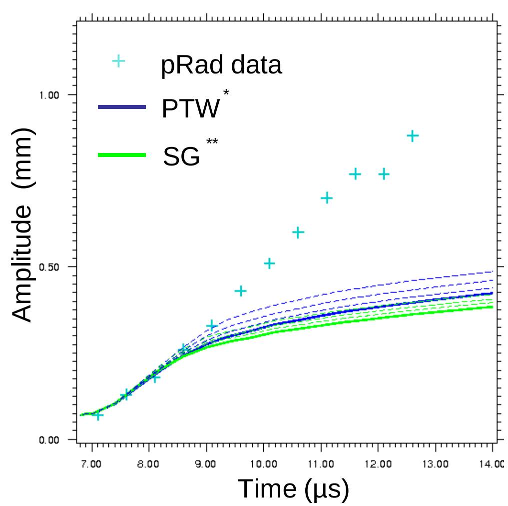

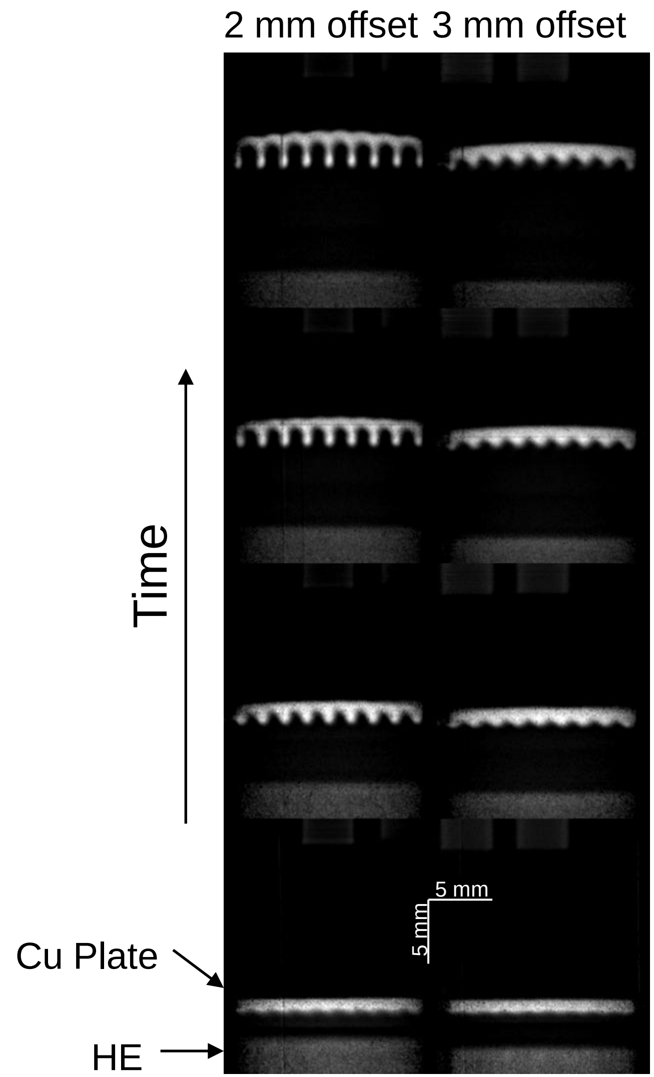

*D.L.Preston, et al. J.Appl. Phys. **93**, 211 (2003). ** D. J. Steinberg, et al. J.Appl. Phys. **61**, 1816 (1987).

Material Strength Experiments

PTW fit to Hopkinson-Bar data*

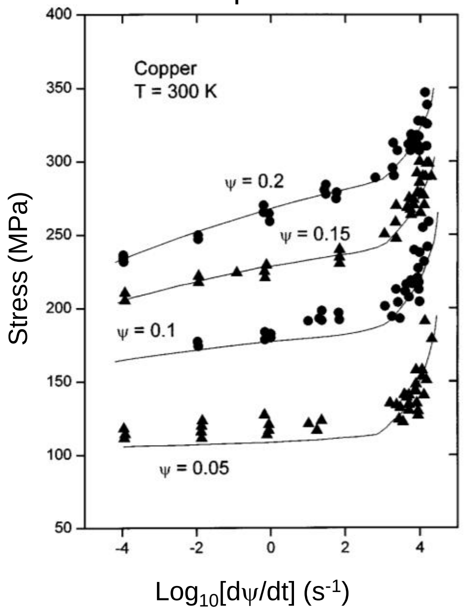

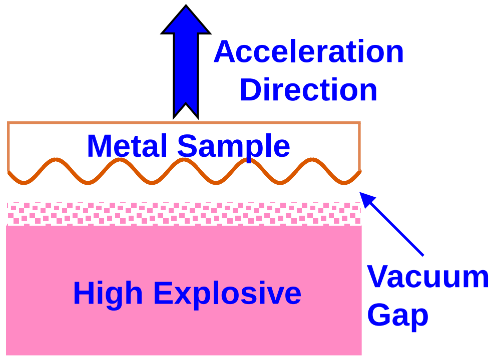

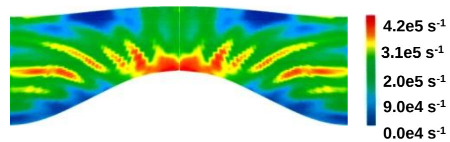

Calculated Strain Rate

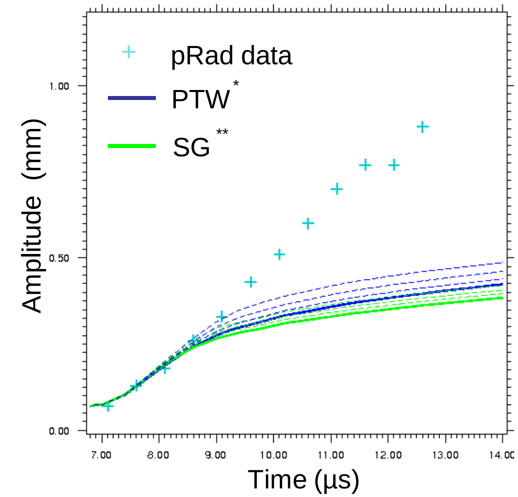

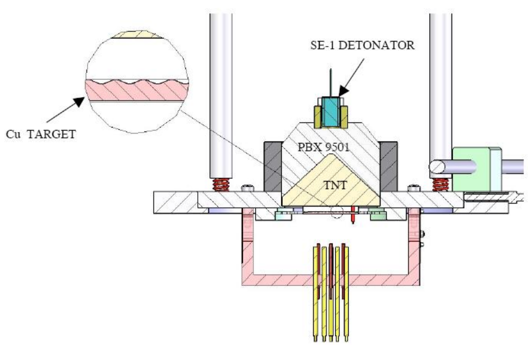

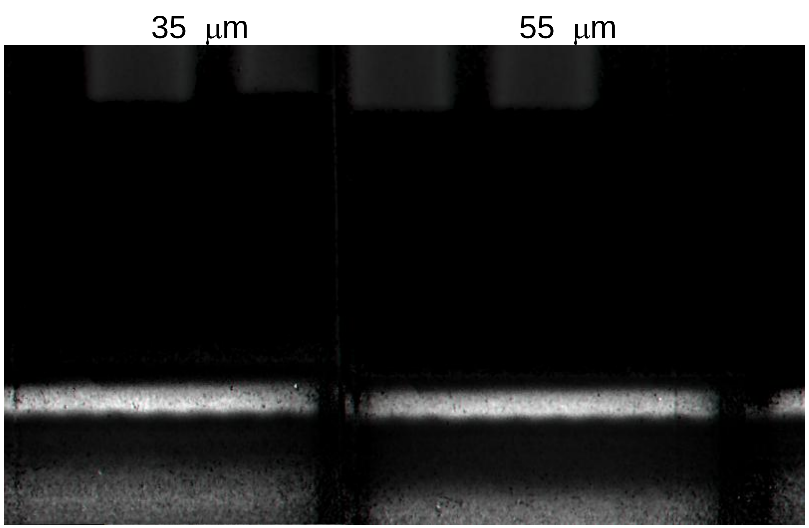

*D.L.Preston, et al. J.Appl. Phys. **93**, 211 (2003).

** D. J. Steinberg, et al. J.Appl. Phys. **61**, 1816 (1987).

Powder Gun Driven Equation Of State Measurements

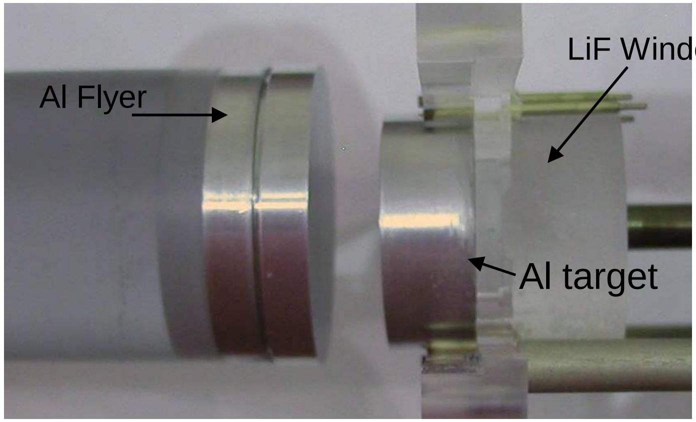

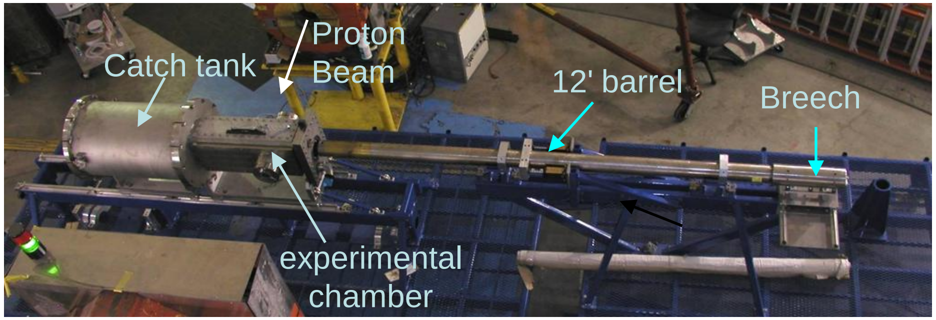

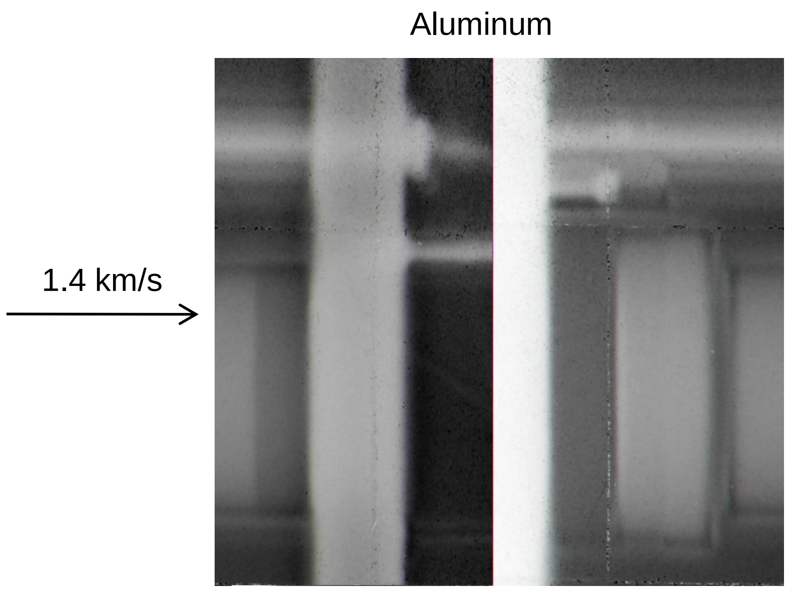

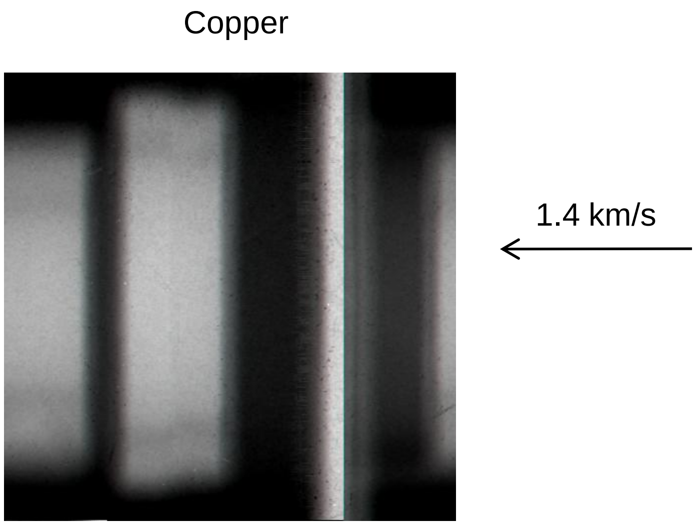

Powder Gun Al/Cu Equation Of State

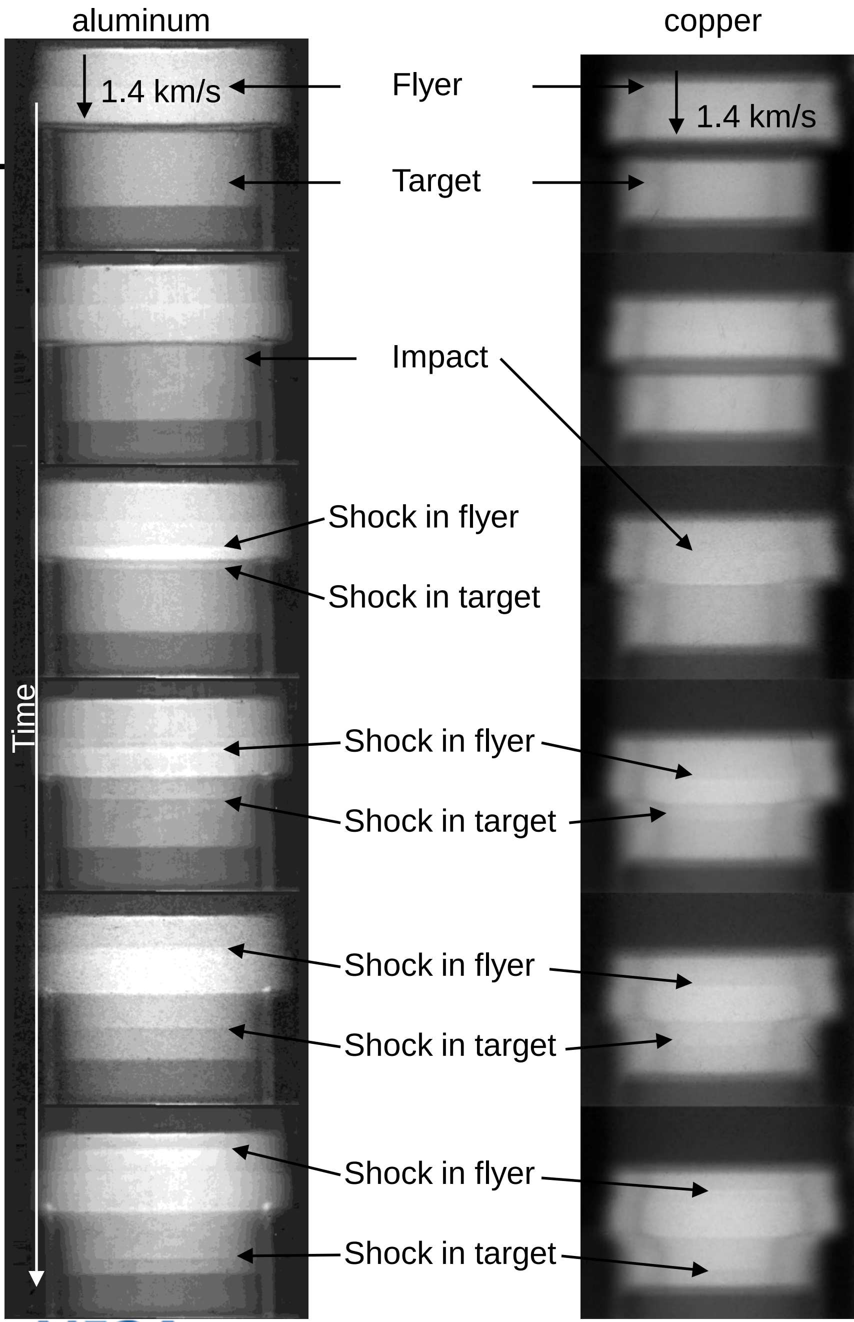

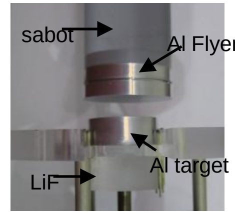

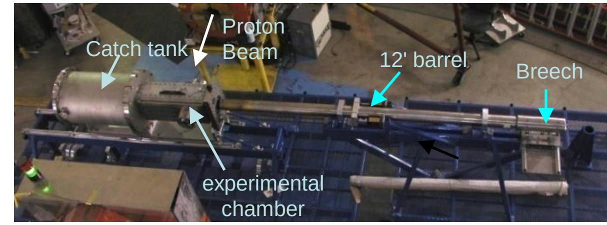

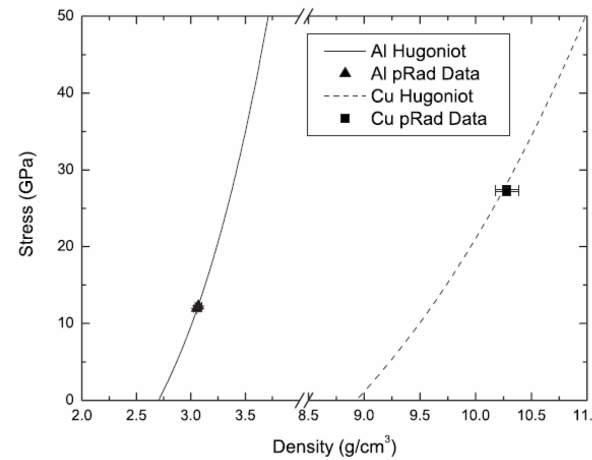

TABLE I. Summary of the experiments with the uncertainties for each quantity shown in parentheses.

Experiment	Impactor/ sample	Impactor velocity (mm/μs)	Peak stress (GPa)	Initial density (g/cm^3)	Calculated density (g/cm^3)	Measured density (g/cm^3)	Agreement
1	Al 6061-T6	1.452 (0.012)	12.27 (0.11)	2.710 (0.003)	3.067 (0.005)	3.070 (0.025)	0.1%
2	Al 6061-T6	1.422 (0.002)	11.98 (0.03)	2.710 (0.003)	3.060 (0.004)	3.056 (0.020)	0.1%
3	OFHC Cu	1.30 (0.04)	28.59 (0.91)	8.928 (0.003)	10.30 (0.05)	10.28 (0.08)	0.2%
4	OFHC Cu	1.249 (0.002)	27.16 (0.06)	8.928 (0.003)	10.241 (0.006)	10.28 (0.08)	0.4%

Solid-Solid Phase Transitions in Iron

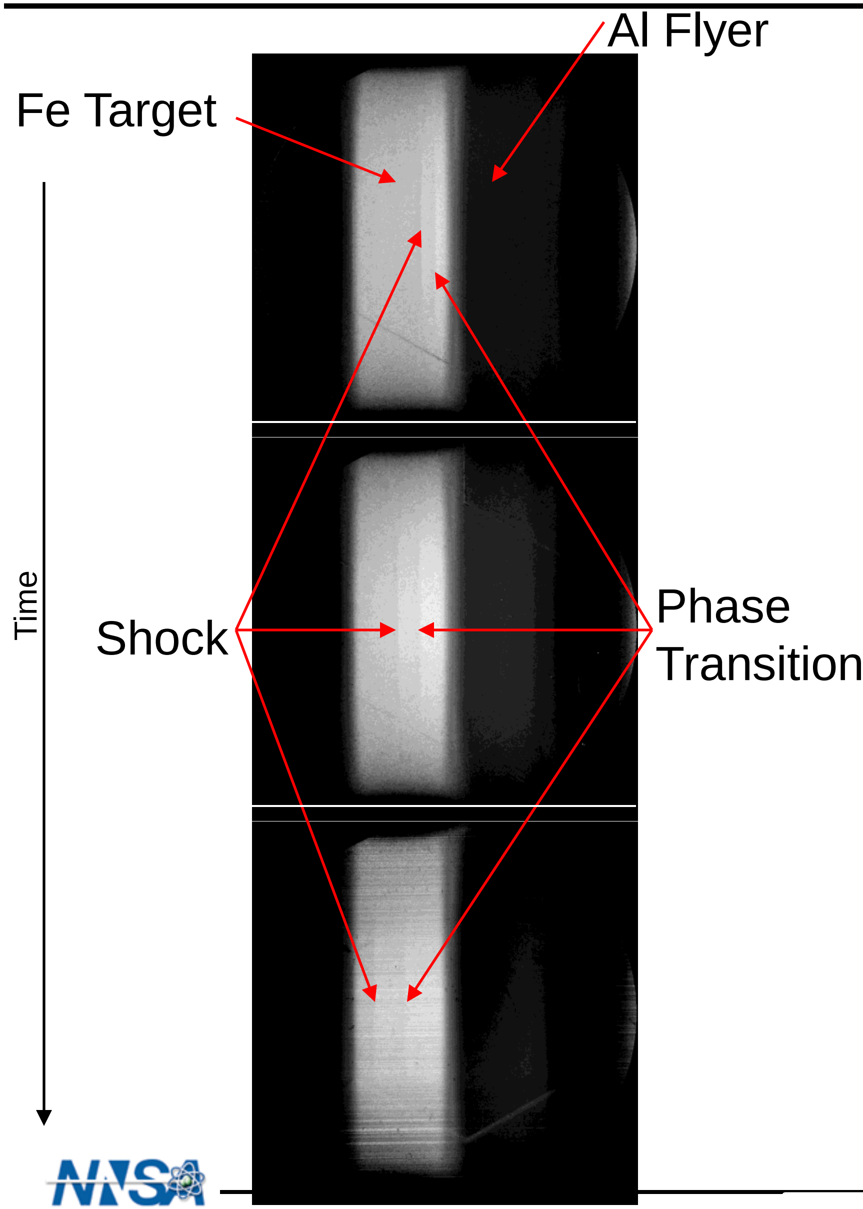

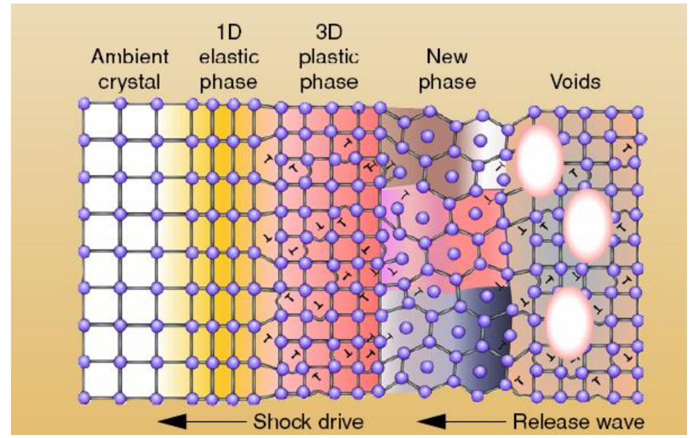

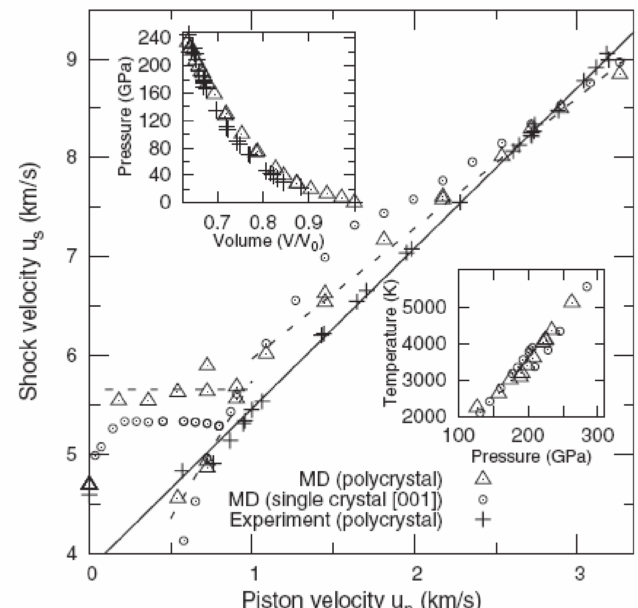

Phys. Rev. Lett. 98 135701 (2007)

pRad has been used to study the failure of materials driven by point detonated high explosives

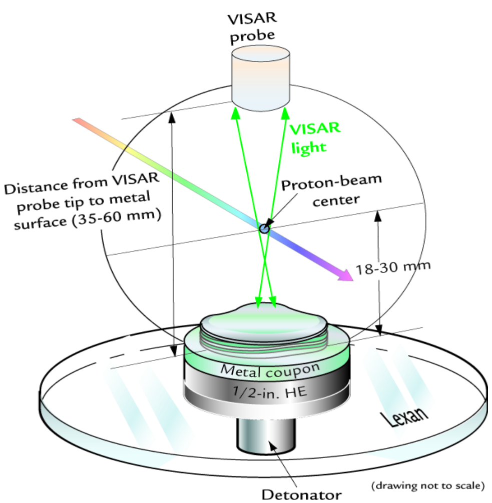

A comparison of spall for different materials

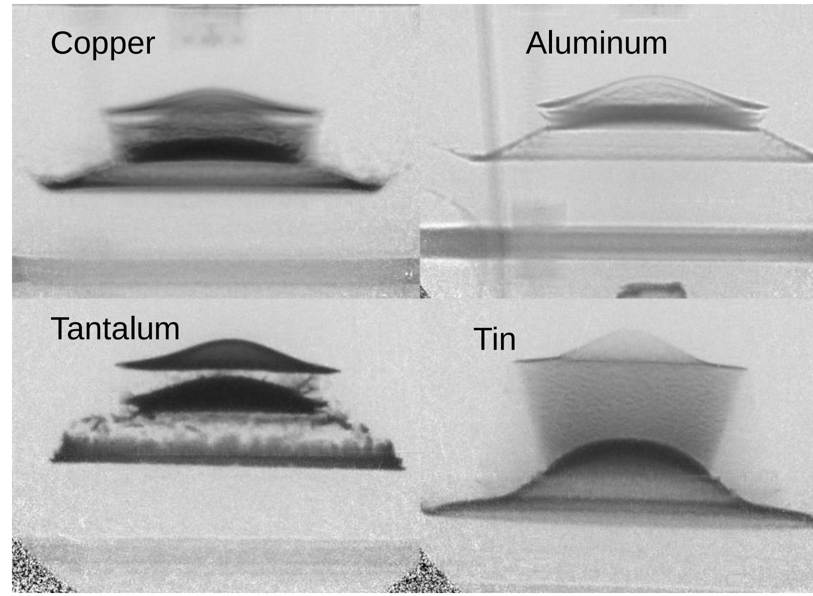

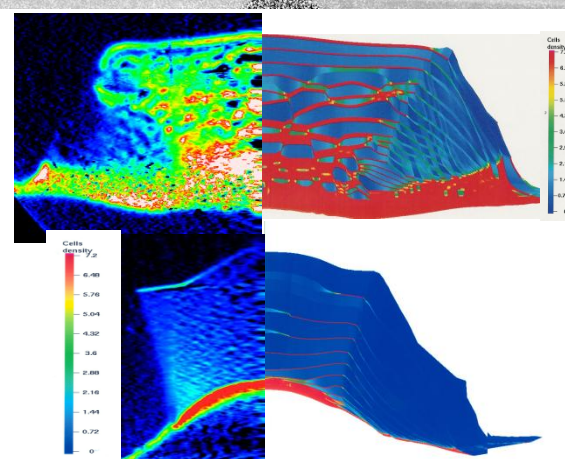

- Experiments were aimed at extending VISAR measurements below the leading spall layer.
- Proton radiographs reveal that the deepest damage layers are not well defined.
- Multiple pRad experiments show that damage formation deep within the metal is “statistical” in nature and dependent on metal.

Complicated Studies of HE Burn Products

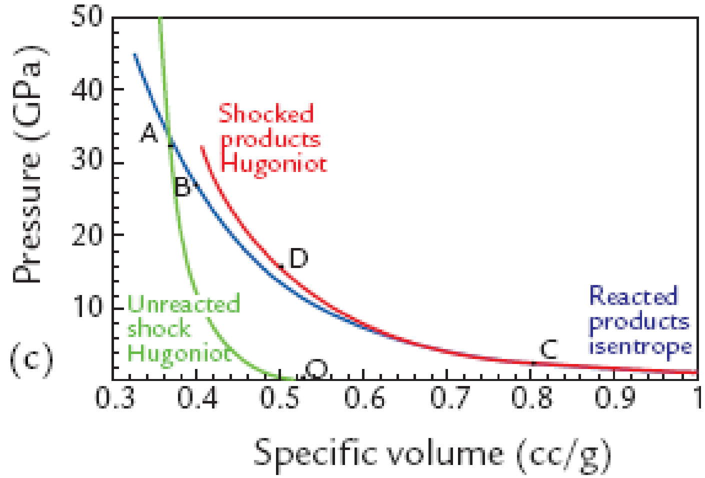

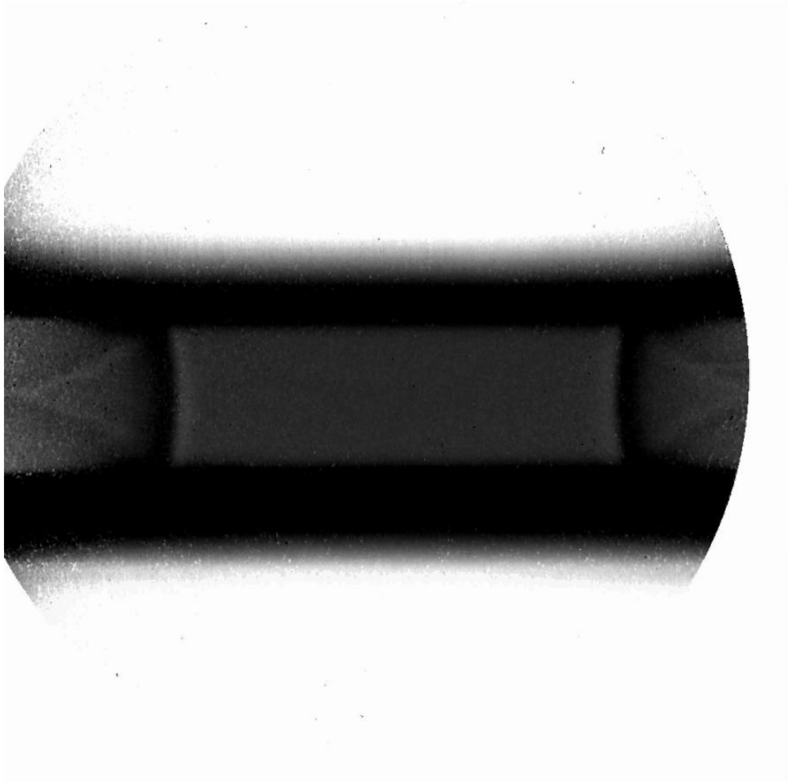

Studies of HE Burn Products

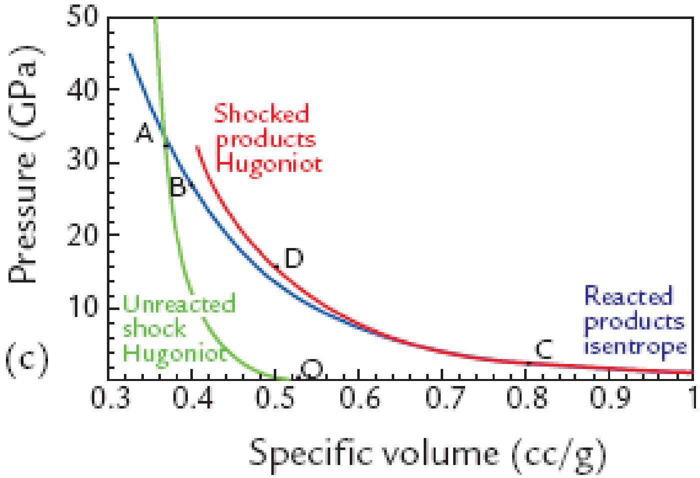

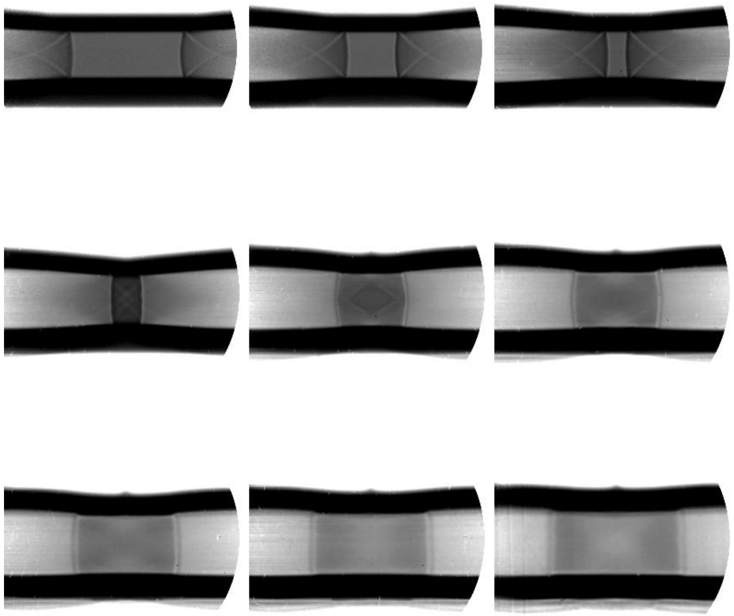

Evolution of Spall Damage

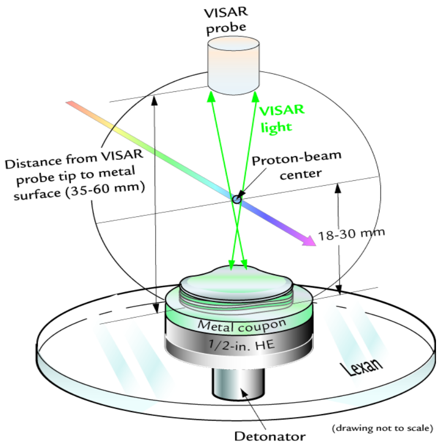

What damage occurs behind the first spall layer?

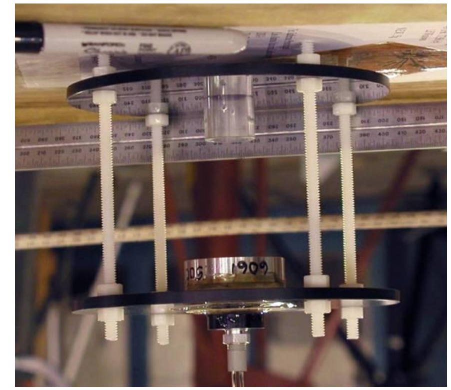

Incipient Spall with Recovery Experiments

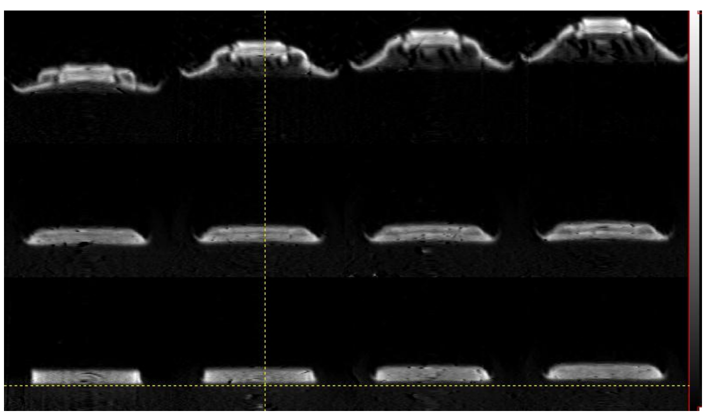

Dynamic Radiograph

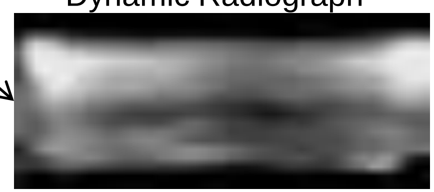

Micrograph

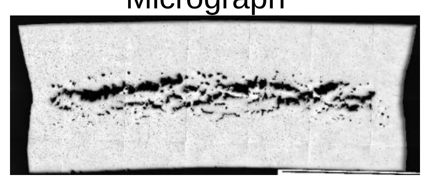

0.8 cm

- How and where are voids formed?
- How do they coalesce to form macroscopic damage?
- Requires improvements in resolution.

Explosively Formed Projectile (EFP)

PRAD486 (Schwartz and Marr-Lyon)

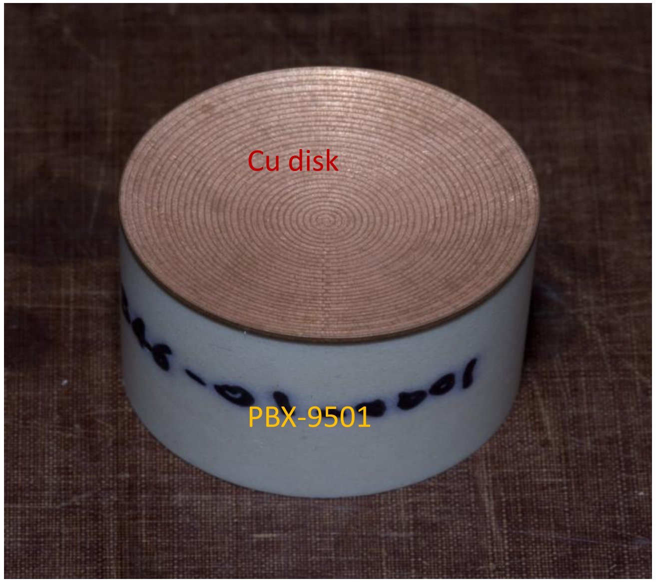

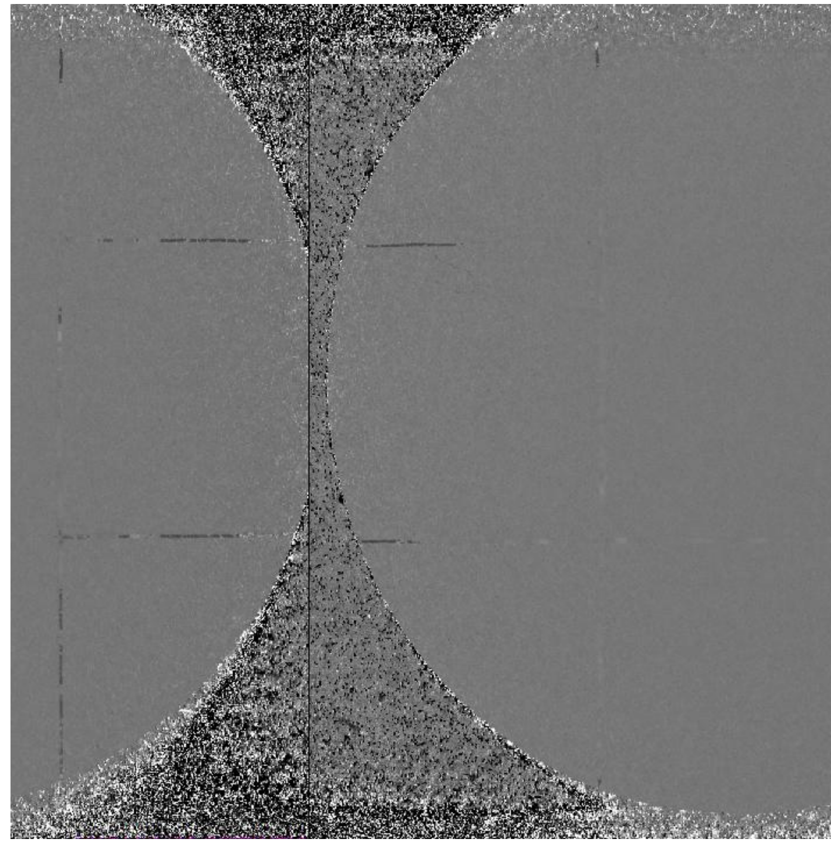

Trial shot for future experiments to study projectile transport thru granular materials (sand)

Tomography of Surrogate Fuel Rods

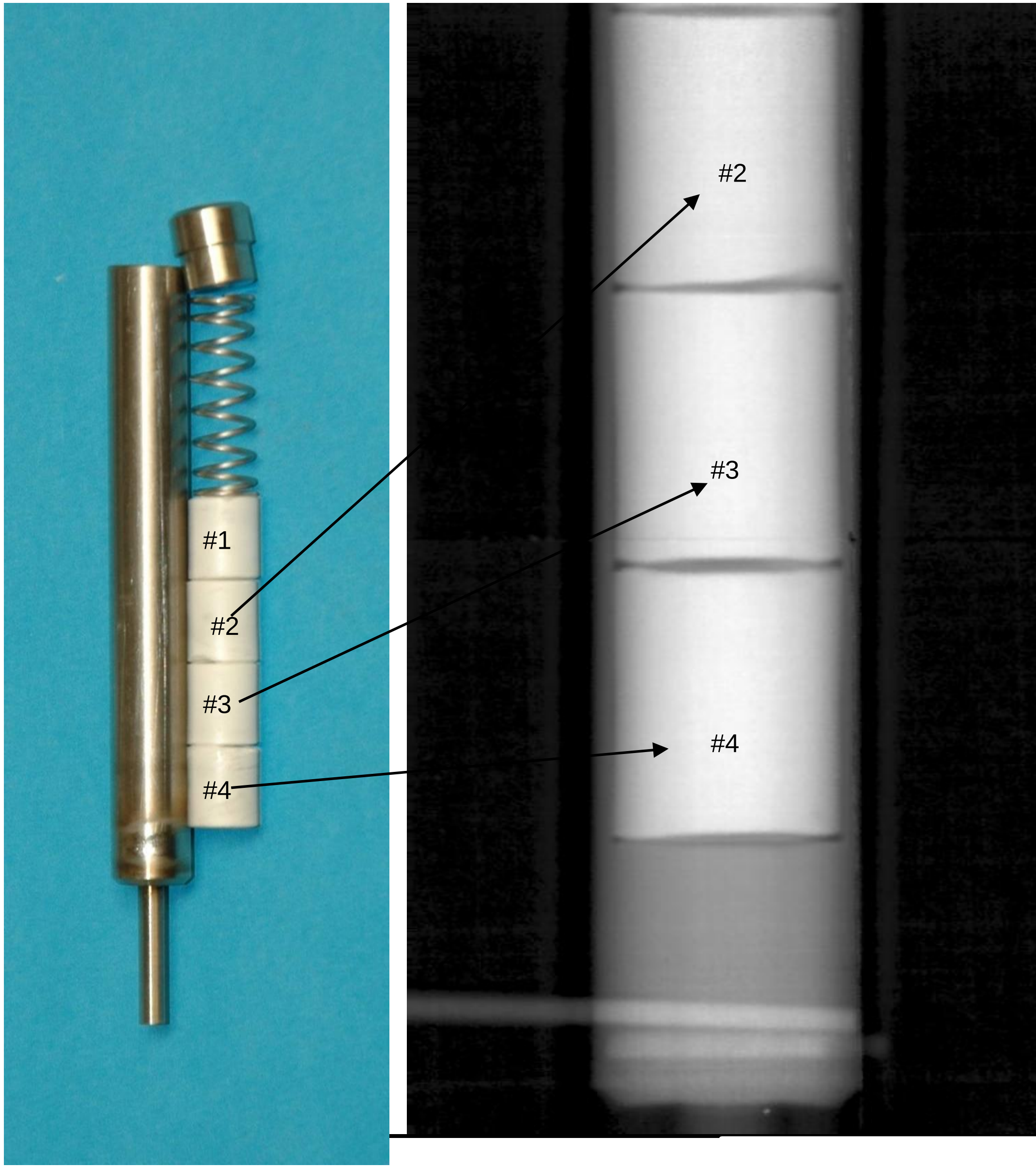

Reconstructed Areal Density of HfO_2 Pellets